

DYNAMIC MODELING OF PROTECTIVE CURRENT TRANSFORMERS

A MASTERS THESIS

in

109906

Electrical and Electronics Engineering

University of Gaziantep

**T.C. YÜKSEKÖĞRETİM KURULU
DOKÜMANTASYON MERKEZİ**

By

Hacı TAŞMAZ

August 2001

Approval of the Graduate School of Natural and Applied Science.



Assoc. Prof. Dr. Ali Rıza TEKİN
Director

I certify that this thesis satisfies all the requirements as a thesis for the degree of
Master of Science.



Prof. Dr. Tuncay EGE
Chairman of the Department

I certify that I have read this thesis and that in my opinion it is full adequate, in scope
and quality, as a thesis for the degree of Master of Science.



Assoc. Prof. Dr. Mehmet TÜMAY
Supervisor

Examining Committee in Charge:

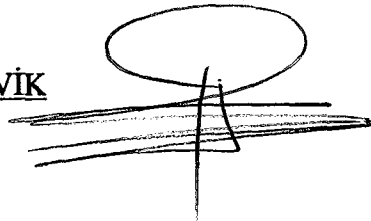
Asst. Prof. Dr. Vedat Mehmet KARSLI
(Chairman)



Assoc. Prof. Dr. Mehmet TÜMAY



Asst. Prof. Dr. Ulus ÇEVİK



ABSTRACT

DYNAMIC MODELING OF PROTECTIVE CURRENT TRANSFORMERS

TAŞMAZ, Hacı

MS. Electrical and Electronics Engineering

Supervisor: Assoc. Prof. Dr. Mehmet TÜMAY

August 2001, 110 pages

Because of its nonlinear core characteristic, it is difficult to analyze current transformer CT performance in any protective scheme under fault conditions. CT core subjected to transient conditions saturates which causes maloperation of protection relays.

To overcome this problem, many mathematical models were proposed for the CT cores in the past, which were mostly complex and inaccurate.

The aim of this study is to investigate the transient characteristic of a CT under fault conditions.

For this reason, a new mathematical model for CT core characteristic was proposed. In addition, a fault current model for a typical power plant was proposed. A 400/1 A current transformer was simulated with various maximum offset fault currents up to 3000 A for different values of burden resistances. A computer program was written using the proposed core model and CT model equations.

The simulation results were seen to be accurate and closely fit into the experimental and simulation results proposed previously.



Keywords; Ferromagnetic hysteresis modeling, Fault current modeling,
Current transformer modeling, Computer simulation,
Graphical analysis,

ÖZET

KORUMA AKIM TRANSFORMATÖRLERİNİN DİNAMİK MODELLENMESİ

TAŞMAZ, Hacı

Yüksek Lisans Tezi, Elektrik Elektronik Mühendisliği

Tez Yöneticisi: Doç. Dr. Mehmet TÜMAY

Ağustos 2001, 110 sayfa

Lineer olmayan nüve (kor) karakteristiği sebebiyle, kısa devre koşullarında akım transformatörlerinin performansını incelemek zordur. Geçici rejim koşullarına maruz kalan bir transformatör nüvesi doyuma gider, ki bu da kendisine bağlı koruma rölesinin hatalı çalışmasına neden olur.

Bu sorunu gidermek için geçmişte, çoğu karmaşık, hassas olmayan pek çok kor modeli geliştirildi.

Bu çalışmanın amacı, akım transformatörlerinin kısa devre şartları altında geçici durum karakteristiğini araştırmaktır.

Bunun için yeni bir kor karakteristiği modeli önerildi. Ayrıca tipik bir güç sistemi için kısa devre akımı modeli önerildi. 400/1 Amper bir akım transformatörü, 3000 Amper'e kadar farklı ofset akımları ve farklı yük dirençleri için simüle edildi. Önerilen kor ve akım transformatörü model denklemleri için bir bilgisayar programı yazıldı.

Simülasyon sonuçlarının hassas olduğu ve daha önce yapılan deneysel ve simülasyon sonuçlarına uyduğu görüldü.



Anahtar Kelimeler: Ferromanyetik histerezis modellemesi, Kısa devre akımı modellemesi, Akım transformatörü modellemesi, Bilgisayar simülasyonu, Grafik analizi.

ACKNOWLEDGEMENT

I am grateful to my supervisor Assoc. Prof. Dr. Mehmet TMAY, for his helpful suggestions, criticisms, and encouragements. Also, I want to express my thanks to Galip TONUÇ and Emin ZCAN for their invaluable help and guidance in computer simulation of this thesis. And, I wish to thank to my roommates Beyhan BAYIK and Hseyin MURATOĐLU, for their, positive criticisms, understanding and morally support during my heavy working period on this thesis.



TABLE OF CONTENTS

| | <u>Page No</u> |
|---|---|
| ABSTRACT | iii |
| ÖZET | v |
| ACKNOWLEDGEMENTS | vii |
| CHAPTER 1 | |
| INTRODUCTION1 | |
| 1.1 | Effects of Offset Currents on CT Performance.....2 |
| 1.2 | Effects of Current Transformer Transient Response on Relays and Protection Circuit Performance.....3 |
| 1.2.1 | Differential Relay Protection.....3 |
| 1.2.2 | Phase Comparison Relay Protection.....4 |
| 1.2.3 | Distance Relay Protection.....5 |
| 1.2.4 | Over current Relay Protection.....5 |
| 1.3 | Review of Previous Methods of Predicting Current Transformer Transient Response.....7 |
| 1.3.1 | Analytical Methods.....7 |
| 1.3.2 | Digital Methods.....8 |
| 1.4 | Scope of Present Work.....11 |
| CHAPTER 2 | |
| FUNDAMENTALS OF CURRENT TRANSFORMERS13 | |
| 2.1 | The Primary Winding.....14 |
| 2.2 | The Magnetic Circuit.....15 |
| 2.3 | The Secondary Winding.....15 |

| | | |
|-------|--|----|
| 2.4 | The Burden..... | 16 |
| 2.5 | Specification of Current Transformers..... | 17 |
| 2.5.1 | Short Time Factor..... | 19 |
| 2.5.2 | Accuracy Limit Factor..... | 19 |
| 2.6 | Effects of Frequency..... | 20 |
| 2.7 | Errors..... | 20 |
| 2.8 | Open-Circuit Secondary Voltage..... | 21 |
| 2.9 | CT Operation..... | 21 |
| 2.10 | Other Types of Current Transformers..... | 24 |

CHAPTER 3

MODELING OF MAGNETIZATION CHARACTERISTICS...26

| | | |
|-------|---|----|
| 3.1 | Magnetic Properties of Soft Iron..... | 26 |
| 3.2 | B-H Loops of Hard and Soft Magnetic Materials..... | 28 |
| 3.3 | Mathematical Representation of B/H Characteristics..... | 30 |
| 3.3.1 | Single valued characteristics..... | 30 |
| 3.3.2 | Multivalued characteristics..... | 33 |

CHAPTER 4

THE JILES-ATHERTON MODEL.....48

| | | |
|-------|--|----|
| 4.1 | The Jiles-Atherton Model..... | 48 |
| 4.1.1 | Experimental Technique..... | 50 |
| 4.2 | The Modified Jiles-Atherton Model..... | 51 |
| 4.3 | Simulation Results of Core Model..... | 61 |

CHAPTER 5

CURRENT TRANSDUCER MODELING.....64

5.1 Fault Current Modeling.....64
5.2 Transient Effects in Current Transformers67
5.3 Dynamic Modeling of Current Transformer.....71
5.4 Air-Core Current Transformer Modeling.....74

CHAPTER 6

**DIGITAL SIMULATION RESULTS OF CURRENT
TRANSFORMER.....77**

6.1 Current Transformer Data..... 77
6.2 Simulation Results for Different Excitations.....78

CHAPTER 7

CONCLUSION AND SUGGESTIONS FOR FURTHER WORK

7.0 Conclusions.....104
7.1. Suggestions for Further Work.....105

REFERENCES.....106

APPENDICES.....109

CHAPTER 1

INTRODUCTION

General

In modern power systems, saturation of current transformers during short circuits is often unavoidable due to slow decaying dc component of fault currents. Saturation causes extensive transient errors, which may adversely affect the performance of the protective relays. Estimation of the expected errors is vital at the stage of designing protective systems.

For the complete transient analysis of any protective system, knowledge of the dynamic behavior of the current transformer is needed. The nonlinear characteristic of core of the CT mainly determines the performance of the CT under fault conditions.

Consequently, the determination of the transient response of a CT feeding a linear or nonlinear load is very complex. Precise analytical methods are often not possible, hence the need for digital methods. Digital computer method requires accurate mathematical models for the CT and load. In the past, different mathematical models have been brought forward most of which do not permit true representation of the exciting circuit, as the models do not closely fit into the exciting curve, especially near the origin.

The present work will examine briefly the quantitative aspects of protection current transformer saturation. An accurate mathematical model for the CT core is proposed. The proposed model is used to simulate the transient response of the CT with R-L load. The effects of variation of the CT parameters and burden, on CT performance under fault conditions are examined and characteristic curves of CT currents are obtained.

1.1 Effects of Offset Currents on CT Performance

The factors determining the performance of a current transformer are its magnetization characteristic, the burden connected, the nature of fault current and steady state errors. The magnetization characteristic of the current transformer depends on the non-linearity of its iron core. This non-linearity is generally represented by a non-linear inductance due to the negligible effect of magnetizing resistance. The magnetizing inductance is high in the normal operating region of the current transformer. However, its value reduces rapidly as the current transformer saturates. In the unsaturated region, only a small fraction of the primary fault current is utilized in establishing core flux, hence transformation errors are quite small. An asymmetric current causes a rapid build up of the core flux, forcing the current transformer into saturation. At this stage, almost all-primary fault current becomes magnetizing current, resulting in high transformation errors, very large distortion and sometimes-complete loss of secondary current. Saturation of current transformers can therefore have adverse effect on associated relays, depending on its design.

Dramatic increase in the current transformer size and decrease in burden reduces the risk of saturation. However, due to costs and limited space available for the current transformers in the primary plant, saturation is still a problem. It should be noted that saturation of the current transformer may occur with steady state symmetrical fault current, but only when relatively high impedance is connected to the current transformer secondary and the fault current is relatively high. Existence of residual flux in a current transformer before fault would aid its saturation, depending on the sign of the residual flux with respect to the primary fault current. If a positive residual flux exists in the current transformer core, an offset fault current that is positively oriented will cause transformer to saturate much faster. The next section would highlight some of the effects of current transformer saturation on relays and protection circuits.

1.2 Effects of Current Transformer Transient Response On Relays and Protection Circuit Performance

The basic function of protection relays is to recognize faults within a protected zone and initiate the operation of the correct circuit breakers at the appropriate time. In reference [1] problems caused by current transformer transient response on relay performance have been outlined. Some of the problems will be examined here. Transient response of current transformers (especially when it is saturated) causes variety of maloperation, which can be classified into three categories:

- Detection of faults where non exists,
- Failure to detect a fault,
- Failure to detect a fault in adequate time.

Different types of protection schemes and effect of current transformer transient response will now be considered.

1.2.1 Differential Relay Protection

In high impedance differential protection, the current transformers may saturate whilst trying to force current through the relays, as in the case of high fault currents within the protected zone. For external faults, such schemes are good. However, in the case of external faults the highly distorted current waveforms can slow down the speed of operation. Differential relaying of transformers, buses and related ac apparatus has been a popular method used for providing selective protection to the device. Relay operation occurs for faults within its zone of protection. The basis of the protection scheme is to sum all currents entering and leaving the zone of protection. If the sum does not equal to zero, the relay operates. Distortion of the current transformer output due to saturation enhances the differential current, thereby causing maloperation of the relay.

1.2.2 Phase Comparison Relay Protection

Briefly, the relay operates in such a system by comparing the phase positions between in flowing and out flowing currents of the protected zone. Figures 1.1 and 1.2 show block diagram of typical phase comparison protection scheme and the output waves generated at different points. Traces 1a and 1b are generated when the current transformer is unsaturated and saturated respectively. Clearly, the current transformer saturation causes the shortening of the local pulse (trace 4), which leads to undesirable effects. This delays the tripping of the appropriate breaker X. The solution of such a problem is to include a pulse stretcher in the circuit [1].

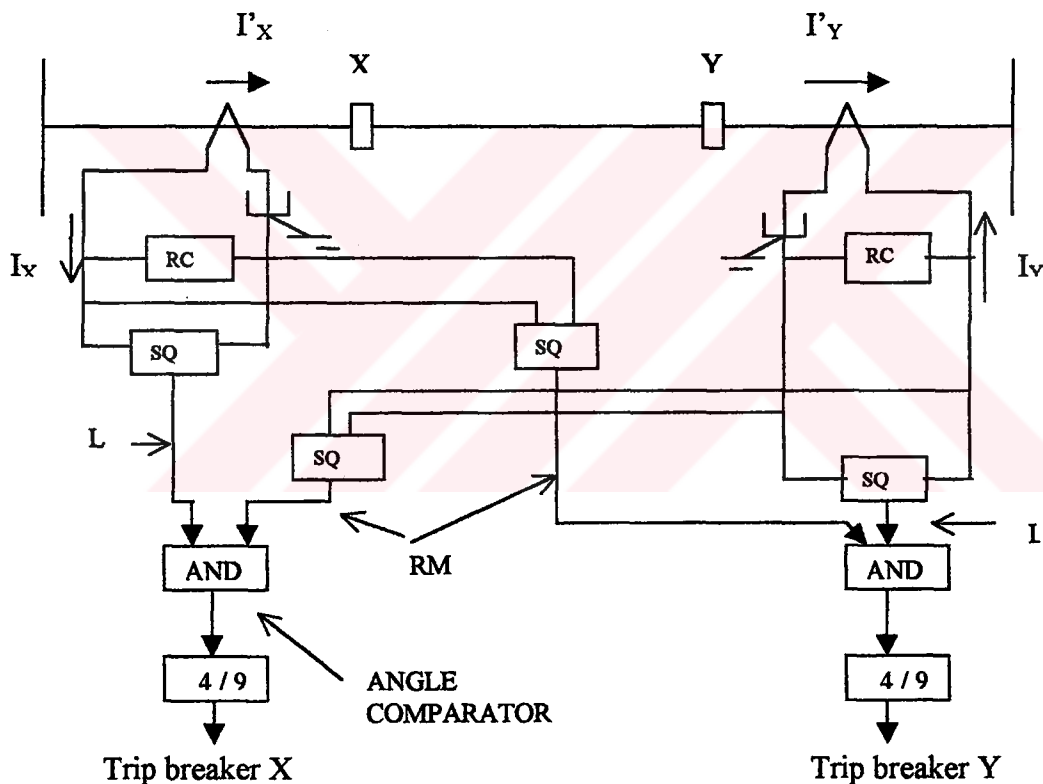


Figure 1.1 Phase Comparison Differential Protection

4/9 - timer, 4 ms operate, 9 ms reset

SQ -squaring circuit

RC- resistor

L- local signal

RM- remote signal

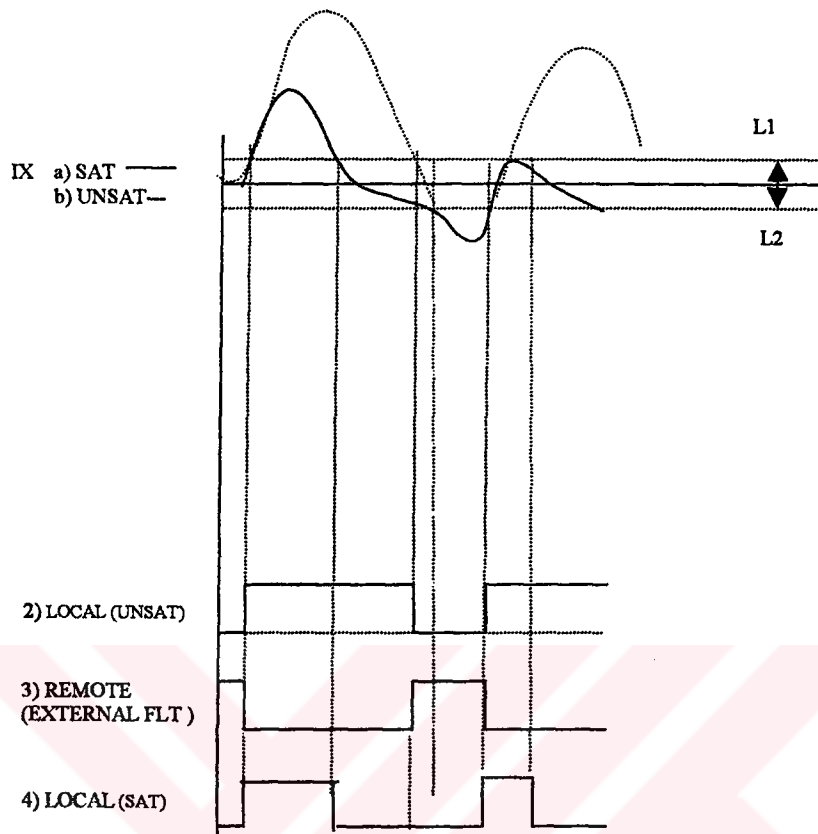


Figure 1.2 Square wave generation at breaker X in figure 1.1

1.2.3 Distance Relay Protection

Distance relays require that a "true" transformation of the primary current be obtained from the current transformer secondary. The current transformers should therefore not saturate before the operation of the relay. In practice, this condition is not satisfied in most types of faults on transmission lines. The current transformers may saturate before the relay has time to operate, thus delaying the operation of the protection system.

1.2.4 Over Current Relay Protection

This type of protection is one of the earliest used in power systems. Over current

relays function differently, depending on the coordinating procedure in the network. Various methods are used to achieve correct relay coordination, among which we have time grading, current grading, or a combination of both. The primary aim of each method is to provide appropriate discrimination and isolation of only the appropriate faulty section of the power system network, leaving the rest of a system undisturbed. The time grading method is achieved by introducing a time delay between the relays controlling the circuit breakers in the power system to ensure that the breaker nearest the fault opens first. Figure 1.3 shows a typical radial system in which time grading relay operation is applied.

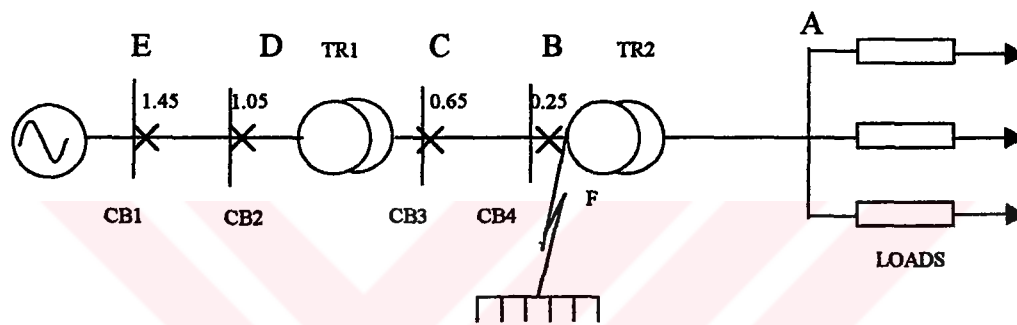


Figure 1.3 Radial power system with time discrimination.

With a fault at point K the relays at B, C, D, and E function as follows: The relay at B causes the breaker at B to operate in 0.25 sec. thereby isolating the fault. Failure of such an operation causes relay C to energize its breaker (at C) in 0.65 sec. and so on. Saturation of the current transformer at B would cause maloperation, possibly slow the initiation of the circuit breaker at B to isolate the fault. If this happens, relay C will cause breaker C to operate, thereby isolating the whole ABC section. Thus, equipment etc. between sections BC, which under normal circumstances should not be affected, is affected. Nowadays, induction disc relays (e.g. IDMT relays), which have improved time grading facility, are used in place of the definite time ones. In addition, inverse time-current relays offer better discrimination and permit lower time settings where level of generation is reasonably constant and fault current is controlled by the fault location. However, since CT saturation cause relays to receive less amounts of current (during saturation), maloperation can occur even in these

improved methods of discrimination. Despite the fact that only a few of the enormous problems caused by the transient response of current transformers have been outlined here, the necessity of accurate determination of the response of current transformers under transient conditions cannot be over emphasized

1.3 Review of Previous Methods of Predicting Current Transformer Transient Response

There are numerous methods with varying degrees of accuracy for predicting the transient response of current transformers. These methods can be categorized into two precise types, analytical and digital. Either of these two types of analysis can be used depending on the amount of information about the power system and the current transformer available and the amount of information required from the obtained results.

1.3.1 Analytical Methods

Analytical methods were the first to be derived by engineers. They were very useful in past years when the development of digital computers had not reached an advanced stage. Even today, some design engineers utilize them for obtaining 'on the spot' estimates of certain transient characteristics of current transformers like time to and time out of saturation, over dimensioning factor, etc. Use of analytical methods does not require a great deal of system or current transformer data. Usually the most important data include current transformer time constant turns ratio, system time constant, degree of fault current offset, percentage remenance flux in the current transformer core, angular frequency of fault current, type and value of current transformer burden. The amount of information obtained from the analytical method is small. This includes the time to saturation of the current transformer [1,2] and time out of saturation, equation for the output currents from the current transformer [3]. Analytical methods include those of Schroot, and Wu. Schroot's [4] method neglects the non-linear aspects of the magnetic material, hysteresis, saturation, and remnant magnetism. A linear relationship between the magnetizing current and flux in the transformer core is assumed. All these assumptions were applied to obtain an

expression of the current transformer magnetizing current and hence the output current in terms of the system and current transformer parameters. Due to the numerous assumptions, most of which might not be true (e.g. neglecting saturation and non-linear core characteristics, etc.), the results obtained are approximate and cannot be used for accurate power system design.

The method determined in IEEE Power Systems and Relaying Committee Report [1] is based on the use of 'time to saturation curves' to determine the time which elapses after the fault, before the current transformer saturates. Saturation curves were derived by if the transformer core has a constant permeability up to the saturation point. The method involves the calculation of the saturation factor and current transformer time constant T_2 . Given the system time constant T_1 , the appropriate saturation curve is used to find the time to saturation (t_g) of the current transformer. Provision is made for remnant flux in the transformer core and partially offset fault current. The method gives better accuracy compared to Schroot's analytical method and is still used by engineers to obtain 'on the spot' approximations of saturation times of current transformers. However, its application is limited due to its incapability to predict the nature of the output current from the current transformer, its time out of saturation (t_{ds}) and the amount of energy dissipated in the core in a given period.

Wu [2] recently revised a new method. Using the same equation, he obtained expressions for the time to saturation (t_g) and time out of saturation (t_{ds}) of the current transformer. Knowing the system and current transformer parameters; system time constant T_1 , angular frequency, current transformer time constant T_2 and burden, turns ratio, current transformer knee point voltage and current, peak value of the fault current and power factor of burden, the time to saturation and time out of saturation can be computed.

1.3.2 Digital Methods

The fast computing facilities provided nowadays by digital computers have revolutionized the analysis of current transformer transient response. Digital

computers are more frequently used to analyze the transient response of current transformers. The degree of accuracy required from the digital results determines the amount of information required for the analysis. Excellent results are obtained by the use of sophisticated core modeling routines and precise knowledge of system and current transformer parameters. For most digital analysis [5,6,7,8,9] non-linear single-valued Φ/I core characteristic is employed. Some employ a more difficult multi-valued hysteresis characteristic [4,10].

Mora's[8] method involves the use of rational fraction model for the core Φ/I characteristic. Single-valued representation is employed. Saturation is accounted for, but hysteresis and eddy currents are neglected. Despite the rigorous computation involved in the method, which includes the inversion of a complicated matrix, the accuracy of determining the transient response of a current transformer obtained is not exceptionally high. Output current from the saturated current transformer, which in real terms should be distorted, appears to show very little sign of distortion.

Yacamini [9] used a single-valued B/H core model to analyze inrush currents in a transformer. Point by point representation of the B/H curve was used. Hysteresis effect was neglected; hence, its use under residual flux situation will not give appreciably accurate results. Despite the fact that this method requires large computer storage, its application is mostly confined to power transformers where the inrush current is relatively very high compared to the magnetizing current in saturated current transformers.

Idoniboyeobu's [11] method, which involves the use of an exponential representation for the Φ/I characteristic of the current transformer core appears to be much easier to implement on a digital computer than the previous two models [8,9]. Single-valued flux/current relationship is assumed, while Range- Kate 4th order, integration routine is used to solve the differential equation obtained from analysis of the current transformer response. Hysteresis and eddy current characteristics were neglected. Although an appreciable accuracy is achieved in modeling the single-valued Φ/I characteristics. This method cannot be used where high residual flux is trapped in the transformer core.

A multi-valued model proposed by Schroot [10] involves the use of a polynomial relationship between the core magnetizing flux and current. Saturation and hysteresis are all accounted for in this model. The effect of hysteresis and residual flux in the transformer core are clearly demonstrated. Residual flux increases the magnetizing current in the first half cycle, hence reducing the time to saturation of the current transformer. Hysteresis effect, however, does not appear to influence the magnitude of saturation, but leads to greater magnetizing currents during the periods of no saturation. Good accuracy is achieved by the use of this method. However, the modeling of the Φ/I characteristic by the Gauss-Jordan method appears to be more difficult than other existing methods.

Frame [10] developed a target point method for representing the Φ/I characteristics of the transformer core. This model is specifically developed for use in a computer in conjunction with the electromagnetic transients program (EMTP), which is widely used on numerous different computers.

The algorithm described in this paper allows the multi-valued hysteresis behavior to be represented as a linear element at each instant of time. It has been implemented together with the EMTP for analyzing the demagnetization of a transformer. However, the use of this method to analyze transient response of current transformers using microcomputers would need the EMTP to be translated to the language applicable to the computer.

The most recent multi-valued model is examined by Hannalla [6]. Here, Hannalla used a rather straightforward formula for expressing the relationship between the flux density and field strength. The problem with this model is that minor loops are not considered in the modeling subroutine. Although it takes less computer storage and time, its ability to model minor loop flux/current excursion is low. Therefore, its use for the solution of problems involving high residual flux in transformer core might not yield very accurate results. However, it should be noted that the simple expression for modeling the hysteresis loops of soft magnetic materials overcomes the computational difficulties in previous methods. It has been used in the solution of

transformer inrush problem [6].

Most of the methods for analyzing current transformer transient response so far described do not yield excellent result. The relatively early method, most of which neglect hysteresis and eddy current, cannot be used for analysis of current transformer response where residual flux exists prior to fault. In addition, minor loop excursion cannot be accounted for. Other methods, including hysteresis, are fairly difficult to implement on PC. The need therefore arises for the development of a relatively easy and accurate method for analyzing current transformer transient response, which can be implemented on a PC. The transformer core model should be represented by a multi-valued Φ/I characteristic which includes hysteresis and eddy current loss and should be capable of representing minor hysteresis loops.

1.4 Scope of Present Work

This thesis is concerned with the development of a digital technique for accurate analysis of transient response of current transformers using a PC. Such a technique requires an accurate mathematical model for the transformer core. The core model should possess the following qualities:

- Multi-valued;
- Include saturation;
- Include hysteresis.

Also, the core model subroutine should be simple and require small computer storage. To appreciate the accuracy of core model, experimental B/H patterns from current transformers would be obtained and compared with those obtained numerically from the computer using the developed algorithm. The effect of current transformer burden resistance, primary fault current, fault angle, and residual flux in current transformer on the transient response of the current transformer will be studied for a single-phase circuit.

In Chapter 2, fundamental aspects of current transformers are examined. The construction of the C.T, (primary and secondary windings, magnetic core, the burden), specification of current transformers, effect of frequency, errors, CT operation, and other types of current transformers are also examined.

In Chapter 3, background theories on representation of the magnetic characteristics of iron are examined. The theories include single-valued representation, multi-valued hysteresis representation and multi-valued hysteresis plus eddy current representation of core Φ/I characteristics. Losses in soft magnetic materials (hysteresis losses, classical and anomalous eddy current losses) were also examined.

Chapter 4 deals with modeling of the core characteristics of the current transformers examined in Chapter 3. Jiles-Atherton model is examined here in detail. Appropriate algorithms were developed for the multi-valued representation of the transformer core characteristics. Simulation results were compared with experimental and simulation results given in ref. [27].

Chapter 5 deals with the representation of saturation and hysteresis of current transformer model including development of computer programs for current transformer transient analysis. Runge Kutta (Merson) fourth Order Integration Routine (Appendix 1) was used for solution of non-linear equations obtained in the analysis.

Chapter 6 deals with the results of the digital simulation and the effects of the primary fault current magnitude and burden impedance on saturation of CT. The technical data of the CT used in the simulation is also given in this chapter.

Chapter 7 includes result, conclusions, and suggestions for further work.

CHAPTER 2

FUNDAMENTALS OF CURRENT TRANSFORMERS

Introduction

The current transformer CT is a device for the transformation of a current of a higher value to one, which is lower, and at a lower potential proportionally. This is usually necessary since power systems operations involve large currents and voltages, which would otherwise be difficult or hazardous to work on. The ideal CT would be one which all-primary conditions are reproduced in the secondary circuit in exact ratio and phase relationship. The basic components of any CT are the primary winding, magnetic core, secondary winding and sometimes included is the secondary burden.

The primary winding of a CT is connected in series with the power circuit whose current is being measured or indicated. The primary current is in no way controlled or determined by the condition of the secondary circuit whereas in the power transformer the current flowing in its primary windings is a representation of that flowing in the secondary circuit. Both however follow the same fundamental mechanism of electromagnetic induction. Therefore, CT operation dominant factor is the primary current.

Current transformers are usually categorized into two types, measuring and protective current transformers according to their duty requirements. A CT designed for measuring purposes usually operates over a range of current up to a specific rated value, which corresponds to the circuit normal rating with specified errors at that value. A protection CT however is required to operate over a larger range, usually up to ten times the circuit rating and frequently liable to be subjected to such over currents.

The electrical isolation of relays, measuring instruments, etc. in the CT secondary circuit from the high potential above earth of the primary circuit is

achieved by the provision of major insulation between primary and secondary windings and between these windings and earth.

The impedance of the CT with secondary burden connected is negligible compared with that of the power circuit but has a slightly higher input impedance with the secondary open circuited. Therefore, the power system impedance governs the current passing through the primary of the CT.

Most current transformers are designed such that the primary winding is the line conductor, which is passed through an iron ring, which also carries the secondary winding. These are known as bar primary or ring-wound CT. Standard CT rated secondary currents are 0.1, 1 and 5 A but in extreme cases, 20 A where primary rating is very high and may need an auxiliary CT to step down to a lower current rating. It is only advantageous to use the lower rating where interconnecting leads to the burden are long.

2.1 The Primary Winding

It is usually single-turn primary but also multi-turn primary for some applications. Single-turn primary winding has the advantage that when a large short-circuit current flows in the primary, the dynamic and thermal stresses subjected to the CT are more onerous in the multi-turn or wound-primary CT.

However it is sometimes necessary to use wound-type primary construction in order to obtain the required performance as in cases where the primary current is low, thus requiring a large core area for a reasonable secondary output.

Clearly, it is more economical to increase the primary windings but at the expense of a higher knee-point voltage due to the corresponding increase in secondary turns. That knee-point voltage is defined as the point where an increase of 10% secondary

voltage would increase the magnetizing current by 50%. (See figure 2.3) The primary winding conductor would also need be of sufficient size to carry the short circuit current of the power systems.

2.2 The Magnetic Circuit

Performance of a CT or accuracy of transformation is determined by the characteristics of the core material and type of core construction adopted. One important parameter in the design of a CT is the frequency of excitation as with any other AC electromagnetic device, i.e. the supply frequency of the primary system.

Normally, grain-oriented sheet-steel strip is wound tightly to form a closed-turned spiral and is then covered with a layer of insulation before the secondary winding is wound over it. Magnetic alloys used include hot-rolled silicon iron, cold-rolled oriented silicon-iron, nickel-iron or “ composite” cores type. (Current transformers which use a different alloy for each of the two sections of the core.)

Choice of the magnetic alloy for the CT core is therefore a matter of its application, since properties such as high permeability and low losses may be preferred for one application but not for others. The less traditional core types are cross like double-oriented and magnetostriction electrical steels (silicon iron alloys). The making of the core by stacked annular laminations has now been superseded by the wound tape method.

2.3 The Secondary Winding

The secondary winding is wound over the insulated core with the appropriate number of turns to produce the required ratio, of wire of sufficient cross-sectional area to carry the rated current. Again, a further layer of insulation is applied over these windings.

Although the flux density in an operating CT is normally low, it is a very important factor in the performance of the CT and is determined by the total impedance of the

secondary circuit. The secondary impedance being the impedances of the leads, windings and burden itself which sometimes the secondary winding is a dominant part of the secondary impedance thus requiring careful attention in the design of a CT.

Especially in applications on protection schemes these current transformers are usually required to deliver high values of secondary current, the secondary winding resistance must be as low as practicable.

Secondary leakage reactance though low but not always negligible, especially for wound primary current transformers are difficult to assess due to the non-linearity of the CT magnetic circuit.

Evenly distributed windings ensure even flux distribution within the core leading to better overall performance of the CT. The secondary winding of a ring-type CT forms a toroid which occupies the whole perimeter of the core, leaving only a small gap between start and finish leads for the insulation.

A reduction of the secondary winding by one or more turns is often used to compensate for small current error introduced by the magnetizing current component. The prospective secondary current is then slightly higher but is reduced by the current error due to the exciting component resulting in the actual current error being very small.

2.4 The Burden

Any device connected to the secondary winding is termed the burden of the CT usually expressed in volt-amperes (VA) or as impedance at rated secondary current and power factor.

All burdens are connected in series and increase in impedance increases the burden on the CT. Transformation errors are dependent on the angle and impedance of the

burden. Therefore, if the rated burden is p (VA) at rated secondary current I_s (A) then the ohms impedance of the burden is given by:

$$Z_b = \frac{P}{I_s^2} \text{ ohms} \quad (2.1)$$

And, with a burden power factor of $\cos \delta$ then the ohm resistance is.

$$R_b = Z_b \cos \delta \quad \text{ohms} \quad (2.2)$$

Moreover, the ohmic reactance would be:

$$X_b = (Z_b^2 - R_b^2)^{0.5} \quad \text{ohms, also,} \quad (2.3)$$

$$= Z_b \sin \delta \quad \text{ohms} \quad (2.4)$$

Precise terminology is required when defining burdens since a burden of constant (VA) is not the same as one of constant impedance Z_b . The error in the secondary current of a CT generally increases with the burden impedance. If the resistance component dominates in the impedance, the distortion increases in the secondary current. i.e. (resistive burden). Similarly, the phase angle error increases with a more dominant reactance in the impedance i.e. (reactive burden). The inductance in the burden impedance however reduces the distortion in the secondary current (ratio error) and vice versa for the phase angle error. As mentioned previously ratio errors may be compensated by the reduction of secondary winding turns, there is however no correction for phase error though usually small for a reactive burden [12].

2.5 Specification of Current Transformers

Protective CTs are specified in detail in BS 3938: 1982 [13]. In this specification they are defined in terms of rated burden, accuracy class and accuracy limit. Standard values of rated burden are 2.5, 5.0, 7.5, 10.0, 15.0 and 30.0 VA. Standard accuracy limit factors are 5, 10, 15, 20, and 30. Since protective equipment is intended to

function at current values above normal rating, current transformers used for this application must retain a reasonable accuracy up to the largest relevant current. The limits of error for class 5P and class 10 P are listed in Table 1. This classification is usually used for overcorrect protection schemes.

Table 2.1 The limits of error in 5P and 10P

| Class | Current error at rated primary current (%) | Phase displacement at rated current (minutes) | Composite error at rated accuracy limit primary current (%) |
|-------|--|---|---|
| 5P | ±1 | ±60 | 5 |
| 10P | ±3 | ±60 | 10 |

Design requirements for current transformers for general protective purposes are frequently specified in terms of knee-point emf, exciting current at knee-point (or some other specified points) and secondary winding resistance. Such current transformers are designated class x.

Table 2.2 Percentage of current error when the burden is 50 % to 100 % of rated burden.

| Class | ± Percentage current (ratio) error at percentage of rated current shown below | |
|-------|---|----|
| % | 50 | 20 |
| 3 | 3 | 3 |
| 5 | 5 | 5 |

For class 3 and class 5, the current error at rated frequency should not exceed the values given in Table 2, when the secondary burden is any value from 50% to 100% of the rated burden.

2.5.1 Short Time Factor

When a CT is used in a power system, it may be subjected to fault currents many times larger than its primary rating. The CT must be able to withstand the effects of these currents for which they are likely to persist. The maximum current, which the CT can carry without injury expressed as a multiple of its rated current is known as "short time factor". For example, a CT of ratio 200/5 which is capable of withstanding a current of 13000 amps would have a short-time factor of 65. Such a short time factor would always be associated with a period of duration of the current, for example, 2 seconds. Smaller currents would be permissible for longer periods, the permissible time increasing as the square of the reduction of current. Larger currents, however, are not necessarily permissible for any period, since electro-magnetic forces have also to be considered.

2.5.2 Accuracy Limit Factor

When a CT is used to energize a protective relay, it must maintain its characteristic ratio up to a current value of some multiple of its rated currents depending upon the characteristic of the protective system. This, multiple which may be 10,20 or some even higher value, has been named the "Accuracy limit factor".

It will be seen that even though the burden of a protective scheme is only a few VA at rated current, if the accuracy limit factor is high the output required from the CT may be considerable. On the other hand, the same CT may be subjected to an alternative condition of very high burden. For example, in the case of overcurrent and earth fault protection having elements of similar VA consumption at setting, if the overcurrent elements are set at 100%, an earth fault element set at 10% would have 10 times the impedance of the overcurrent elements. Although saturation of the relay elements modify this consideration somewhat, it will be seen that the earth fault element is a increment of magnetizing current 50%. Design requirements for current

transformers for general protective purposes are frequently laid out in terms of knee-point emf magnetizing current at the knee-point or alternatively at some other specified point and secondary impedance.

2.6 Effects of Frequency

For a given current and a fixed burden impedance, the flux density decreases with increase in frequency. This is in effect reducing the magnetizing and core-loss components of the primary current of the CT. In practice, most burdens are inductive so that its impedance and phase angle both increase with frequency. These have the adverse effect of increasing the errors due to the increase of the magnetizing and core-loss components. Harmonics in the primary current waveform has a similar effect as an increase in frequency. Their effect on accuracy is usually quite negligible unless it reaches abnormal proportions

2.7 Errors

Errors arise because of the shunting of the burden by the exciting impedance. This uses a small proportion of the input current for exciting the core thus reducing the amount passed to the burden. Reference is made to Section 2.1.9, Fig.2.1, $I_s = I_p - I_e$ where I_e (the magnetizing current) is dependent on the secondary emf, I_s is the actual secondary current and I_p is the primary current referred to the secondary side.

Current or ratio error is the difference in magnitude between I_p and I_s and is equal to I_e , the component of the I_e which is in phase with I_s .

Where, I_q is the component of I_e in quadrature with I_s , results in the phase error θ but as mentioned previously for moderately inductive burdens with I_p and I_e approximately in phase, there will be little phase error and the exciting component will result almost entirely in current error.

Composite error is defined as the rms value of the difference between the ideal secondary current and the actual secondary current, which also includes current and

phase errors, and the effects of harmonics in the exciting current. In practice, the exciting impedance is non-linear, leading to some harmonics in the exciting current, which increases its rms value and thus increasing the composite error. This effect is more noticeable when the core goes into saturation.

2.8 Open-Circuit Secondary Voltage

The secondary circuit of a CT must never be broken with the primary current flowing. Most CT has a shorting link across its secondary terminals for removal the secondary circuit when necessary.

With the secondary circuit open, the entire primary acts on the core as a magnetizing quantity since there is no opposing mmf in the secondary. The core is driven into saturation on each half wave and the high rate of change of flux while the primary current passes zero induces a high peak emf in the secondary winding.

Emf produced may be a few hundred volts for a small CT of several kilovolts for a large, high ratio protective CT with rated primary current flowing.

However, with system fault current flowing, the voltage would be raised in nearly proportion to the current value. Such voltages are dangerous especially to personnel who might be working in the vicinity including damages to the insulation, overheating of the CT, and connected apparatus.

2.9 CT Operation

The equivalent circuit of a CT is shown in Fig.2.1. The primary resistance, primary leakage inductance and secondary leakage inductance have been neglected since they are very small.

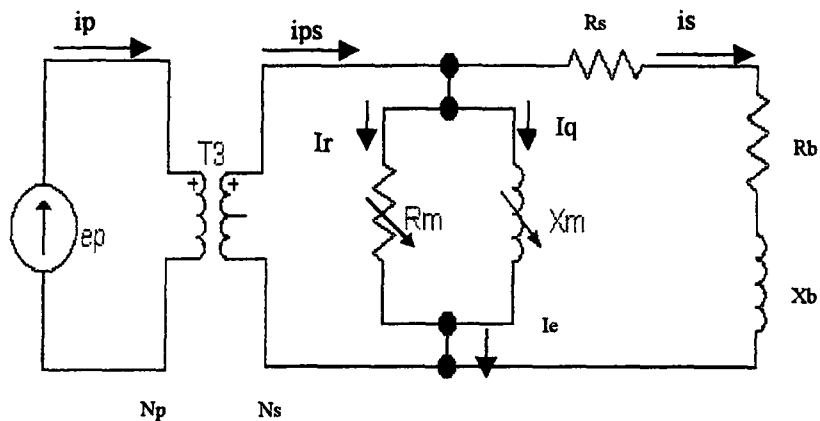


Figure 2.1 Equivalent circuit of a CT

Where;

i_p = primary current

i_{ps} = primary current referred to the secondary

i_s = secondary current

i_e = magnetizing current

R_s = secondary winding resistance

R_b, X_b = burden impedance

R_m, X_m = magnetizing impedance

e_p = applied primary voltage

Also,

$$i_{ps} = i_p N_p / N_s$$

Where;

N_p = number of primary turns

N_s = number of secondary turns

Lead resistance and secondary winding inductance are included in the burden impedance.

When a vector diagram of the CT is drawn, the ratio error, which is the difference in magnitude of I_p and I_s and θ , the phase angle error can be seen as in Fig.2.2

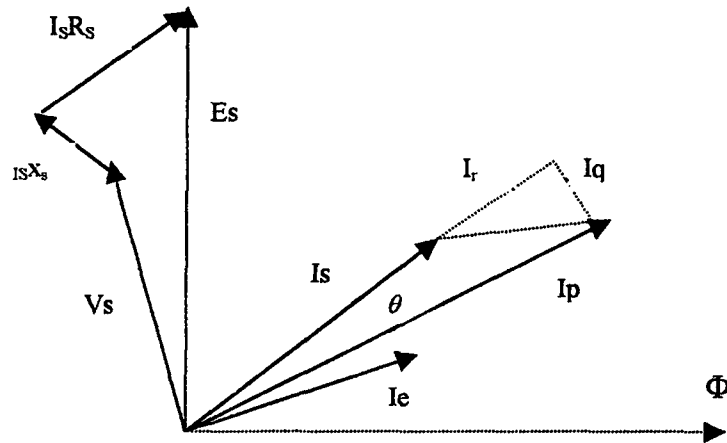


Figure 2.2 Vector diagram of the CT

Where;

I_p = primary current

I_s = secondary current

E_s = secondary induced emf

V_s = secondary output voltage

θ = Phase angle error

$I_s R_s$ = secondary resistance voltage drop

$I_s X_s$ = secondary reactance voltage drop

I_s = exciting current

I_r = component of I_s in the phase with I_s

I_q = component of I_s in quadratur with I_s

Φ = flux

It can also be seen from the vector diagram of Fig.2.2 that if the burden was wholly resistive then the ratio error would be a minimum and phase-angle error maximum, whereas if the burden was wholly reactive then the ratio error would be maximum and phase-angle error minimum.

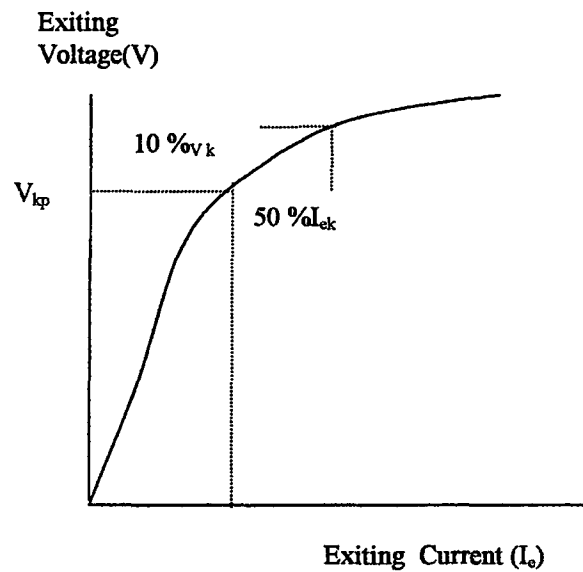


Fig.2.3 Magnetizing characteristic for a current transformer

Where,

V_{kp} = knee-point voltage

i_o = current at which magnetization curve departs from air-gap line

2.10 Other Types of Current Transformers

- Summation current transformers have a winding arrangement to give a single-phase output signal having a specific relationship to the three-phase current input normally used in a measuring or on an auxiliary CT.
- Quadrature or Air-gap current transformers are made with an air gap so that most primary ampere-turns are used to magnetize the core. The secondary voltage is proportional to the rate of change of flux and therefore lags the primary current by 90 degrees.
- Core-balance current transformers have split cores and are normally mounted over a cable at a point close to the switchgear or other apparatus. They are of ring

type where the cable is passed through the center for earth fault protection schemes, advantage being only one CT core is used in place of three phase current transformers are optimizing the effective primary pick-up current.

- Over dimensioned current transformers are in general extremely bulky and make large demands on the mounting space available in CT housings. However, they possess the most faithful transformation of all continuous core current transformers but are prone to remnant core flux caused by previous heavy current conditions, which may have detrimental effects on following measurements.
- Anti-remenance current transformers are a variation of the over dimensional class of current transformers but have small gap(s) in the core magnetic circuit, thus reducing the possible remnant flux. Errors in current transformation are thereby significantly reduced when compared with the gapless types.
- Separately mounted current transformers are freestanding units when bushings are not available to mount these EHV current transformers. Primary is bent into an elongated U-form and is contained winding and core are mounted on the lower part of the U and several cores and secondary windings for separate functions are provided on the one primary conductor

Conclusions

Throughout this chapter, fundamental characteristics of current transformers were detailed. The concepts short time factor and accuracy limit factor were explained. The factors effecting CT performance under fault conditions, which are core material, load parameters and the effect of frequency were examined.

The specifications of current transformers, rated burden, accuracy class and accuracy limit were also detailed. The CT operation was explained in detail.

CHAPTER 3

MODELING OF MAGNETIZATION CHARACTERISTICS

Introduction

The dynamic and transient responses of power system circuits are usually simulated using digital computers. Circuits containing magnetic material can only be approximately analysed if all the circuit components are represented mathematically.

The transient analysis of a protective scheme may be achieved if the transient response of CT used in the system is known. The behaviour of a CT depends mainly on its core which has non-linear flux density-field strength characteristics. Accurate determination of a protective CT performance therefore depends on the accuracy of flux variation with respect to the magnetic field strength.

For many years, there have been several attempts to represent the magnetic nature of iron cored inductors and transformers mathematically. The main problem in such exercises is the representation of the iron core. To do this would require an understanding of the magnetic properties of soft iron.

3.1 Magnetic Properties of Soft Iron

It has been observed and widely reported that unmagnetized soft iron sheets contain several magnetic domains separated by domain walls. Within a domain, the atoms have identical directional spins. Figure 3.1 shows the domain pattern of a single crystal of iron +3.8% silicon [14].

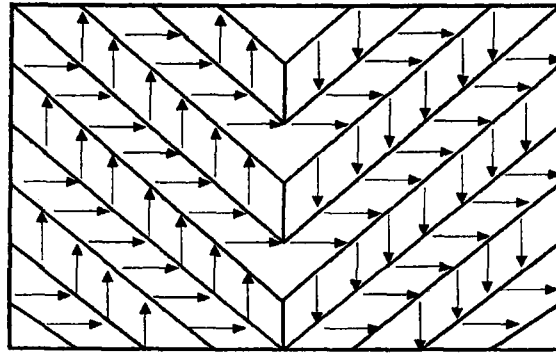
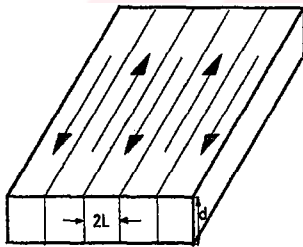


Figure 3.1 Domain pattern of single crystal of iron +3.8 % silicon

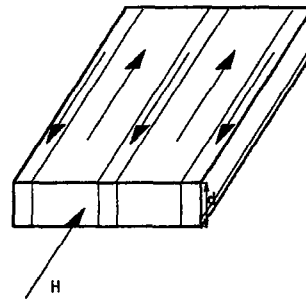
The fundamental domain structure of grain oriented silicon iron is very simple and widely reported [15,16,17]. It consists of equal width parallel 180° domains that are in line with the rolling direction (Figure 3.2.a). In an unmagnetized specimen, the domains are oriented in different directions the net magnetisation being zero. If a magnetic field H is applied, there is a small rotation of magnetisation within the domain an overall magnetisation in the direction of H (Figure 3.2.b).



(a) Unmagnetized

d- width of sheet

2L- width of domain



(b) Partially Magnetised

Figure 3.2 Domain walls in a sheet of grain oriented silicon iron

Figure 3.3 shows the variation of magnetisation with applied field. Along AB, the main contribution of magnetisation is movement of domain walls. If the applied

field is gradually reduced, the original path is retraced, i.e. BA. Beyond B, removal of the field does not return the magnetisation to zero and therefore could result in remanent condition. Beyond C, magnetisation results mainly from rotation of domains, thereby resulting in a complete alignment of the domains with respect to the applied field.

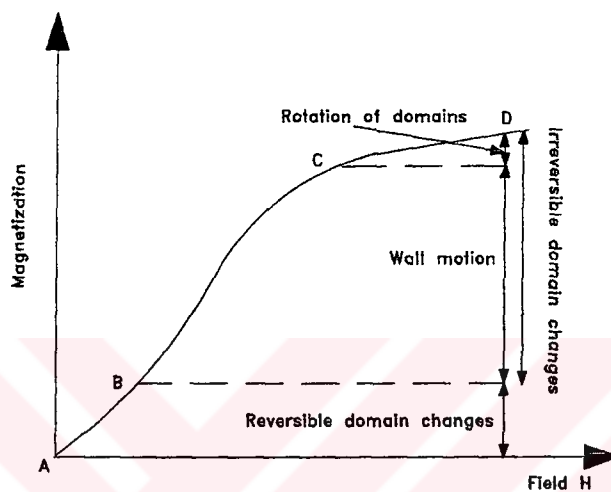
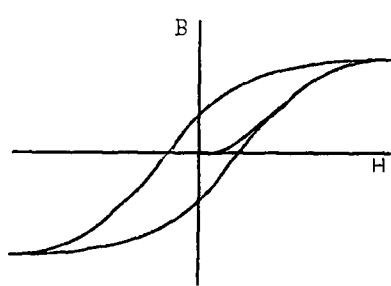


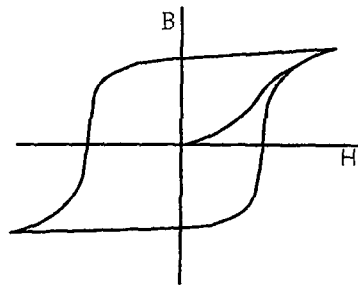
Figure 3.3 Variation of magnetisation with applied field.

3.2 B-H Loops of Hard and Soft Magnetic Materials (Iron)

Hard magnetic materials are usually more difficult to magnetise. They require a greater magnetising force. Also, they retain their magnetism much longer after the magnetising field is removed. Consequently, their B-H loops are larger and more square compared to those of soft magnetic materials. They are mostly used for production of permanent magnets. B-H loops of soft magnetic materials are smaller and inclined. Figure 3.4 shows the relative differences between typical soft and hard magnetic materials.



(a) Soft magnetic material



(b) Hard magnetic material

Figure 3.4 B-H loops of soft and hard magnetic material

If an unmagnetized ferromagnetic material is placed in a magnetic field and the field is varied from minimum to maximum, and from the maximum value in the previous direction to the maximum value in the opposite direction over a complete cycle, the graph of the flux density (B) in the material against the field strength (H) is shown in Figure 3.5. This is well known hysteresis loop.

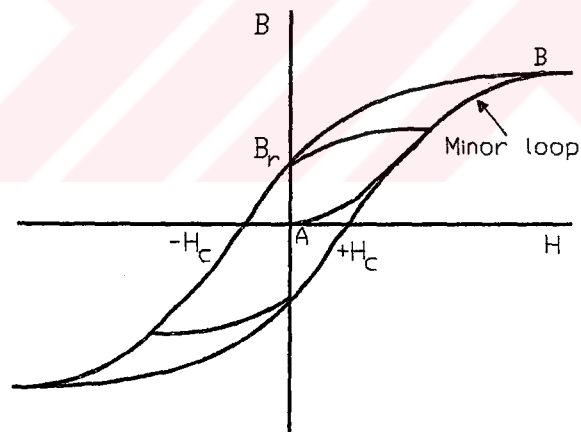


Figure 3.5 Hysteresis loop for ferromagnetic materials

The initial magnetisation region is AB. B_r is the remnant flux density in zero field while H_c is the coercive force required to reduce the remnant flux to zero. This shape of the hysteresis loop and its size vary for different ferromagnetic materials.

Work is done in taking the specimen round the hysteresis loop by the applied field. The area enclosed by the loop is called hysteresis loss and is usually dissipated as heat in the core.

3.3 Mathematical Representation of B/H Characteristics

There are a considerable number of mathematical equations to represent the B/H characteristic of a ferromagnetic core. These characteristics can be categorised into single valued and multivalued B/H characteristics.

3.3.1 Single valued characteristics

The points on the magnetisation curve generated by both increasing and decreasing the magnetisation coincide for a given intensity of magnetisation. Both increasing and decreasing magnetisation curves pass through the origin.

Macfadyen et al [18] used an exponential model to express the relationship between flux density in the magnetic material and the field strength. Consider the B/H characteristic shown in Figure 3.6. The basic principle is expressed by equation 3.1.

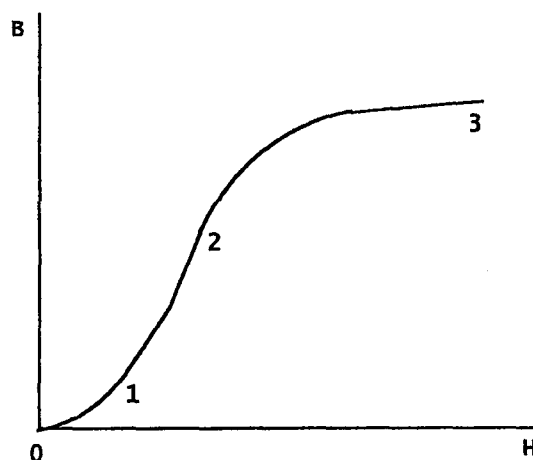


Figure 3.6 B/H characteristic of magnetic material.

The region 0-1 is represented by:

$$B = k_1(1 - \exp(D_1 H)) + k_2 H \exp(-D_2 H) \quad (3.1)$$

Beyond 1, The effect of the second term of the equation 3.1 almost vanishes resulting in the characteristic represented by equation 3.2 .

$$B = k_1(1 - \exp(D_1 H)) \quad (3.2)$$

Beyond 2, saturation of the material is achieved. The exponential in equation 3.2 vanishes. A new term $\mu_0 H$ is introduced to represent this saturation. The general equation for the characteristic over the whole range is therefore given by:

$$B = \sum_{i=1}^n k_i(1 - \exp(D_i H)) + k_{n+1} H \exp(-D_{n+1} H) + \mu_0 H \quad (3.3)$$

Where k_i and D_i are constant coefficients determined by iterative process from a set of observed points. Accuracy of the model is improved by increasing the number of exponential terms.

A model developed by Shimatani and Fujita [19] is similar to the Macfadyen et al model described earlier. However, use of this model is based on knowledge of the physical properties of the core material. It is generally expressed in the form:

$$B = K_1(1 + \exp(-K_2 H)) - K_3 H(-K_4 H^m) + \mu_0 H \quad (3.4)$$

Where K_1, K_2, K_3, K_4 and m are constants.

Representing the model in Φ / I form gives,

$$\Phi = A \left[K_1 \left(1 + \exp \left(-K_2 \frac{NI}{l} \right) \right) - K_3 \frac{NI}{l} \exp \left(-K_4 \left(\frac{NI}{l} \right)^m \right) + \mu_0 \frac{NI}{l} \right] \quad (3.5)$$

Where,

l is the average length of the core,

N is the number of secondary turns,

A is the cross section area of the core.

Krishnamoorthy and Venugopa[20] proposed a similar model where the magnetising current is the independent variable while the core flux is the dependent variable. The general equation for this model is of the form:

$$\Phi = C_1 i_m + C_2 \left(1 - \exp(-C_3 i_m) \right) \quad (3.6)$$

C_1, C_2 and C_3 are constant coefficients which are usually calculated by the least square error method from a set of observed points.

Idoniboyeobu [11] improved Krishnamoorthy and Venugopal's model by inserting two more exponential terms into the equation 3.6.

Prusty et al [21] proposed a model described in terms of a polynomial which is completely different from earlier described exponential models. The variation of magnetising current with respect to the core flux is an odd polynomial function.

The general equation for this model is of the form:

$$i_m = C_1 \Phi + C_3 \Phi^3 + C_5 \Phi^5 \dots \dots \dots C_n \Phi^n \quad (3.7)$$

where n is an odd integer and $C_1, C_3, \dots \dots \dots C_n$ are constants.

In many cases, a two term approximation is sufficient, that is:

$$i_m = C_1\Phi + C_n\Phi^n \quad (3.8)$$

Where $n=5,7,9,11$ etc.

Constants in equations 3-7 and 3-8 can be determined by the use of observed data points and least square error technique.

3.3.2. Multivalued characteristics

The magnetic properties of iron indicate that the path followed by the magnetisation curve when an iron core is continuously being magnetised is different from that followed when the magnetising signal is gradually reduced after reaching a particular level. That is, the path followed during demagnetisation is not same as that originally followed during magnetisation. The B/H characteristic of an iron core is therefore multivalued.

O'Kelly [22] was brought forward multivalued exponential model. In this model, the flux is defined by three parameters, viz., μ , slope of the magnetisation characteristic, W , width of the hysteresis effect and T , the exponential coefficient of the hysteresis effect (Figure 3.7). O'Kelly's linear model is of the form:

$$[H - B / \mu - W] = -2W \exp\left[-(B - B_d) / T\right] \quad (3.9)$$

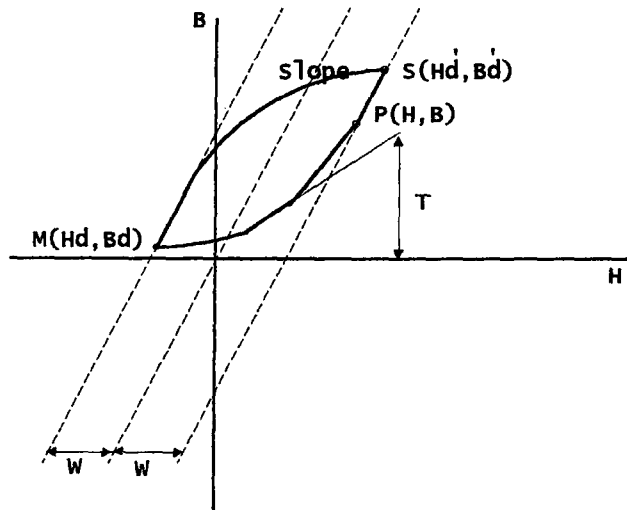


Figure 3.7 B/H characteristic.

for increasing values of H , where B_d, H_d are the co-ordinates of the initial point of the exponential. For decreasing values of H , the equation is given by:

$$[H - B / \mu + W] = 2W \exp\left[-(B'_d - B) / T\right] \quad (3.10)$$

Where B'_d and H'_d are the co-ordinates of the initial point of the decreasing exponential. Considering any point between M and S , say $P(H, B)$ with known values of H and B , the initial point of the exponential B_d and hence H_d can be computed by substituting the known values in equation (3.9)

Refinement of the linear model is carried out to obtain a more accurate representation, viz., non-linear model. Saturation is included by defining the central characteristic to have a non-linear relationship for magnetising force in terms of flux density, i.e. $H_k(B)$. The general non-linear model therefore takes the form

$$\left[H - H_k(B) - W(B) \right] = -2W(B) \exp \left[- (B - B_d) / T(B_d) \right] \quad (3.11)$$

for increasing H

$$\left[H - H_k(B) + W(B) \right] = 2W(B) \exp \left[- (B'_d - B) / T(B'_d) \right] \quad (3.12)$$

for decreasing H.

Figure 3.8 shows the basic non-linear model.

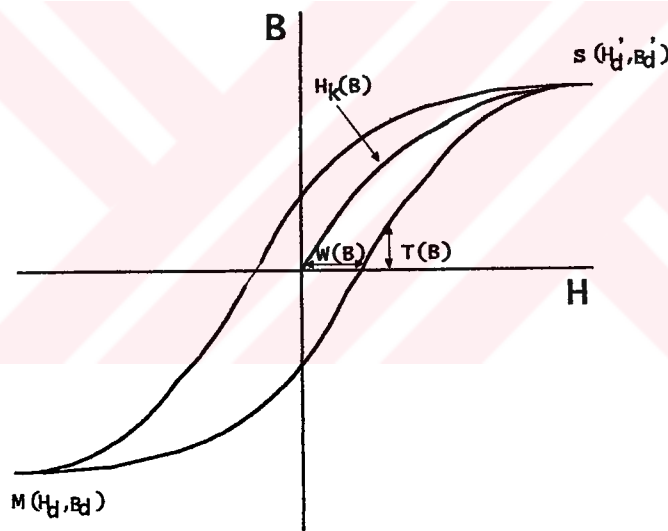


Figure 3.8 B/H characteristic: Non-linear model.

C.E.Lin [23] et al proposed a new method for representation of hysteresis loop. The dynamic hysteresis loop in iron core is composed of two symmetrical parts. The normal magnetising curve, as the first part marked by "aoc" in Figure 3.9, is the locus of the mid points of the hysteresis loop. This can be obtained by the measured hysteresis data. The loss part, as the second part marked by distances such as "ef" in Figure 3.9, represents loss in the hysteresis loop. It is also termed as the "consuming function" because the main part contributes proper shape and

area of the hysteresis loop. The distance "ef" changes periodically by a half wave symmetry. The periphery of the hysteresis loop is obtained by adding or subtracting the consuming function to the normal magnetising curve. Usually for modern transformers, the normal magnetising curve can be approximated by four line sections. The equations of these lines are:

$$i = (i_1 - m_1 \Phi_1) + m_1 \Phi, \quad \Phi_0 < |\Phi| \leq \Phi_1 \quad (3.13a)$$

$$i = (i_2 - m_2 \Phi_2) + m_2 \Phi, \quad \Phi_1 < |\Phi| \leq \Phi_2 \quad (3.13b)$$

$$i = (i_3 - m_3 \Phi_3) + m_3 \Phi, \quad \Phi_2 < |\Phi| \leq \Phi_3 \quad (3.13c)$$

$$i = (i_4 - m_4 \Phi_4) + m_4 \Phi, \quad \Phi_3 < |\Phi| \leq \Phi_4 \quad (3.13d)$$

Where,

$$\Phi = \Phi_m \text{Cos}(\omega t) \quad (3.14)$$

Subscripts 1,2,3 and 4 denote for the sampled points on Figure 3.10 and m is slope of the line sections. The nature of the function is a reverse function of the normal magnetising curve. It reaches maximum when the normal magnetising goes to zero, and vice versa. Hence the function can be represented by,

$$\begin{aligned} f(\Phi) &= D \left(\frac{d\Phi}{dt} \right) \\ &= -D\omega\Phi_m \text{Sin}(\omega t) \\ &= -Ob \text{Sin}(\omega t) \end{aligned} \quad (3.15)$$

Where D is a coefficient, and Ob is the maximum distance between the midpoint locus and the periphery of the hysteresis loop. The hysteresis loop is represented by combining equations 3.14 and 3.16. By fitting the four line sections into the normal magnetising curve, the periphery of the hysteresis loop turns out a composition of sixteen line sections. The mathematical expression for the hysteresis loop becomes:

$$i = (i_k - m_k \Phi_k) + m_k \Phi - Ob \sin(\omega t) \tag{3.16}$$

Where $\Phi_{k-1} < |\Phi| \leq \Phi_k$

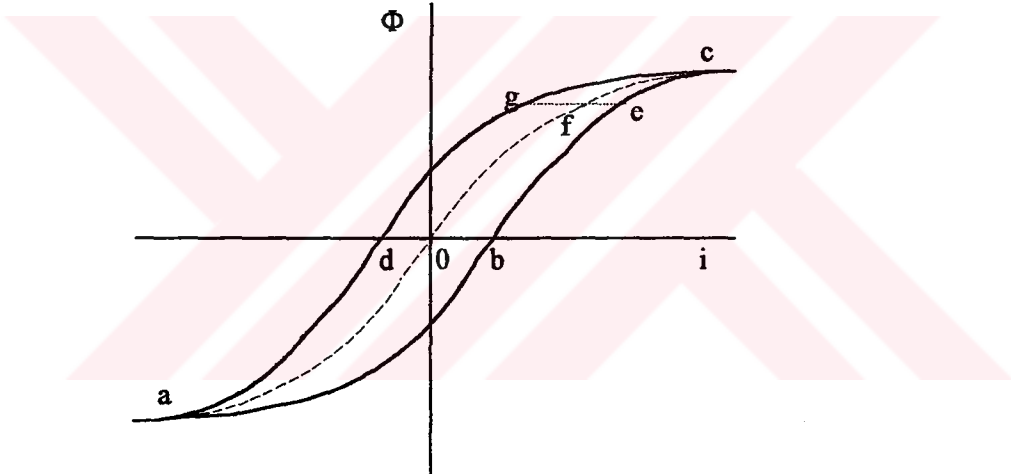


Figure 3-9 Simple hysteresis curve

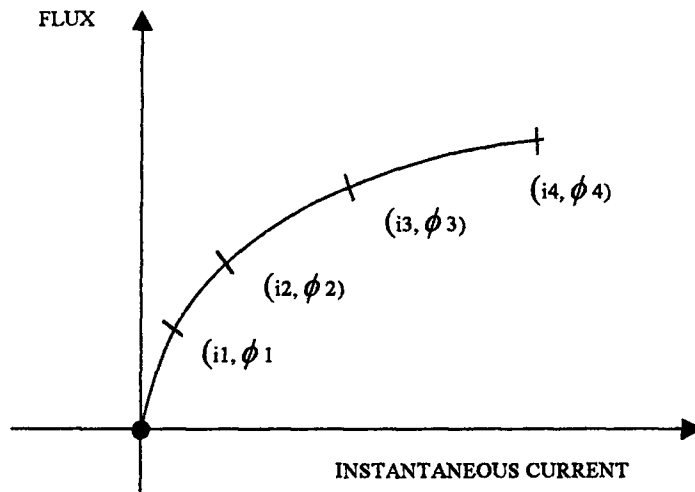


Figure 3-10 Approximated variation of normal magnetisation curve.

Hanalla-Macdonal's [24] approximation can be used to model the characteristics of a ferromagnetic core. For flux density/field strength characteristic, the flux density is considered the independent variable while the field strength is dependent variable.

Consider the relationship between sinusoidal voltage and current in a single series RL circuit, which is elliptical (Figure 3-11). The basic equation is

$$V = Ri + L \frac{di}{dt} \quad (3.17)$$

This loop has some characteristics of the hysteresis loop. The relationship between H and B for a ferromagnetic core material can be represented by:

$$H = \nu B + \xi \frac{dB}{dt} \quad (3.18)$$

Where,

$\nu = 1/\mu_r \mu_0$ is the core-reluctivity, analogous to the resistance and ξ analogous to the inductance.

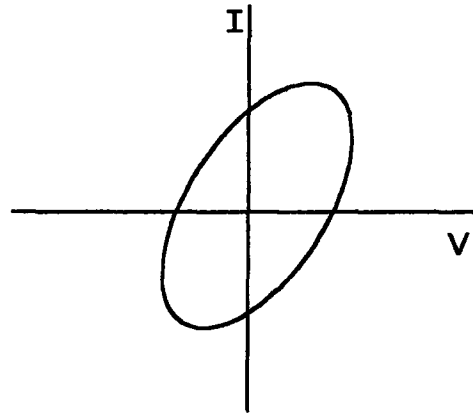


Figure 3.11 Voltage/current relationship of RL series circuit.

Improvement of the model is achieved by making ν dependent on B and expressing ξ as:

$$\xi = \alpha(T_1 - t_1)$$

Where,

α is the hysteresis parameter

T_1 , the time between last two occasions at which dB/dt changed its sign.

t_1 , the time since the last peak value B .

so,

$$H = \nu B + \alpha(T_1 - t_1) \frac{dB}{dt} \quad (3.19)$$

For sinusoidal excitation

$$B = B_m \cos \omega t$$

Where,

B_m is the sinusoidal value of the flux density wave.

Also for the sinusoidal excitation,

$$\alpha = \left(\frac{2}{\pi} \right) \frac{H_0}{B_m} \quad (3.20)$$

$$\text{and } f = \frac{1}{T} \quad ; \quad T_1 = \frac{\pi}{\omega}$$

where H_0 is the coercive force corresponding to the last peak of the flux density (B_m), and f is the frequency.

Substituting equation 3.20 in equation 3.19 gives:

$$H = \nu B_m \cos \omega t - \alpha \left(\frac{\pi}{\omega} - t_1 \right) B_m \omega \sin \omega t$$

$$H = \nu B_m \cos \omega t - 2H_0 \left(1 - \frac{2t_1}{T} \right) \sin \omega t \quad (3.21)$$

Where T is the periodic time.

A typical variation of the last peak value of the flux density (B_m) with the corresponding coercive force (H_0) for permalloy is shown in Figure 3.12. For accurate representation of the core characteristics, curve α' is used to represent

the hysteresis parameter in equation 3.19. However, a mean value α determined by straight line (Figure 3-12) was found satisfactory for most applications.

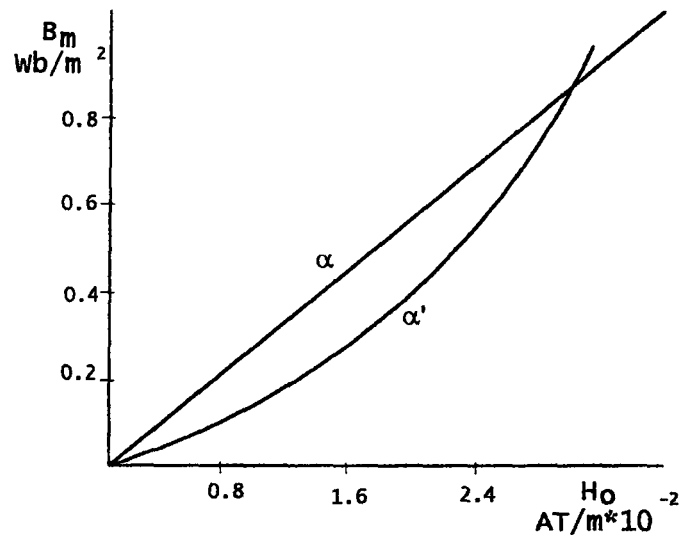


Figure 3.12 Variation of H_0 with B_m

Rivas et al [25] brought forward a rational fraction method. Here, the flux density in the core (B) is represented as a function of the magnetic field strength (H) and the intensity of magnetisation (M). The flux density-field strength curve is made up of auxiliary curves B_1 and B_2 , such that

$$B_1 = \frac{f_1 + f_2}{2} \quad (3.22)$$

$$B_2 = \frac{f_1 - f_2}{2} \quad (3.23)$$

Where f_1 and f_2 are the descending and ascending branches of the hysteresis loop respectively (Figure 3.13).

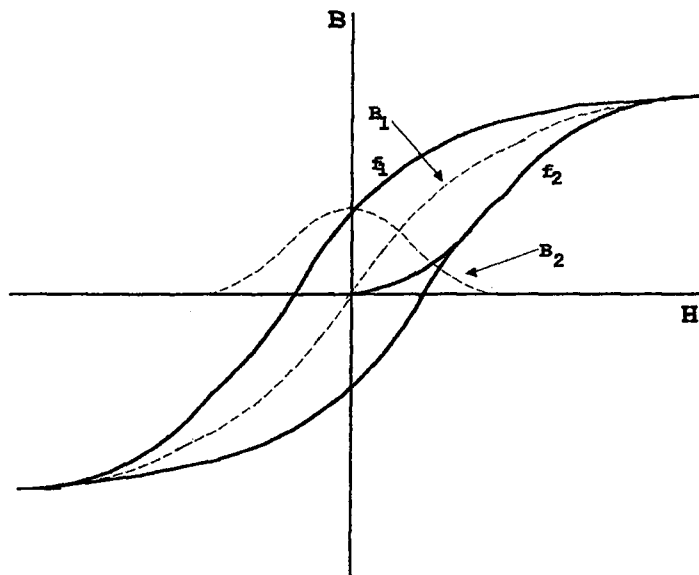


Figure 3.13 B/H characteristic of ferromagnetic core

$$B = B_1 \pm B_2 \quad (3.24)$$

Plus sign for descending portion and minus sign for ascending portion of the loop.

B_1 and B_2 are also defined in terms of the field strength.

$$B_1 = \mu_0 \left[H + \frac{a_1 H + a_2 H|H|}{1 + b_1 |H| + b_2 H^2} \right] \quad (3.25)$$

$$B_2 = \mu_0 \left[\frac{c_1 (H_m - |H|) + c_2 (H_m^2 - H^2)}{1 + b_1 |H| + b_2 H^2} \right] \quad (3.25)$$

The constants are evaluated as follows:

From equation 2.25, when $H = 0, B = B_R$ where B_R is the residual flux density

$$a_1' = \frac{1}{\mu_0} \frac{dB}{dH} - 1 \quad (3.27)$$

at point $H = H_m, B = B_m$ where H_m and B_m are maximum values of field strength and flux density respectively.

$$a_2' = \frac{B_m - \mu_0 H_m}{H_m^2} (1 + b_1 H_m + b_2 H_m^2) - \frac{a_1'}{H_m} \quad (3.28)$$

Where,

$$b_1 = \frac{\alpha \lambda + x}{M_s - \alpha x} \quad (3.29)$$

$$b_2 = \frac{\lambda M_s + x^2}{M_s (M_s - \alpha x)} \quad (3.30)$$

Parameters α, λ, x, M_s are constants as in reference [25]. These are usually supplied by the manufacturer.

For the B_2 curve, at $H = 0, B_2 = B_R, \frac{dB_2}{dH} = 0$

$$C_1 = \frac{b_1 B_R}{\mu_0} \quad (3.31)$$

and

$$C_2 = \frac{B_R}{\mu_0 H_m^2} (1 + b_1 H_m) \quad (3.32)$$

Macfadyen [26] et al model: The single term exponential series representation of magnetisation characteristic is found to be inadequate for representing both positive and negative values of H for multivalued magnetisation curve. Refinement of the single term representation gives:

$$B = K_1 (1 - \exp(-K_2 H)) / (1 + \exp(-K_0 H)) \quad (3.33)$$

Where,

K_1, K_2 and K_0 are constants.

This equation was found to be satisfactory, especially for the condition K_0 much greater than K_2 . In such a case the positive and negative regions are effectively represented as, $K_1 (1 - \exp(-K_2 H))$ and $(1 + \exp(-K_0 H))$ respectively.

The non-unique B/H relationship for magnetic materials may be considered as an infinite number of single-valued trajectories, or curves, which are bounded in the B/H plane by the limit cycle or outer hysteresis loop as shown in Figure 3.14.

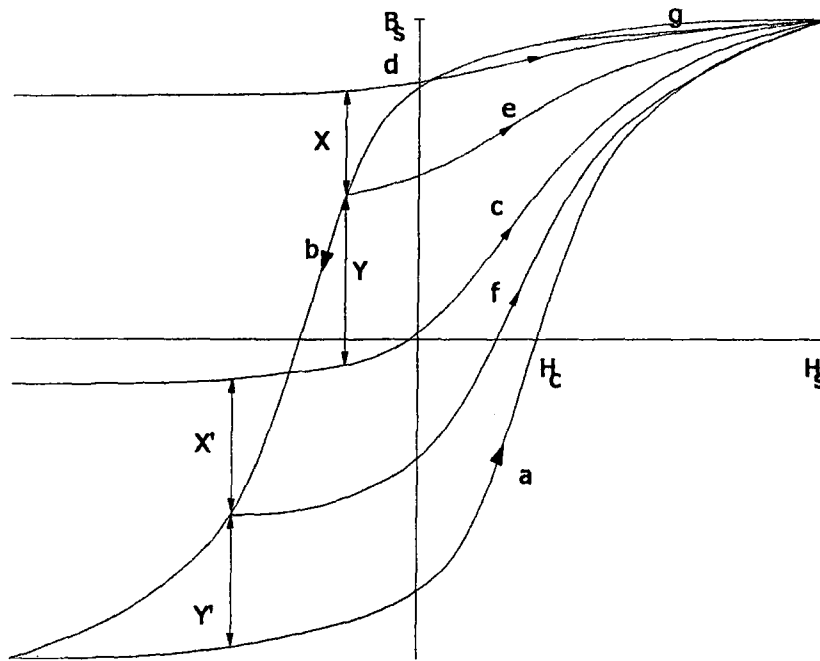


Figure 3.14 Multivalued characteristic of magnetisation curve

It is only necessary to represent the curves for H increasing positively, since in general, decreasing curves may be obtained by rotating the corresponding increasing characteristic by 180° about the origin. Trajectories (e) and (f) in Figure 3.14 are examples of increasing characteristics, all of which originate on the boundary curve (b) and pass through the positive saturation point, (H_s, B_s) . It is assumed that the increasing trajectories, and consequently the decreasing curves, do not intersect.

In order to be able to represent all increasing curves, an expression must initially be obtained for at least two curves in the plane, preferably curves (a) and (d). Any other curve can be evaluated knowing one point on the required trajectory defined by initial conditions or turning points in the B/H plane. The curve (c) may be expressed as,

$$B_c = (B_d - B_a) / 2 \quad (3.34)$$

Greater accuracy may be achieved by obtaining expression for intermediate curves such as curve (c). Thus if trajectories (a), (c), and (d) are explicitly defined, the expressions for characteristic (e) and (f) become,

$$B_c = B_c + (B_d - B_c) \frac{Y}{Y+X} \quad (3.35)$$

$$B_f = B_a + (B_c - B_a) \frac{Y'}{Y'+X'} \quad (3.36)$$

It is therefore possible to represent all curves in the B/H plane using equation 3.35 to obtain the characteristic lying above (c), and equation 3.36 for those below (c). The accuracy of representation of the generated curves can be improved by obtaining expressions for intermediate curves. A general exponential equation for the model is of the form:

$$B = B_0 + \mu_0(H - H_0) + \sum_{i=1}^n K_{2i-1} \frac{[1 - \exp(-K_{2i}(H - H_0))]}{[1 + \exp(-K_0(H - H_0))]} + \sum_{j=n+1}^m K_{2j-1} \frac{[1 - \exp(K_{2j}(H - H_0))]}{[1 + \exp(K_0(H - H_0))]} \quad (3.37)$$

Where (B_0, H_0) is the point of maximum gradient and K_0, K_1, \dots, K_{2j} are constants determined by iterative process using a set of observed data points. Two points from the curve being represented are required for each exponential term. The greater the number of exponential terms, the better the accuracy of the model.

Conclusions

The single valued and multivalued models were discussed. The multivalued models had a better accuracy for modelling core characteristic compared to the

single-valued models. Several multivalued models were highlighted, some of which were quite accurate. A brief comparison of these models will now be made.

The rational fraction method is mostly useful when the constants, initial magnetic susceptibility and saturation magnetisation are known. Its use is mainly limited to symmetrical excitation, which does not always apply to transient analysis. Another disadvantage is that minor loops are not represented in the model.

Hannalla's model gives errors within 5% of the maximum flux density. It is very easy to implement this model.

C.E. Lin et al methodology results in a very practical model. The error between simulation and experiment is within 2%. But minor loops are not represented in this model.

Accuracy achieved by the use of O'Kelly's model is 1.8% for the minor loops. For the major loops, error tends to be larger (10.5%). Due to the flexibility of this model, it can be easily adopted to model any type of core.

Macfadyen's exponential model yields an error of less than 1% for six term exponential representing the boundary curve. This model has not been used to analyze performance of a current transformer with the inclusion of positive and negative region of the curves. It has been used successfully by the authors to study the transient and steady-state behaviour of a single phase 1KVA 250V transformer

The hysteresis model we used in this thesis (Jiles Atherton Model) will be highlighted in detail within chapter 4 .

CHAPTER 4

THE JILES-ATHERTON MODEL

Introduction

In this chapter, the Jiles-Atherton Model will be examined in detail. First of all the physical background and some modifications and improvements in the model are going to be investigated. Moreover, the model equations are going to be derived. A computer sub-program will be written to solve the model equations. The 4th Order Implicite Runge Kutta Merson method will be used in solution of the model equations. The simulation results of the core model will be given and will be compared to the results given in reference 27.

4.1 The Jiles-Atherton Model

The mathematical model for ferromagnetic hysteresis introduced by Jiles and Atherton in 1983 [28] is based on physical principles, rather than strictly mathematical arguments or experimental curve fitting. Magnetization of a ferromagnet contains both reversible and irreversible process. As an example for reversible mechanism include bowing of the domain wall between positions where it is held by pinning sites, planar domain in regions free of pinning sites. Examples of irreversible magnetization mechanisms include discontinuous domain wall motion through pinning sites.

The magnetization in a ferromagnetic material is notated as M, the magnetic field intensity by H, and the magnetic flux density will be;

$$B = \mu_0(H+M) \quad (4.1)$$

And the effective flux density,

$$Be = \mu_0 (H + \alpha M) \quad (4.2)$$

The differential equation for M defined by J-A is

$$M = M_s \ell\left(\frac{Be}{a}\right) - \delta k \frac{dM}{dBe} \quad (4.3)$$

Where,

$$\ell(x) = \coth(x) - \frac{1}{x} \quad (4.4)$$

is known as Langevin Function (Appendix 2) and M_s , a and k are parameters of the model, and δ is the sign of the dH/dt . If the parameters a and k are constants or functions of Be only, then equation (4.3) is a non-homogeneous, first-order linear differential equation whose solution may be obtained by standard solution methods. The solution of the corresponding homogeneous equation is,

$$M_h = M_o \exp\left(-\delta \int_0^{Be} \frac{1}{k} dBe\right) \quad (4.5)$$

Where M_o is constant, then the complete solution is,

$$M = M_h + M_p \quad (4.6)$$

Where,

$$M_p = M_h \delta \int \frac{M_s \ell(Be/a)}{k M_s} \quad (4.7)$$

M_h and M_p must be calculated with the same value of δ , yielding two cases, one for $\delta=1$ and one for $\delta=-1$. If the parameters a and k are constants, then the solution for M_p can be obtained as a series by iteration in the differential equation as an alternative to solving the integrals in (4.6) and (4.7).

$$M_p(\text{Be}) = M_s \sum_{n=0}^{\infty} (-1)^n \left(\frac{k\delta}{a}\right)^n \ell^{(n)}\left(\frac{\text{Be}}{a}\right)^n \quad (4.8)$$

Where $\ell^{(n)}(x)$ is the nth derivative of the $\ell(x)$.

The solution for M as a function of Be given in (4.8) is only implicit solution for M in term of either B or H as the independent variable. But (4.3) may be restated with either H or B as the independent variable by eliminating the other two of Be, B and H by means of the defining equations for B and Be. These differential equations for dM/dH or dM/dB are more useful for direct numerical solution for M given H or B. The discussion here will continue to use Be as the independent variable to avoid complexity in the equations unnecessarily.

The functions for M obtained above in integral form or the corresponding functions would be obtained by the numerical solution of equation (3.3). The geometrical meaning of that integration is the major loop or outer hysteresis curve, is composed of the solutions for M_p for the two values of δ and M_h which gives the exponential approach of the initial magnetization curve to the major loop as Be increases. However if the direction of dH/dt is reversed or in other words δ changed from 1 to -1.

4.1.1 The experimental technique

There are many experimental techniques for J-A model for magnetization. The Atherton and Schonbachler technique is as follows; the measurement has all been made on a sample of one-percent manganese pipeline steel in a standard laboratory electromagnet. System reversible (backward) differential magnetization components as distinct from the total (forward) differential magnetization are obtained by small field reversals. Provided that sufficiently small field reversals are used, these minor loops show negligible hysteresis and their slope therefore gives the reversible permeability. The numerous magnetization cycles are all performed under microcomputer control, which is also used to log all data. This has upgraded with Zenith 150 PC and Tecmar. Master data acquisition system and the elimination of the

use of an X-Y recorder during the normal using favor fully automatic data recording and subsequent outputting on a digital plotter. Computer control is essential to obtain consistent demagnetization's and to obtain anhysteretic points as efficiently as possible to minimize the effects of drift in the integrating flux meter even so anhysteretic curves take several hours to measure.

The other experimental process improved by Y.Bi and D.C.Jiles [29] in September 1999. The chosen material was a Mn-Zn ferrite in the form of a toroid with an outer diameter of 14.4 mm an inner diameter of 6.5 mm and a length of 28.4 mm. The AC excitation field was applied along the circumferential direction by a 12-turn toroidally wound coil and the flux density was measured along the same direction by a 10 turn toroidally wound coil. This field is perpendicular to the AC excitation field everywhere in the material. The toroidal structure of the specimen (Mn-Zn) allowed the internal magnetic field to be calculated from the excitation current by using Ampere's law. Hysteresis measurements were made using an AMH-401 hysteresisgraph from Walker Scientific Inc. A Hall sensor at the center of the solenoid measured the axial applied orthogonal field.

4.2 The Modified J-A Model

J-A theory was developed as an attempt to create a quantitative model of hysteresis based on a macromagnetic formulation. The model describes isotropic polycrystalline materials (multidomain grains) with domain wall motion as the major magnetization process. The theory begins with the development of an equation for the anhysteretic curve using a mean field approach as follows. [30]

The energy per unit volume E of a typical domain with magnetic moments per unit volume m and an internal magnetic field H is,

$$E = -\mu_0 mH \quad (4.9)$$

The total energy of the ferromagnetic solid must also consider the coupling between domains. This can be most easily expressed by;

$$E = -\mu_0 M H_e \quad (4.10)$$

Where,

$$H_e = H + \alpha M \quad (4.11)$$

Where, α is an experimentally determined mean field parameter representing interdomain coupling. The response of the magnetization, in the direction of the applied field, to this effective field may be written as.

$$M_{an} = M_s f(H_e) \quad (4.12)$$

Where f is an arbitrary function that takes the value zero when H_e is zero and one when H_e goes to infinity. M_s is the saturation value. Jiles and Atherton derived, for the case of an isotropic ferromagnet, a function that obeys these criteria, namely a modified Langevin function,

$$M_{an} = M_s \left[\coth\left(\frac{H_e}{a}\right) - \left(\frac{a}{H_e}\right) \right] \quad (4.13)$$

Substituting equation 4.11 into 4.13 we have,

$$M_{an} = M_s \left[\coth\left(\frac{H + \alpha M}{a}\right) - \left(\frac{a}{H + \alpha M}\right) \right] \quad (4.14)$$

Where,

M_{an} is anhysteretic magnetization (Represents global minimum energy state at a given field H .) and a is a constant with dimensions of magnetic field.

Calculated hysteresis loops, based on this function, are shown for various values of α . At this stage hysteresis is introduced only by means of interaction through the parameter a . When a is small, M is single valued. This therefore leads to an expression that may represent the anhysteretic curve. A sufficiently high value of a

is able to generate a hysteresis loop but gives spontaneous magnetization. The general shapes of these loops caused by interaction are however always very sharp with most vertical sides.

Hysteresis resulting from strong interaction between domains is not appropriate for modeling the smoother loops, measured on soft materials. The J-A model can be made more realistic by considering the frictional effects during domain wall displacement. Frictional forces are due to pinning of domain walls by defect sites at dislocations, impurities, grain boundaries, etc., inside the ferromagnet, which cause opposing forces resisting any changes in magnetization. Hence, for this purpose, an additional energy term is introduced. It represents the energy lost by the pinning and unpinning of the wall.

The pinning sites are considered to all have the same energy and to be uniformly distributed. Suppose the pinning energy per unit volume for a given pinning site is ε_p . If there are n pinning sites per unit volume the energy lost by moving a 180 domain of surface area A through a distance dx is,

$$dE_p = \mu_0 n \varepsilon_p A dx \quad (4.15)$$

While the change of magnetic moment will be

$$dM = 2MsAdx \quad (4.16)$$

Then for the volume distribution of pinning sites dE_p is proportional to the magnetic moment change. Hence

$$dE_p = kdM \quad (4.17)$$

Where k is a micro structural parameter proportional to the pinning site density and to pinning site energy. It is taken to be constant here. Of course if $k=0$, there is no pinning and the domain walls can move freely. Isotropy is assumed in this model and if a , the interaction parameter, is also small which is true for soft ferromagnetic

materials then the curve is the single-valued curve given by (4.13). Hysteresis has been eliminated, so this is the anhysteretic curve that represents the global thermodynamic equilibrium state.

The energy of the material is then equal to the energy supplied to the material if it were anhysteretic, reduced by the energy lost in overcoming the pinning sites, so the energy balance becomes

$$\mu_0 \int M_{irr} dH = \mu_0 \int M_{an} dH - \mu_0 \int k d(M_{irr}/dH)dH \quad (4.18)$$

This equation describes only irreversible magnetization changes M_{irr} . A reversible magnetization component due to reversible domain wall bowing of a supposedly flexible wall and reversible rotation needs to be added. This has the form where c is a constant Hence the total magnetization is

$$M_{rev} = c(M_{an} - M_{irr}) \quad (4.19)$$

$$M = M_{rev} + M_{irr} \quad (4.20)$$

The model is then defined by the following equations:

$$\frac{dM_{irr}}{dH} = \frac{M_{an} - M_{irr}}{\delta k - \alpha(M_{an} - M_{irr})} \quad (4.21)$$

$$\frac{dM_{rev}}{dH} = c \left(\frac{dM_{an}}{dH} - \frac{dM_{irr}}{dH} \right) \quad (4.22)$$

$$\frac{dM}{dH} = \frac{dM_{irr}}{dH} + \frac{dM_{rev}}{dH} \quad (4.23)$$

Where,

$$\delta \text{ is sign of } \frac{dH}{dt} \quad (\delta = 1 \text{ if } \frac{dH}{dt} > 0 \text{ and } \delta = -1 \text{ if } \frac{dH}{dt} < 0)$$

Major or minor loops are obtained depending on the integration constants defined by the initial and final values to be reached on the curve. Hence, this model uses five different equations (4.19 through 4.23) together with An hysteretic Magnetization, M_{an} , (represented by Modified Langevin Function, (see Appendix 2) and five different physical parameters given below which obtained experimentally.

(M_s), the saturation magnetization,

(k), the pinning coefficient,

(α), Mean field parameter representing inter-domain coupling.

(a), parameter which characterizes the shape of anhysteretic curve.

(c), defines the reversible magnetization component.

Table 4.1 Effects of parameters on model [31]

| | |
|-------|--|
| Alpha | Increased value leads to steeper slopes for anhysteretic and magnetization curves. |
| a | Increased value decreases slope of M_{an} . |
| k | Increased value produces wider hysteresis curve. |
| c | Decrease in value leads to wider hysteresis curve. |
| M_s | Increase leads to large saturation value for magnetization. |

Assuming a uniform distribution of pinning sites and treating each one as having the mean pinning energy, the total work done against pinning is proportional to the change in magnetization. By manipulation of the equations obtained based on this concept, Jiles and Atherton have shown that, irreversible susceptibility can be expressed as in the equation (4.1)

$$\frac{dM_{irr}}{dH} = \frac{(M_{an} - M_{irr})}{\delta k - \alpha(M_{an} - M_{irr})}$$

Where, M_{irr} is Irreversible magnetization,

Considering bulging of domain walls due to displacement of magnetization from the anhysteretic, and assuming that a domain wall bisects a spherical grain boundary, Jiles and Atherton have shown that M_{rev} can be expressed in the form. [32]

$$\frac{dM_{rev}}{dH} = c \left(\frac{dM_{an}}{dH} - \frac{dM_{irr}}{dH} \right)$$

Where, M_{rev} is Reversible magnetization.

Summation and rearrangement of Reversible and Irreversible Differential Susceptibilities gives the Total Differential Susceptibility. From equations 4.19 and 4.22 we have Total Differential Susceptibility as follows.

$$\frac{dM}{dH} = (1 - c) \frac{M_{an} - M_{irr}}{\delta k - \alpha(M_{an} - M_{irr})} + c \frac{dM_{an}}{dH} \quad (4.24)$$

Since the Total Differential Susceptibility given in equation (4.23) includes three variables (H , M , M_{irr}) it is difficult to take the derivative $\frac{dM}{dH}$. To overcome this problem two approximations have been used to simplify the equation.

H.G. Brachtendorf and R.Laur [32] used one of them. They expressed that “The rate of change of the irreversible part of magnetization M_{irr} is approximately proportional to the distance of the total magnetization to an equilibrium state which is called anhysteretic magnetization M_{an} ”.

They have given the equations in the form;

$$\frac{dM_{irr}}{dH} = \frac{M_{an} - M}{\delta k - \alpha(M_{an} - M)} \quad (4.25)$$

$$\frac{dM_{rev}}{dH} = c \left(\frac{dM_{an}}{dH} - \frac{dM_{irr}}{dH} \right) \quad (4.26)$$

By substituting the new equations, we obtain the Total differential susceptibility in the form.

$$\frac{dM}{dH} = (1-c) \frac{(M_{an} - M)}{\delta k - \alpha(M_{an} - M)} + c \frac{dM_{an}}{dH} \quad (4.27)$$

Taking derivative of M_{an} with respect to (H) we have,

$$\begin{aligned} \frac{dM_{an}}{dH} &= M_s \left\{ -\frac{1}{a} \operatorname{cosec}^2 \left(\frac{H + \alpha M}{a} \right) \left(1 + \alpha \frac{dM}{dH} \right) + \frac{(1 + \alpha \frac{dM}{dH}) a}{(H + \alpha M)^2} \right\} \\ &= M_s \left(1 + \alpha \frac{dM}{dH} \right) \left\{ -\frac{1}{a} \operatorname{cosec}^2 \left(\frac{H + \alpha M}{a} \right) + \frac{a}{(H + \alpha M)^2} \right\} \end{aligned} \quad (4.28)$$

Substituting equation (4.28) into (4.27) we obtain;

$$\frac{dM}{dH} = (1-c) \frac{(M_{an} - M)}{\delta k - \alpha(M_{an} - M)} + M_s \left(1 + \alpha \frac{dM}{dH} \right) \left\{ -\frac{1}{a} \operatorname{cosec}^2 \left(\frac{H + \alpha M}{a} \right) + \frac{a}{(H + \alpha M)^2} \right\}$$

Moreover, rearranging we get the total differential susceptibility in the most general form.

$$\begin{aligned} \frac{dM}{dH} &= \left\{ (1-c) \frac{(M_{an} - M)}{\delta k - \alpha(M_{an} - M)} + c \left(-\frac{1}{a} \operatorname{cosec}^2 \left(\frac{H + \alpha M}{a} \right) + \frac{a}{(H + \alpha M)^2} \right) \right\} / \\ &M_s c \alpha \left(-\frac{1}{a} \operatorname{cosec}^2 \left(\frac{H + \alpha M}{a} \right) + \frac{a}{(H + \alpha M)^2} \right) \end{aligned} \quad (4.29)$$

And since from equation 4.1,

$$B = \mu_0(H+M)$$

$$\frac{dB}{dH} = \mu_0 \left(1 + \frac{dM}{dH}\right) \quad (4.30)$$

By solving equations, 4.29, 4.30 and 4.31 by the numerical method mentioned before,

H, M, B, $\frac{dM}{dH}$ and $\frac{dB}{dH}$ values can be calculated.

We used the form given in equation (4.29) in our work. Using Fourth Order Runge Kutta Method and writing a computer program, we solved the equation (4.29). (See Runge Kutta (Merson) Method in appendix 1)

Other approach used by R.P. Jayasinghe and P.G. McLaren [33] they used Reversible Magnetization as follows,

$$M_{rev} = c(M_{an} - M) \quad (4.31)$$

This is slightly different from equation (4.19)

From equation (4.19) and (4.20) we obtain;

$$M = (M_{irr} + c(M_{an} - M))$$

$$M = \frac{M_{irr}}{(1+c)} + \frac{cM_{an}}{(1+c)} \quad (4.32)$$

Taking 1st derivative of equation (4.32) we obtain;

$$\frac{dM}{dH} = \frac{1}{(1+c)} \frac{dM_{irr}}{dH} + \frac{c}{(1+c)} \frac{dMan}{dH} \quad (4.33)$$

Rearranging equation (4.32),

$$M_{irr} = (1+c)M - cMan \quad (4.34)$$

Substituting equation (4.34) into (4.21) we get,

$$\frac{dM_{irr}}{dH} = \frac{(Man - [(1+c)M - cMan])}{\delta k - \alpha(Man - [(1+c)M - cMan])} = \frac{Man - M}{\delta k/(1+c) - \alpha(Man - M)} \quad (4.35)$$

Substituting equation (4.35) into (4.33) we obtain total differential permeability as;

$$\frac{dM}{dH} = \frac{1}{(1+c)} \frac{Man - M}{\delta k/(1+c) - \alpha(Man - M)} + \frac{c}{(1+c)} \frac{dMan}{dH} \quad (4.36)$$

These two results were tested in the simulation program developed and were seen to be giving the same results.

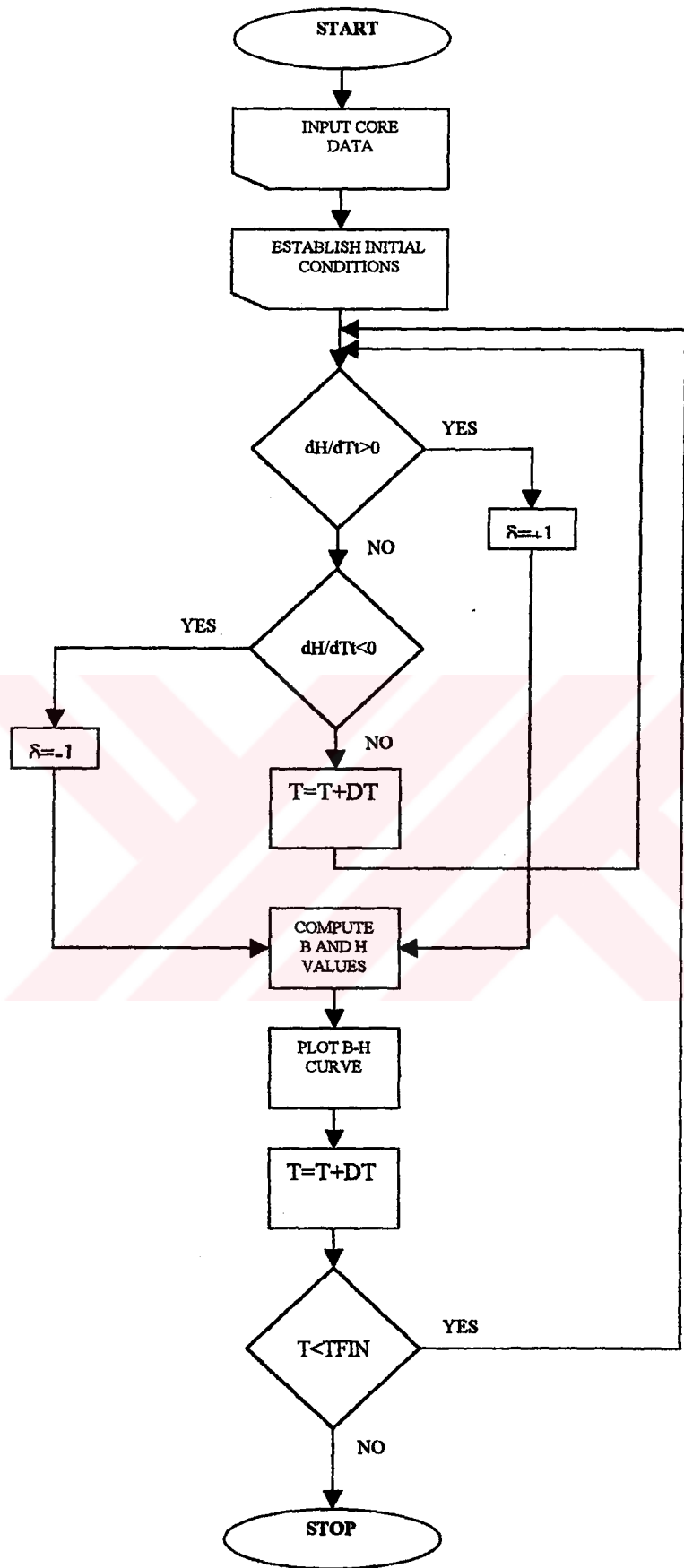


Figure 4.1 Flow chart of sub-program (core modeling)

4.3 Simulation Results of the Core Model

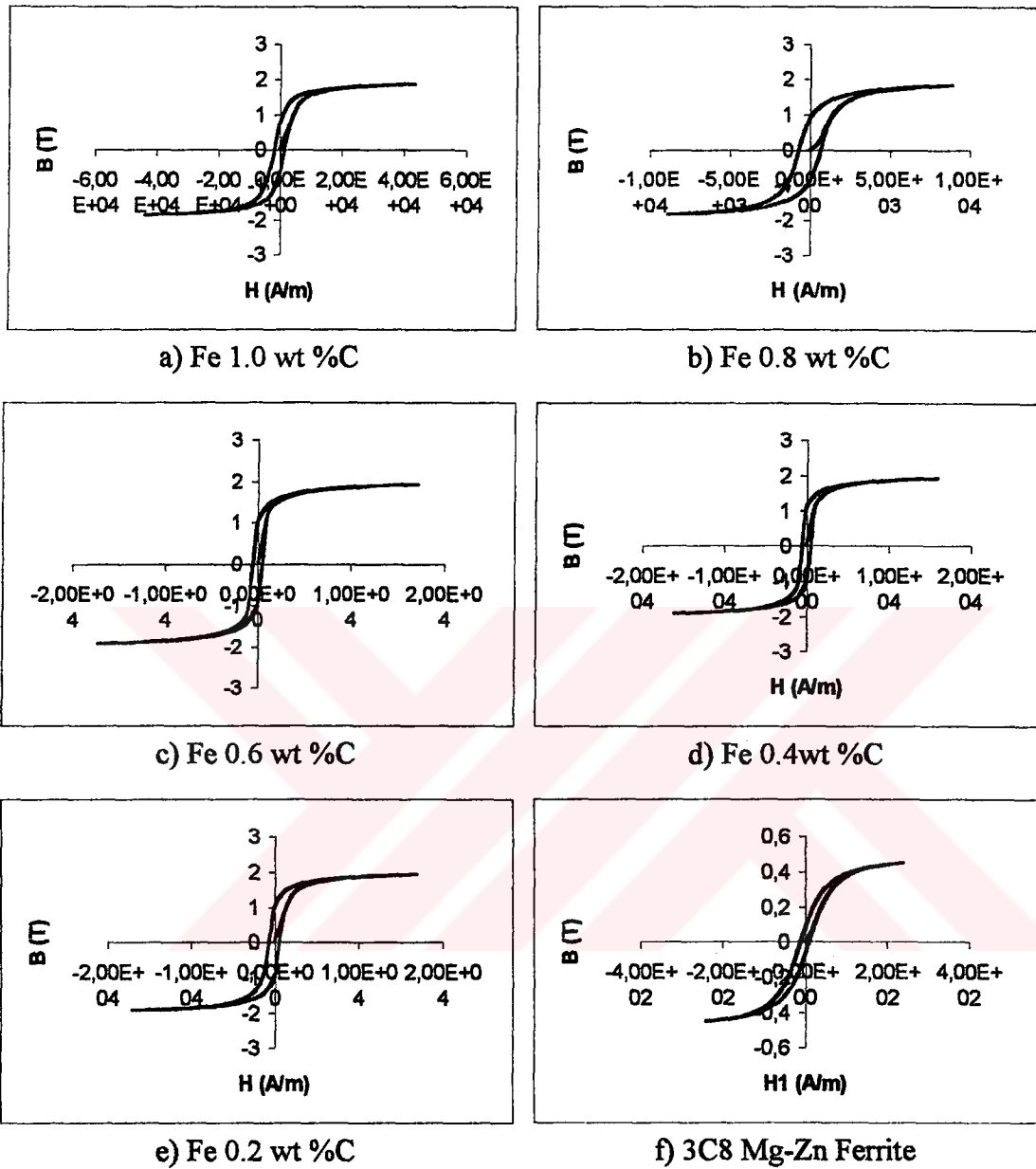


Figure 4.2 Simulation results (B-H curves) obtained from various materials whose constants are given in table 4.2

Table 4.2 Simulation results, compared with the simulation and experimental results given in ref. [27]

| | | Fe 1.0 wt %C | Fe 0.8 wt%C | Fe 0.6 wt%C | Fe 0.4 wt%C | Fe 0.2 wt%C | 3C8 Mg-Zn ferrite |
|---|---------|--------------------|-------------------|-------------------|-------------------|-------------------|-------------------------|
| Experimentally obtained data (By D.C.jiles at all) | Hm(A/m) | 43600 | 8883 | 17000 | 16000 | 17200 | 240 |
| | Bm(T) | 1.88 | 1.62 | 1.85 | 1.83 | 1.94 | 0.46 |
| | Br(T) | 0.72 | 0.81 | 1.1 | 0.91 | 0.88 | 0.1 |
| | Hc(A/m) | 1509 | 693 | 620 | 400 | 315 | 16 |
| | | | | | | | |
| Core model constants, from experimental data | Ms | 1.5E+6 | 1.6E+6 | 1.6E+6 | 1.6E+6 | 1.6E+6 | 0.4E+6 |
| | a | 1800 | 1000 | 972 | 1010 | 1085 | 27 |
| | k | 1800 | 700 | 672 | 455 | 320 | 30 |
| | Alpha | 0.4E-3 | 0.14E-3 | 0.14E-3 | 1.8E-3 | 2E-3 | 5E-5 |
| | c | 0.14 | 0.22 | 0.14 | 0.21 | 0.3 | 0.55 |
| | | | | | | | |
| D.C.Jiles at all. simulation results | Hm | 40000 | 9000 | 17000 | 16000 | 17200 | 240 |
| | Bm | 1.87 | 1.6 | 1.82 | 1.81 | 1.91 | 0.44 |
| | Br | 0.68 | 0.71 | 0.85 | 0.86 | 0.91 | 0.1 |
| | Hc | 1538 | 617 | 624 | 441 | 337 | 15 |
| | | | | | | | |
| Our simulation results | Hm | 43600 | 8880 | 17000 | 16000 | 17200 | 240 |
| | Bm | 1.86 | 1.66 | 1.92 | 1.92 | 1.92 | 0.45 |
| | Br | 0.7 | 0.89 | 0.98 | 1.02 | 0.96 | 0.1 |
| | Hc | 1510 | 679 | 630 | 451 | 340 | 15 |
| | | | | | | | |

Conclusion

Simulation results were compared with the experimental and simulation results given in previously proposed papers. The B-H loop (Hysteresis Curve) and features such as remnant point, coercive point, and tip points were also compared with the previous results proposed by D.C.Jiles, J.B.Thoelke and M.K.Devine [27] and were seen to be closely fit. The core model developed was used in the simulation of CT in Chapter 5.



CHAPTER 5

CURRENT TRANSFORMER MODELLING

Introduction

In order to be able to simulate a CT under fault conditions, a suitable input signal equation representing actual transient fault signal and an equivalent circuit of CT are needed. The accurate mathematical equations representing primary, secondary and magnetic core of the CT are needed as well.

The present chapter is concerned with the derivation of fault current equations in a typical power network, development of CT equivalent circuit and CT characteristic equations. The air core transformers and their specifications are also examined.

5.1 Fault Current Modelling

Most of the power system networks can be represented by a series of interconnected source e.m.f. and impedances. The impedances consist of series and parallel resistances and inductances and in some cases capacitors. Figure 5.1 shows a typical power system network [11].

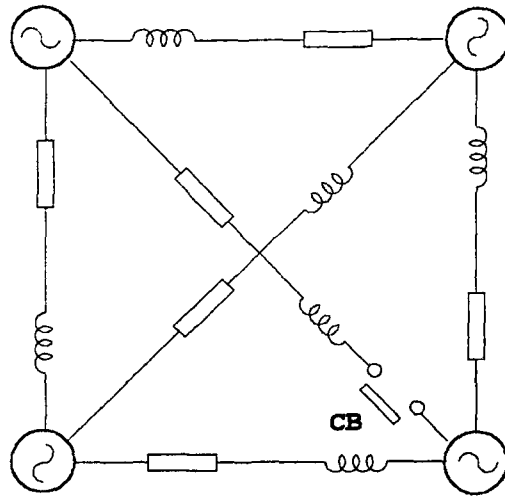


Figure 5.1 Typical power network

Closing of the circuit breaker gives rise to current flow which depends on the open circuit voltages across the circuit breaker terminals presented by the sources of the e.m.f. and Thevenin impedance. The current flowing in the C.B. is given by equation 5.1

$$i_1(t) = \frac{V_{oc}(t)}{Z_{sc}(t)} \quad (5.1)$$

Where,

$i_1(t)$ is the short circuit current flowing in the CB.

$V_{oc}(t)$ is the pre-fault voltage across the CB terminals.

$Z_{sc}(t)$ is the Thevenin impedance across the CB terminals.

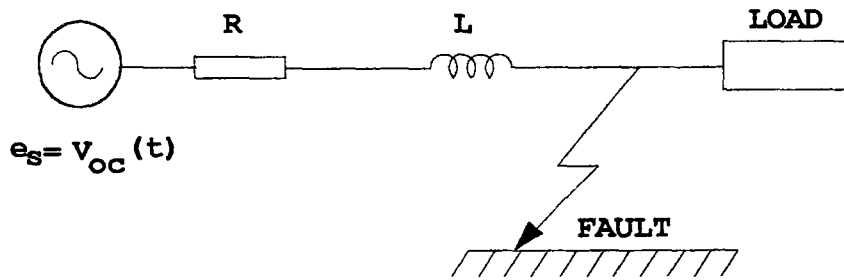


Figure 5.2 Fault on circuit fed at one end

Considering a circuit fed only at one end (Figure 5.2) for sinusoidal source of e.m.f., the general fault current equation can be represented by:

$$i(t) = \frac{V_{pm}}{Z} [\sin(\omega t + \varepsilon - \phi) - \exp(-Rt/L)\sin(\varepsilon - \phi)] \quad (5.2)$$

Let $\delta = \varepsilon - \phi$

Then,

$$i(t) = \frac{V_{pm}}{Z} [\sin(\omega t + \delta) - \exp(-Rt/L)\sin\delta] \quad (5.3)$$

Where,

ε is the fault angle from the last voltage zero,

ϕ is $\tan^{-1}\left(\frac{\omega L}{R}\right)$ (phase angle)

t is the time after the occurrence of fault.

ω is the angular frequency in radians,

$i_1(t)$ is the instantaneous value of current,

R is the effective source resistance,

L is the effective source inductance

V_{pm} is the maximum peak value of voltage

Several cases occur depending on what happened before the fault as well as the fault angle [11]. Two major cases can be singled out among the variety of cases. These are

- when no current was flowing before the fault,
- current was flowing before the fault.

5.2 Transient Effects In Current Transformers

In order to fully understand the transient phenomena to which protection current transformers are subjected it is appropriate to first consider an approximate analysis. This analysis considers the effect of burdens together with their influence on the saturation characteristics of these devices.

Restating the expression for the fault current in the form

The fault current in equation 5.3 may be expressed as the sum of two components.

$$i(t) = \frac{V_{pm}}{Z} [\sin(\omega t) \cos \delta + \sin \delta \cos(\omega t) - \exp(-\gamma t) \sin \delta] \quad (5.4)$$

$$i_1 = I_{pm} [\cos(\omega t) - \exp(-\gamma t)] \sin \delta \quad (5.5)$$

$$i_2 = I_{pm} [\sin \omega t \cos \delta]$$

Where, $I_{pm} = \frac{V_{pm}}{Z}$ and $\gamma = \frac{R}{L}$

Two extreme cases occur depending on the instance of fault occurrence. (Assuming no current flow prior to fault)

- For $\delta = 0$,

$i(t) = I_{pm} [\sin(\omega t)]$ symmetrical fault current, without any transient component.

- For $\delta = +\pi/2$ or $\delta = -\pi/2$, fully offset fault current

For $\delta = -\pi/2$, fully offset fault current (the worst case).

$$i(t) = I_{pm} [-\cos(\omega t) + \exp(-\gamma t)] \quad (5.6)$$

Considering the reduced circuit diagram Figure 5.3 for the current transformer and primary current reduced by turns ratio N.

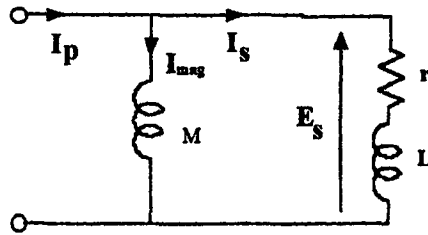


Figure 5.3 Reduced circuit diagram

Ignoring L as being small compared to r and considering transient component only

$$i_s = \frac{i_p}{p + \gamma} \frac{pM}{pM + r} \text{ by laplace transform,} \quad (5.7)$$

Resolving by using partial fraction,

$$i_s = I_{pm} \left[\frac{r \exp((-r/M)t) - M\gamma \exp(-\gamma t)}{r - M\gamma} \right] \quad (5.8)$$

And the voltage across the current transformer,

$$v_s = r I_{pm} \left[\frac{r \exp((-r/M)t) - M\gamma \exp(-\gamma t)}{r - M\gamma} \right] \quad (5.9)$$

But the flux $\Phi_s = \int_0^t v_s dt$

$$\Phi_s = M I_{pm} \left[\frac{\exp(-(r/M)t) - \exp(-\gamma t)}{\frac{M\gamma}{r} - 1} \right] \quad (5.10)$$

The magnetising current due to the transient component only is Φ_s / M .

$$i_{\text{mag}} = I_{\text{pm}} \left[\frac{\exp(- (r/M)t) - \exp(- \gamma t)}{\frac{M\gamma}{r} - 1} \right] \quad (5.11)$$

Considering the expression above equation 5.11 is shown typically in Figure 5.4

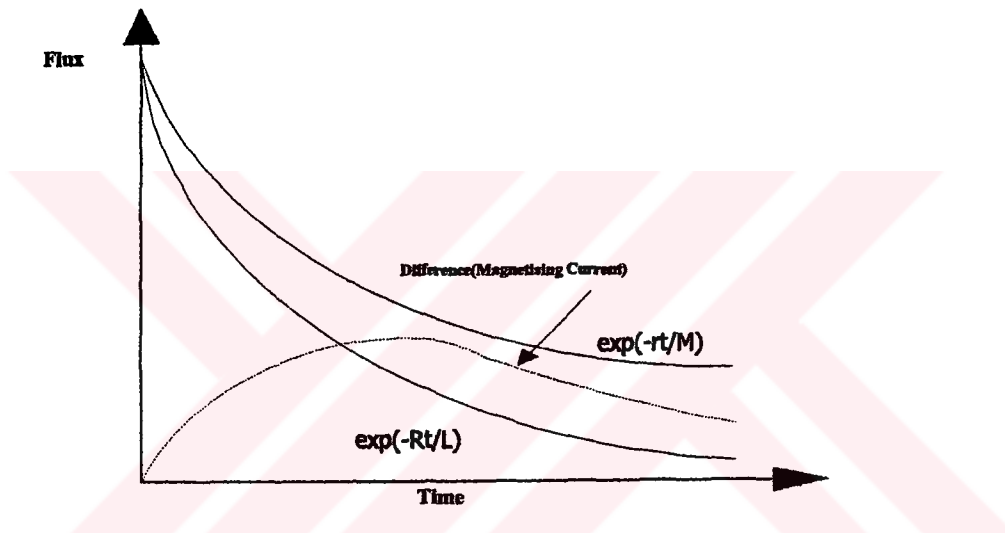


Figure 5.4 Magnetizing current due to transient component Φ_s / M .

Maximum flux occurs when $d\Phi_s/dt = 0$

Or,

$$r \exp(- (r/M)t) - \gamma M \exp(- \gamma t) = 0$$

Assume $M/r \gg 1/\gamma$

Then,

$$\exp(- (r/M)t) \cong 1 \text{ and } \exp(- \gamma t) = \frac{r}{M\gamma}$$

The maximum flux may be given approximately by,

$$\begin{aligned}\Phi_{\max} &= \frac{M I_{\text{pm}} \left[1 - \frac{r}{M\gamma} \right]}{\frac{M\gamma}{r} - 1} \\ &= \frac{r}{\gamma} I_{\text{pm}}\end{aligned}\quad (5.12)$$

$$i_{\text{mag}_{\max}} = \frac{r I_{\text{pm}}}{M\gamma} \quad (5.13)$$

The peak value of the magnetising current $I_{\text{mag}_{\text{pm}}} = i_{\text{mag}_{\max}}$ due to the transient component + $i_{\text{mag}_{\text{pm}}}$ due to the steady state component. The first component is given by equation 5.13. The second component is derived as follows

$$i_{\text{mag}_{\text{ss}}} = \frac{V_{\text{pm}}}{Z} \sin \alpha t \frac{r}{\gamma M} \quad (5.14)$$

$$i_{\text{mag}_{\text{pm}_{\text{ss}}}} = \frac{r I_{\text{pm}}}{\omega M} \quad (5.15)$$

$$i_{\text{mag}_{\text{pm}}} = \frac{r I_{\text{pm}}}{\gamma M} + \frac{r I_{\text{pm}}}{\omega M} = \frac{r I_{\text{pm}}}{M} \left\{ \frac{1}{\gamma} + \frac{1}{\omega} \right\} \quad (5.16)$$

$$\text{The ratio } i_{\text{mag}}/i_{\text{mag}_{\text{ss}}} = \frac{\frac{r I_{\text{pm}} \left\{ \frac{1}{\gamma} + \frac{1}{\omega} \right\}}{M}}{\frac{r I_{\text{pm}}}{\omega M}} = \frac{\omega L}{R} + 1 \quad (5.17)$$

Where L and R are constants of the primary circuits and $\frac{\omega L}{R} + 1$ may be expressed as $Q+1$.

This means that the current transformer may experience high currents to a value of $(Q+1)$ times the steady state during fault conditions which will cause saturation. The factor $Q+1$ will increase as the impedance angle of the primary circuit i.e. the factor increases almost linearly over the transmission range 132kV to 400kV. The worst condition arises with a resistive burden. Figure 5.5 illustrates the transients for magnetising current for various burdens.

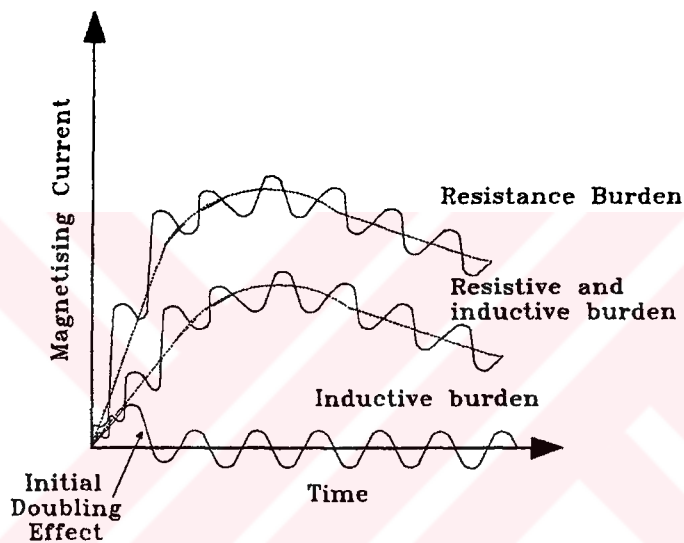


Figure 5.5 Transients for magnetising current for various burden

5.3 Dynamic Modelling of Current Transformer

The general equivalent circuit of a current transformer should contain the primary section and the secondary section combined with the burden. Figure 5.6 shows an equivalent circuit of a current transformer and its excitation circuit. It consists of a lumped inductor L_p and R_p which represent the primary system inductance and

resistance respectively. L_s and R_s represent the secondary lumped equivalent inductance and resistance respectively, while R_b represent the burden equivalent resistance. The magnetising branch is represented by a non-linear inductance. The eddy current loss is considered to be negligible so no resistance has been included in the circuit for this power loss.

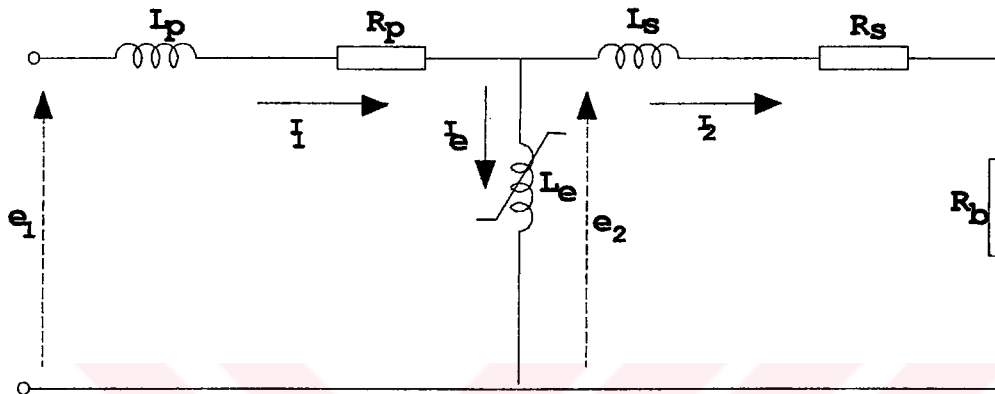


Figure 5.6 Equivalent circuit of current transformer.

Assuming no current flow prior to fault and under the full offset fault current condition. Applying Kirchoff's current law to Figure 5.6

$$i_1(t) = i_2(t) + i_e(t) \quad (5.18)$$

The induced voltage in the core $e_2(t)$ is given by the equation :

$$e_2(t) = N \frac{d\Phi(t)}{dt} \quad (5.19)$$

$$N \frac{d\Phi(t)}{dt} = i_2(t)R + L_2 \frac{di_2(t)}{dt} \quad (5.20)$$

Where,

$$R = R_s + R_b \quad (\text{If } L_b \neq 0)$$

$$L_2 = L_s + L_b$$

The main problem now is to establish the relationship between the excitation current and flux.

Generally

$$i_e(t) = f(\Phi(t)) \quad (5.21)$$

So,

$$\frac{d\Phi(t)}{dt} = \frac{NA}{\ell} \frac{dB}{dH} \frac{di_e(t)}{dt} \quad (5.22)$$

Where

N is the turn ratio of the transformer

A is the area of the core

ℓ is the length of the magnetic path

$\frac{dB}{dH}$ is the differential permeability or the slope of the B/H characteristic.

Substituting for $i_2(t)$ in equation 5.20 using equation 5.18 , we have:

$$\begin{aligned} \frac{d\Phi}{dt} &= \frac{1}{N} \left[(i_1(t) - i_e(t))R + L_2 \frac{d}{dt} (i_1(t) - i_e(t)) \right] \\ &= \frac{1}{N} \left[Ri_1(t) + L_2 \frac{di_1(t)}{dt} - Ri_e(t) - L_2 \frac{di_e(t)}{dt} \right] \end{aligned} \quad (5.23)$$

Equation 5.22 and 5.23 give

$$\frac{di_e(t)}{dt} = \frac{1}{L_2 + \frac{N^2 A}{\ell} \frac{dB}{dH}} \left[Ri_1(t) - Ri_e(t) + L_2 \frac{di_1(t)}{dt} \right] \quad (5.24)$$

$\frac{dB}{dH}$ is found from the equation 4.30 in Chapter 4.

Equation 5.24 is solved by using Runge-Kutta fourth order method for solving first order differential equation by numerical analysis (Appendix 1).

Now we have a value of magnetising current at time t , which could then be substituted into equation 5.18 to find $i_1(t)$.

5.4 Air-Core Current Transformer Modelling

Although iron-cored current transformers are and have been used in conjunction with power-system protective equipment for almost a hundred years, they are not ideal because of the non-linearity of their excitation characteristics and their ability to retain large flux levels in their cores. Protective schemes, in which the outputs of non-ideal current transformers at different points in a power system are compared, could operate correctly provided that the current transformers each had the same percentage transformation errors at each instant. This situation cannot be achieved in practice, however, with protective schemes protecting multi-ended units, such as busbars, because the output of a current transformer carrying a large current might be required to balance with the sum of the outputs of a number of transformers carrying small currents. The transformers would be operating at different points on their excitation characteristics and when these are non-linear the errors of the transformers would differ, preventing perfect balance being achieved. Even in those cases where the outputs of only two current transformers carrying the same primary currents are compared, unbalance would occur if they were retaining different remnant fluxes because they would not then be at the same points on their excitation characteristics and would not have the same errors.

The above difficulties clearly would not arise if protective schemes were energised from transformers with cores of unit relative permeability, i.e. of wood or air, because such transformers are unable to retain flux in their cores when their excitation is removed and always behave in a proportional or linear manner. These devices, which are usually called linear couplers, do not produce secondary currents approximating

to those which would be provided by an ideal current transformer ($i_s = i_p N_p / N_s$) and consequently protective equipment must be specially designed to operate from them.

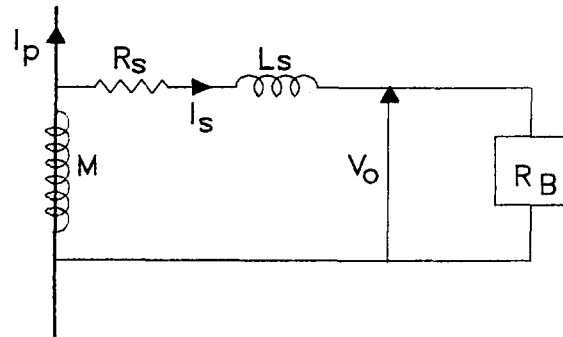


Figure 5.7 The equivalent circuit of air-cored current transformers

The mathematical equations for the output voltage can be written as follows:

$$v_o = M \frac{di_p}{dt} - L_s \frac{di_s}{dt} - R_s i_s \quad (5.25)$$

$$v_o = L_B \frac{di_s}{dt} + R_B i_s \quad (5.26)$$

the secondary differential current can be calculated from equation 5.25 and 5.26,

$$\frac{di_s}{dt} = \frac{1}{L_B + L_s} \left(M \frac{di_p}{dt} - (R_s + R_B) i_s \right) \quad (5.27)$$

where M is the mutual inductance which is,

$$M = \frac{\mu_o AN}{2\pi r_o}$$

r_o = mean radius of core

5.5 Conclusions

In this chapter, the dynamic modelling of the protective and the air-core current transformers were explained. From the CT equivalent circuit, the magnetising current was modeled. Together with the core model described in Chapter 4 and Kirchhoff's current laws, a complete CT model was developed and a computer program was written. For the solution of the model equations, the Fourth Order Runge Kutta (Merson) Routine was used. The model is applied to a 400/1 A CT. Results of the simulation are given in Chapter 6.



CHAPTER 6

DIGITAL SIMULATION RESULTS OF CURRENT TRANSFORMER

Introduction

The digital analysis is carried out by numerically integrating equation (5.25) using 4th Order Runge-Kutta Merson Integration Routine (Appendix1). The computer program for the digital analysis consists of a main program and a subprogram, which are chained at several intervals when required. Flow chart of main program is shown in Figure 6.1.

The transformer parameters are referred to the secondary side. After inputting the CT parameters the initial conditions are established, e.g. in case of no residual flux. The time step is made as small as to minimize the errors. A value of 0.2 milliseconds was found to be satisfactory.

6.1 Current Transformer Data

- Core Data

Core material: 3C8 Mg-Zn Ferrite

Model Constants: $M_s=0.4 \text{ E}+6$

$a= 27$

$k= 30$

$\text{Alpha}=5\text{E}-5$

$c=0.55$

- CT Data

Turn ratio: 400/1

Core material: 3C8 Mg-Zn ferrite

Area of the core: 14.52 cm^2

Mean length of magnetic path: 39.9 cm
Type of transformer: protection

- Burden Data

Load type: Linear R-L (Inductive)

Load resistance: Various resistance values are tested (0.5 Ohm- 60 Ohm) depending on primary current value

Load Inductance: 0.2 mH. (Constant)

Load impedance is taken to be dominant at the secondary circuit.

6.2 Simulation Results for Different Excitations

A 400/1 A CT was simulated. Figures 6.1 to 6.24 show selected simulation results. The following graphical outputs were produced for different values of burden resistance and primary fault current magnitude.

- Primary current &time.
- Secondary current &time.
- Magnetizing current &time.
- Transformation error &time.
- Flux &time.
- Burden power &time.
- Magnetizing reactance& magnetizing current.
- B-H curve.

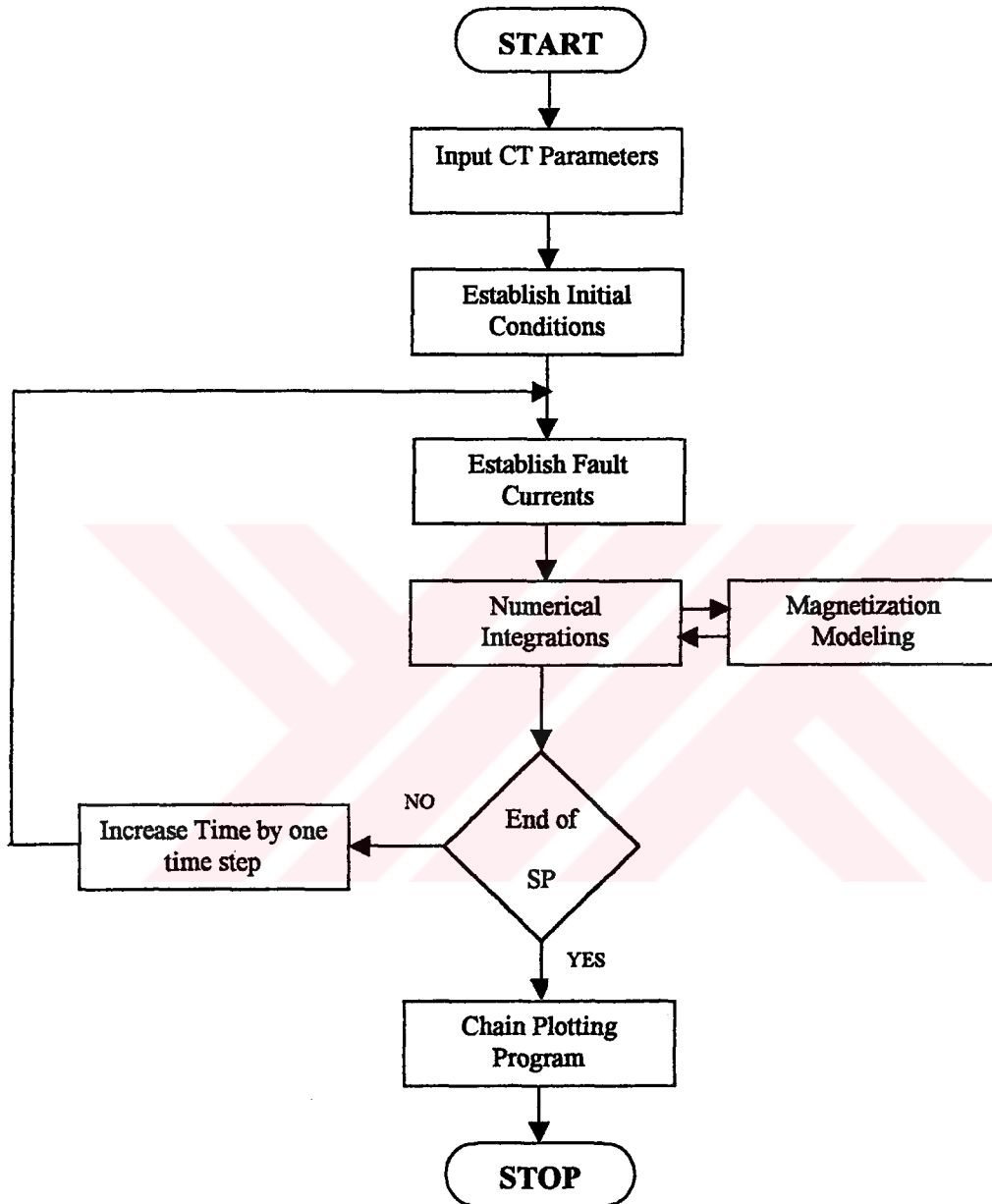


Figure 6.1 Flow Chart of Main Program

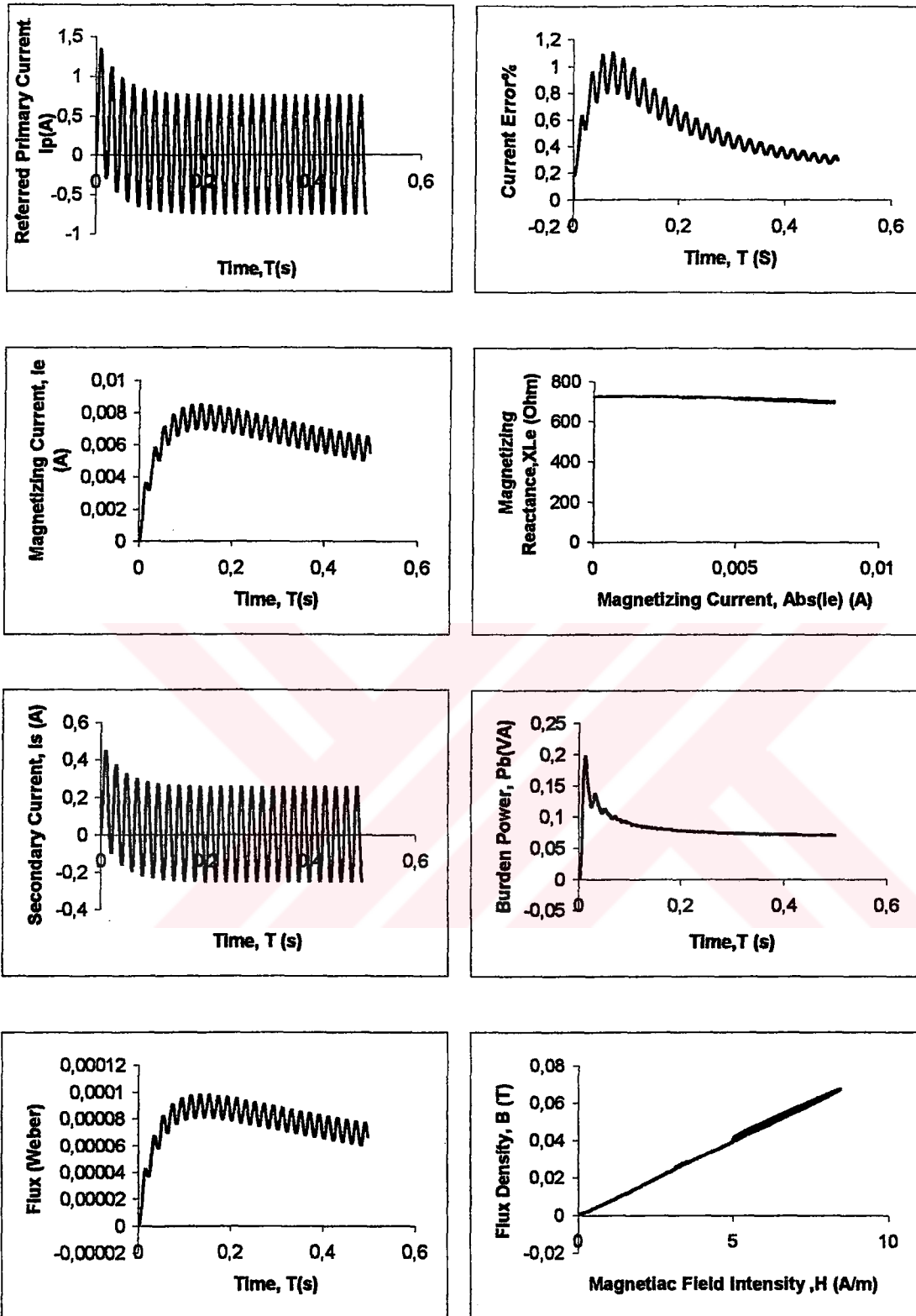


Figure 6.1 Variation of CT characteristics with respect to primary current.

$$I_p=100A, R_b=2\Omega$$

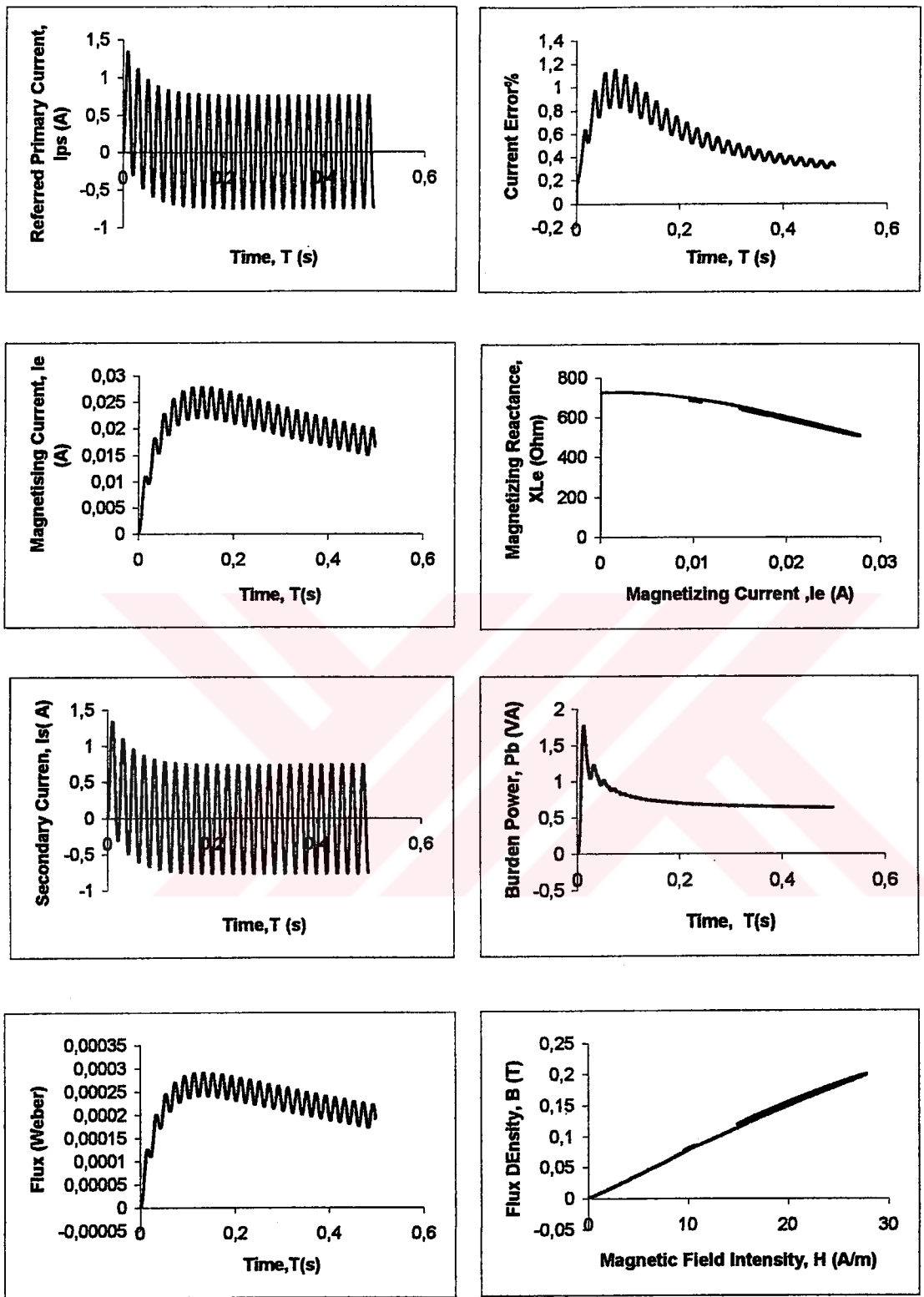


Figure 6. 2 Variation of CT characteristics with respect to primary current.

$$I_{pm}=300A, R_b=2\Omega$$

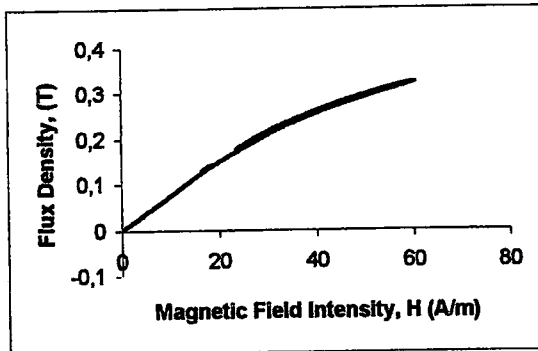
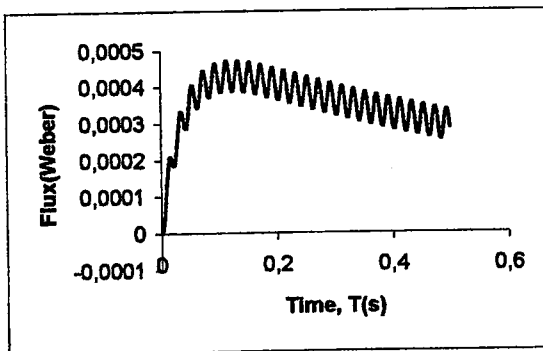
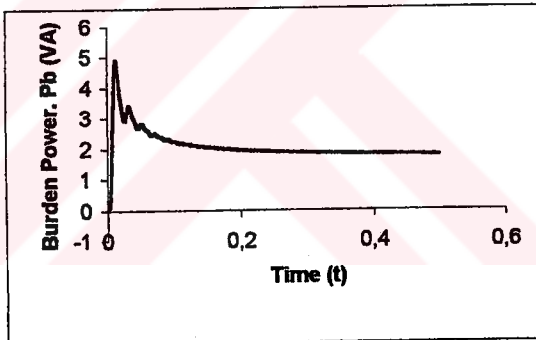
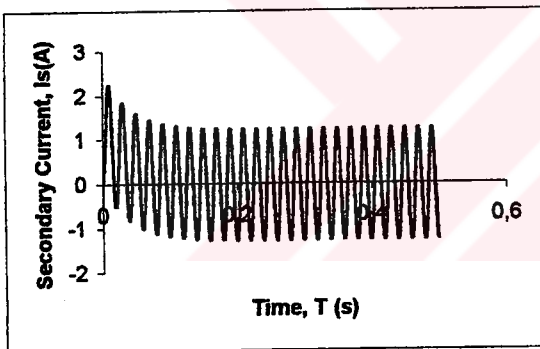
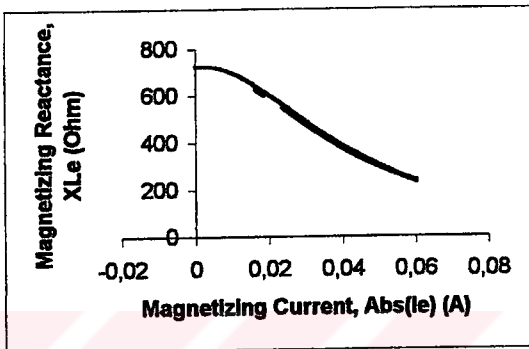
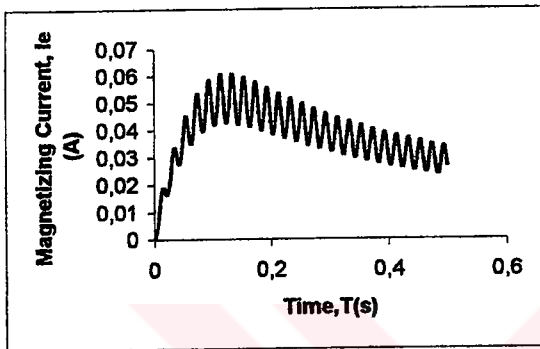
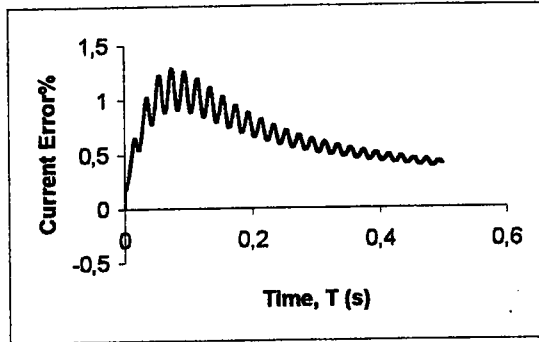
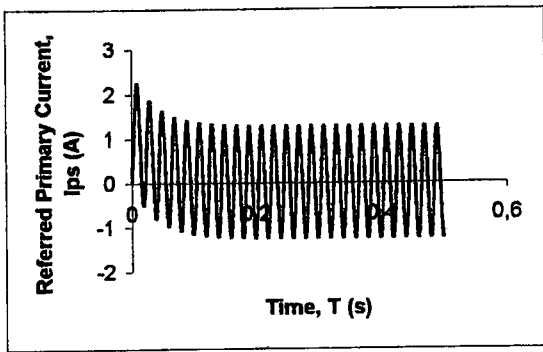


Figure 6.3 Variation of CT characteristics with respect to primary current.

$$I_{pm}=500A, R_b=2\Omega$$

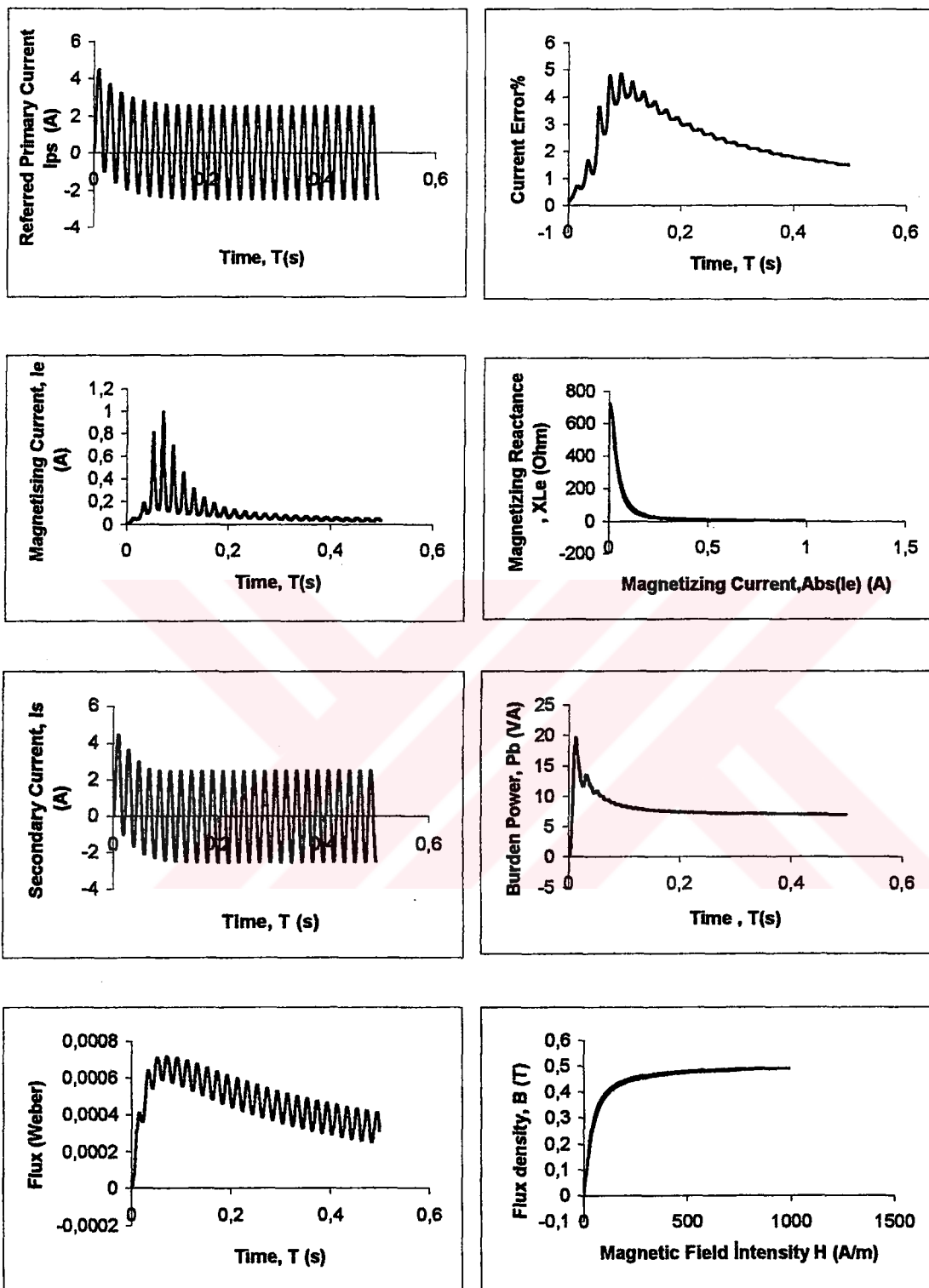


Figure 6. 4 Variation of CT Characteristics With Respect To Primary Current.

$$I_{pm}=1000A, R_b=2\Omega$$

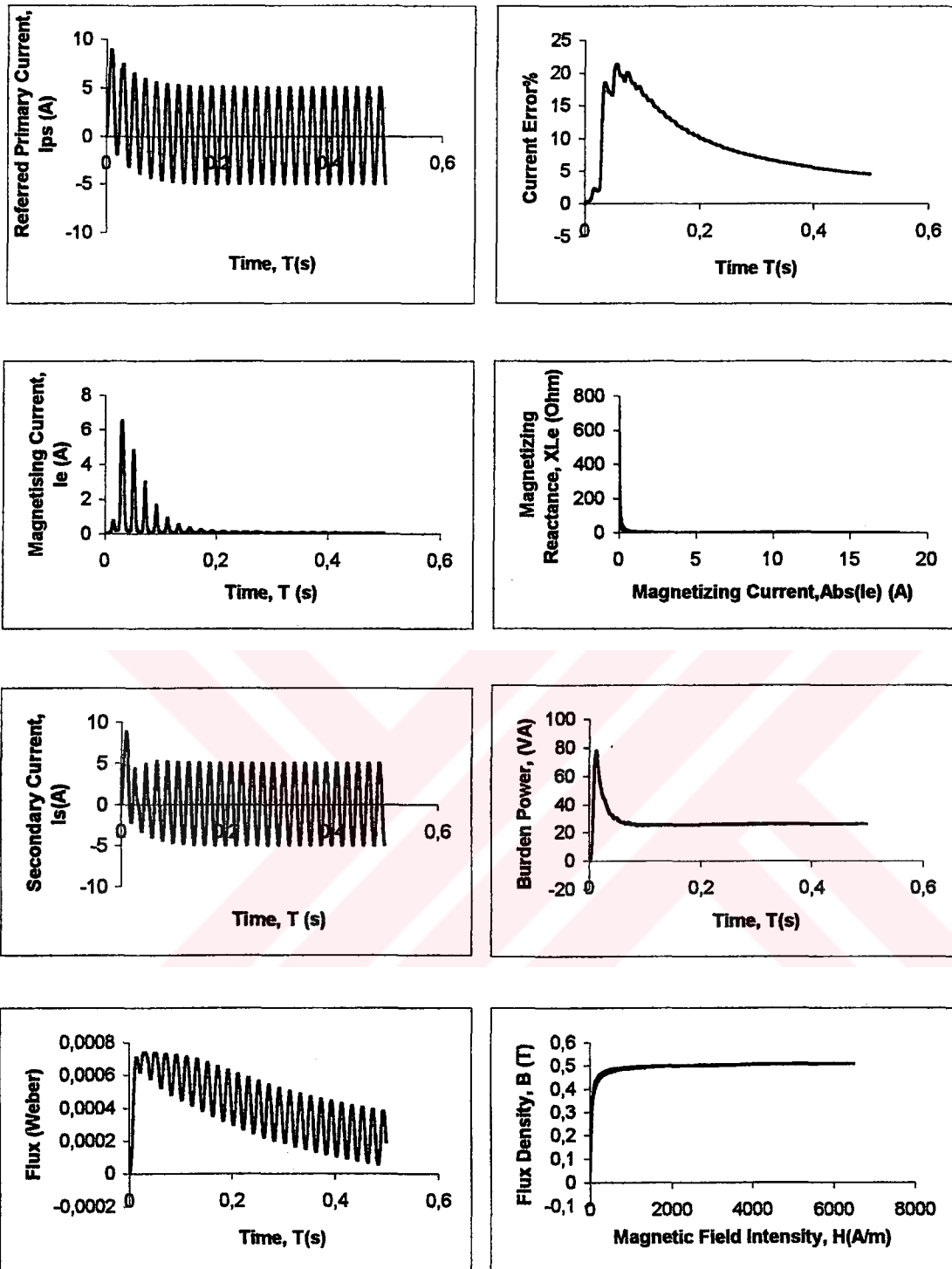


Figure 6.5 Variation of CT characteristics with respect to primary current.

$I_{pm}=2000$ A, $R_b= 2$ Ohm

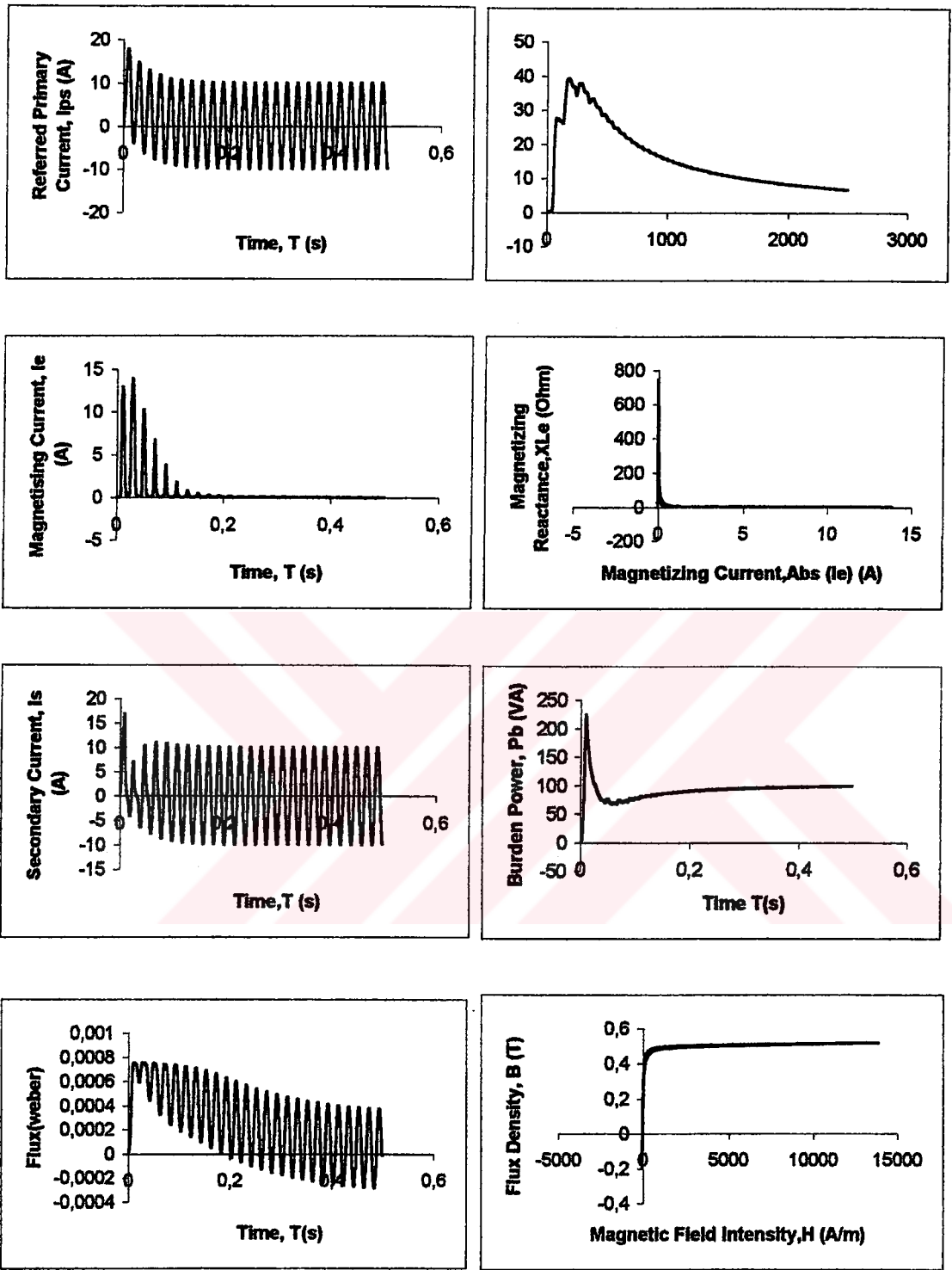


Figure 6. 6 Variation of CT characteristics with respect to primary current.

$$I_{pm}=4000 \text{ A, } R_b= 2 \text{ Ohm}$$

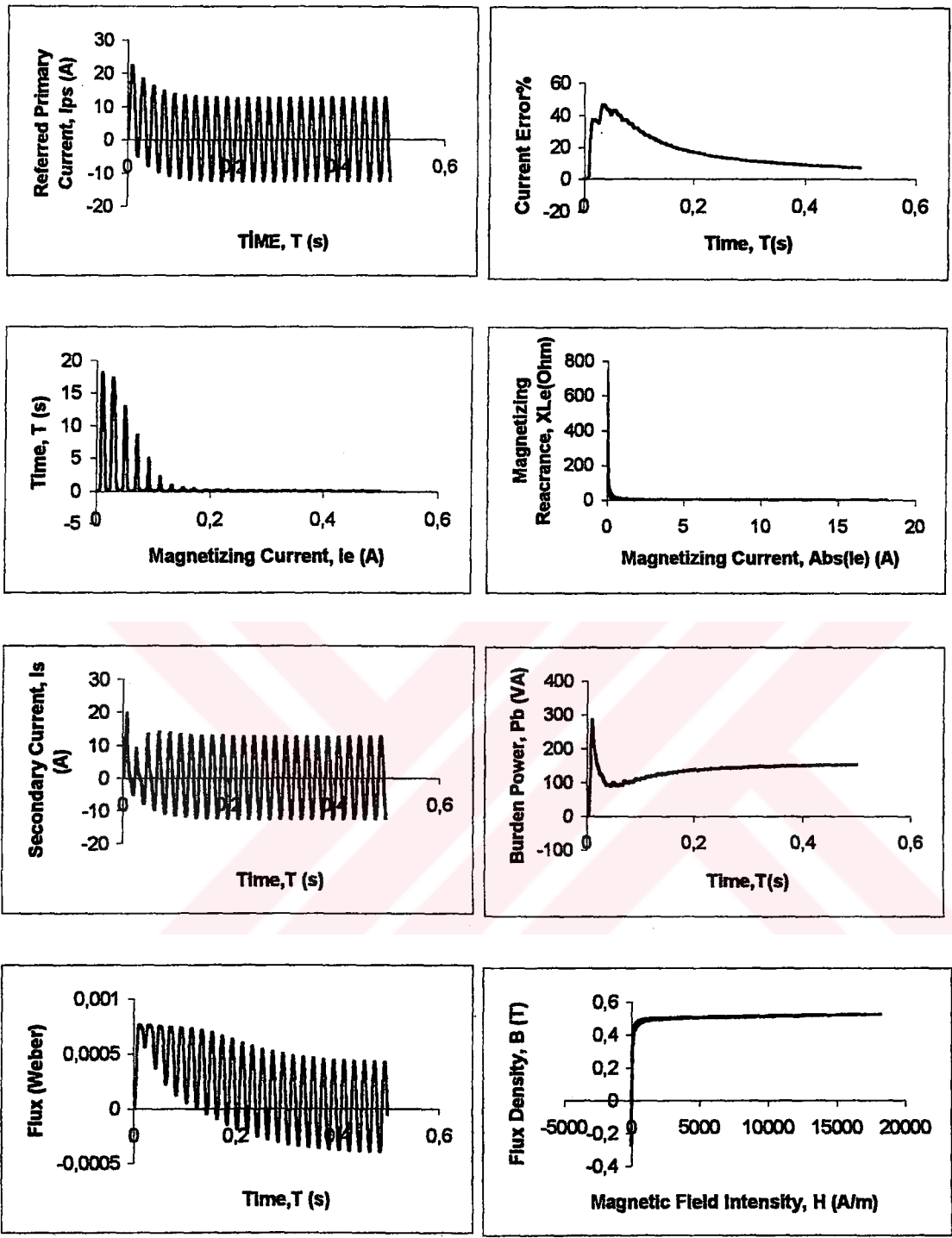


Figure 6.7 Variation of CT characteristics with respect to primary current.

$$I_{pm}=5000 \text{ A, } R_b= 2 \text{ Ohm}$$

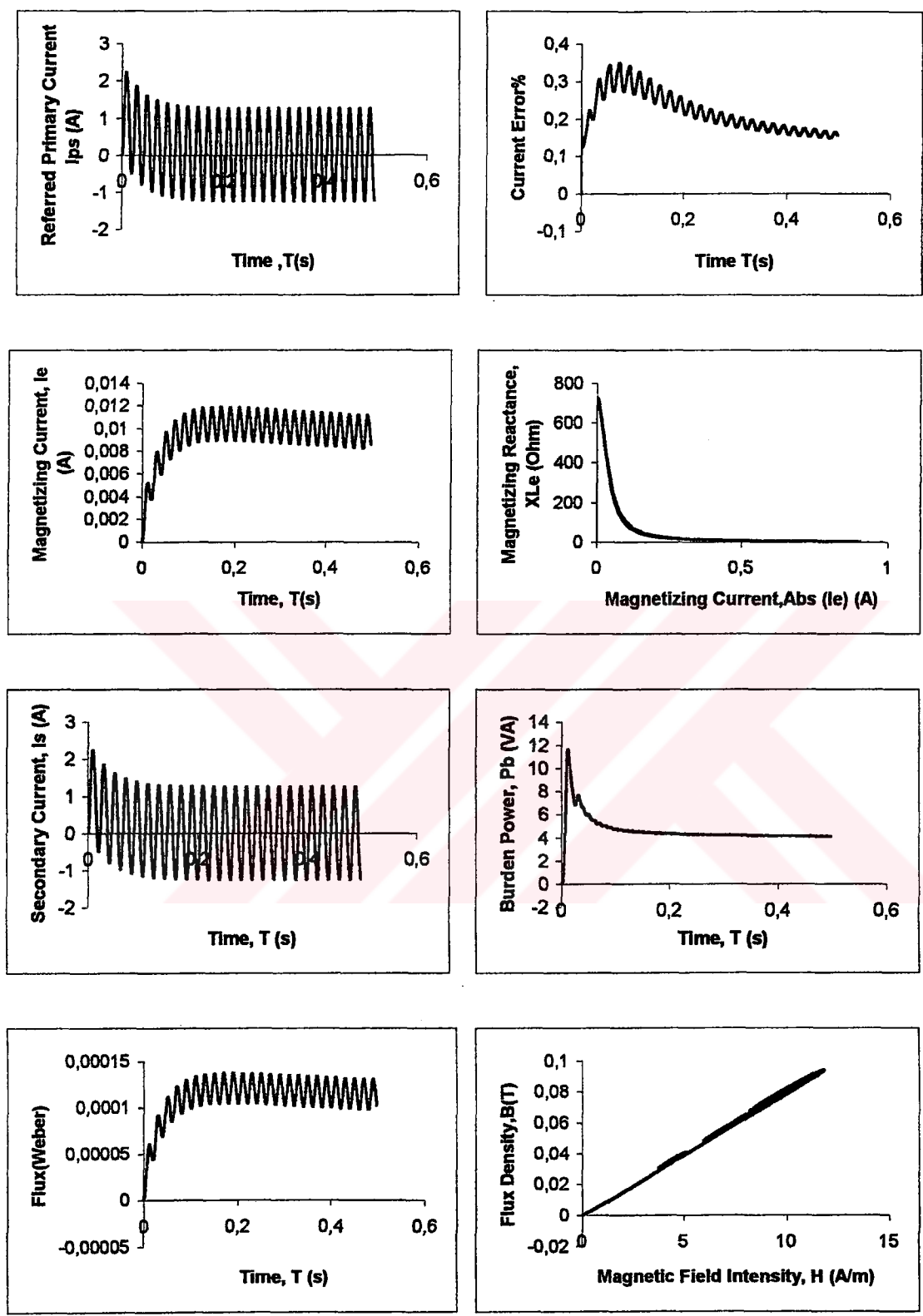


Figure 6.8 Variation of CT parameters with respect to load resistance.

$$I_{pm} = 500A, R_b = 0.5 \Omega$$

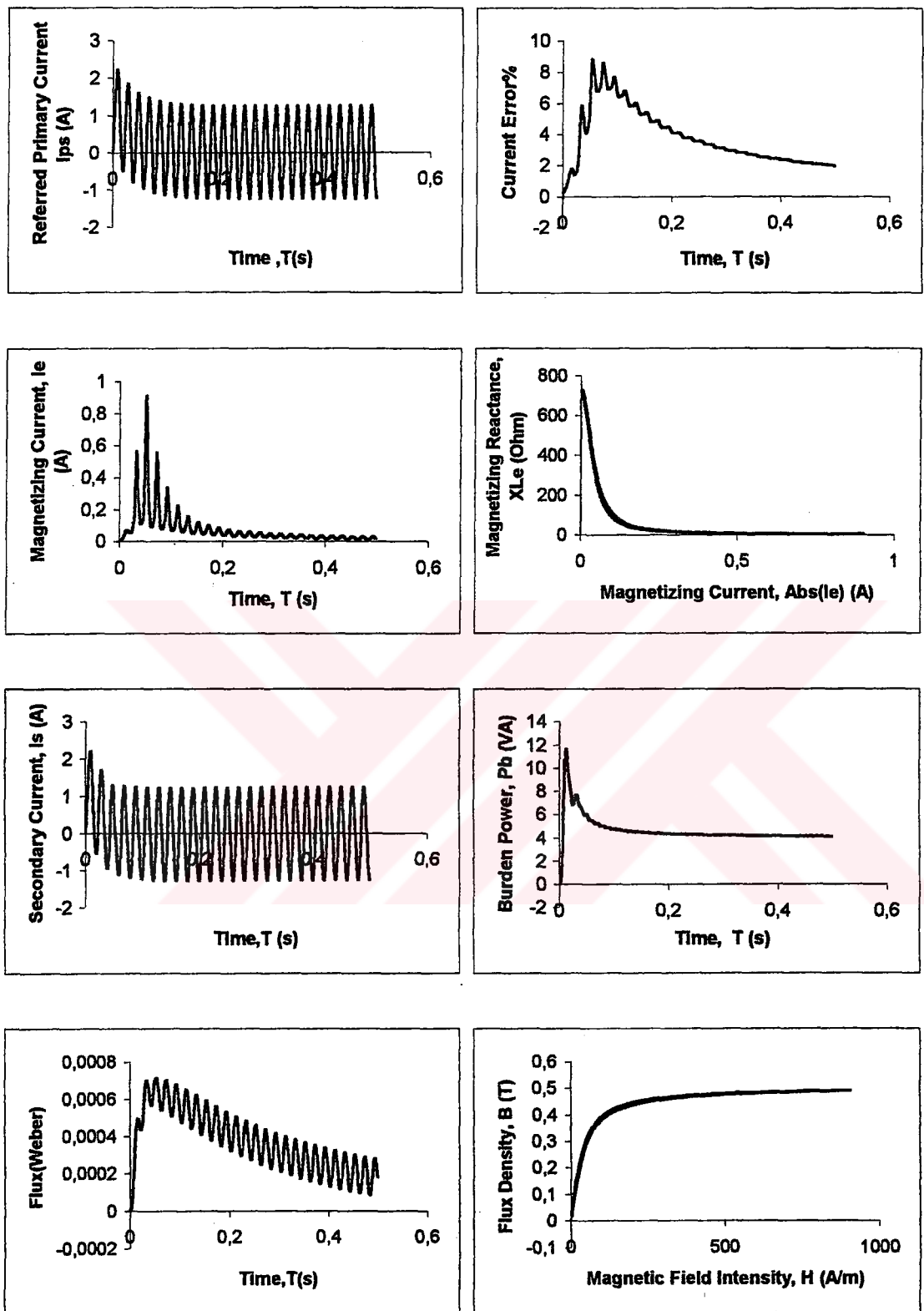


Figure 6.9 Variation of CT characteristics with respect to burden resistance.

$$I_{pm}=500 \text{ A, } R_b =5 \Omega$$

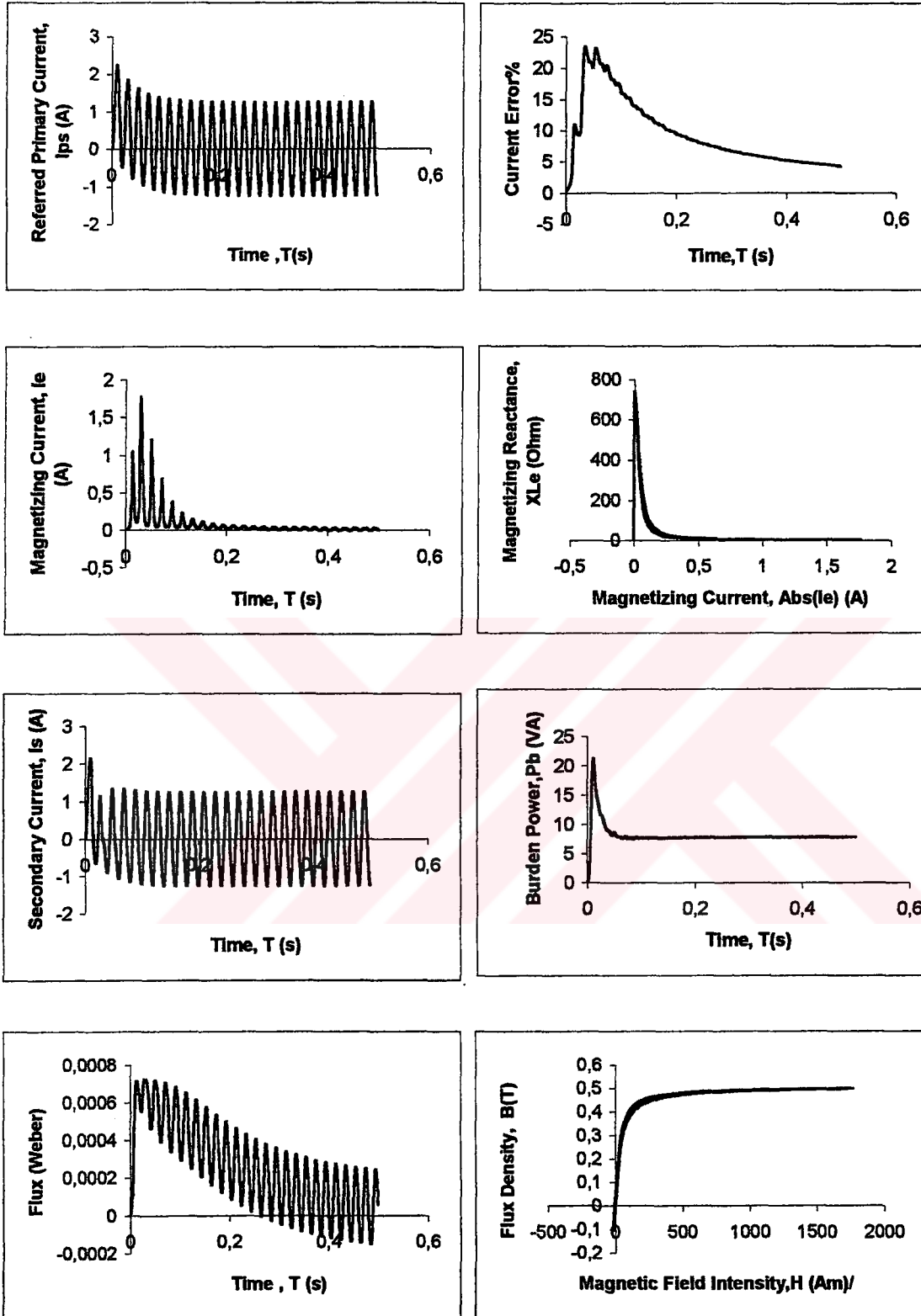


Figure 6.10 Variation of CT parameters with respect to load resistance

$$I_{pm} = 500A, R_b = 10 \Omega$$

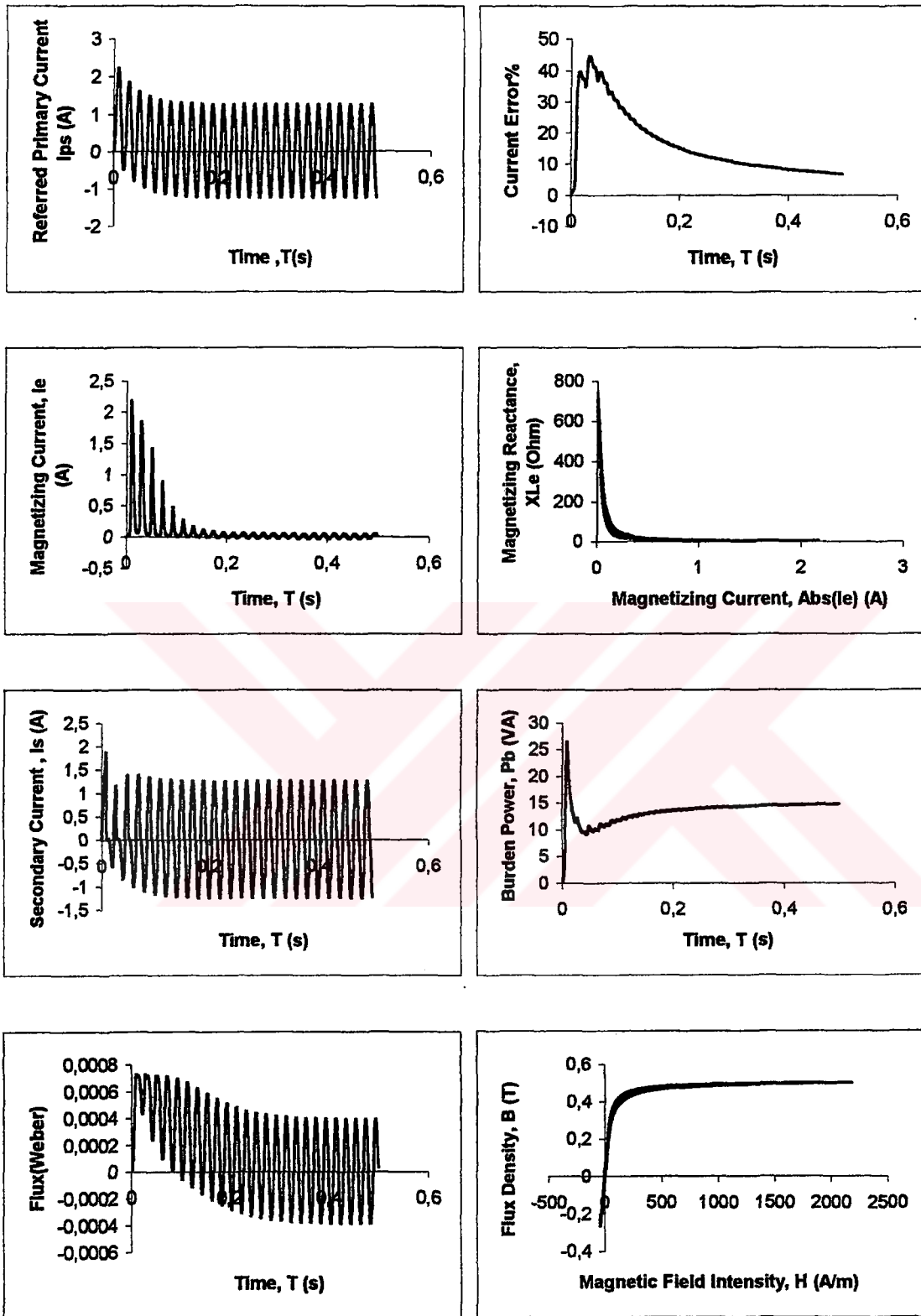


Figure 6.11 Variation of CT parameters with respect to load resistance.

$$I_{pm} = 500 \text{ A}, R_b = 20 \Omega$$

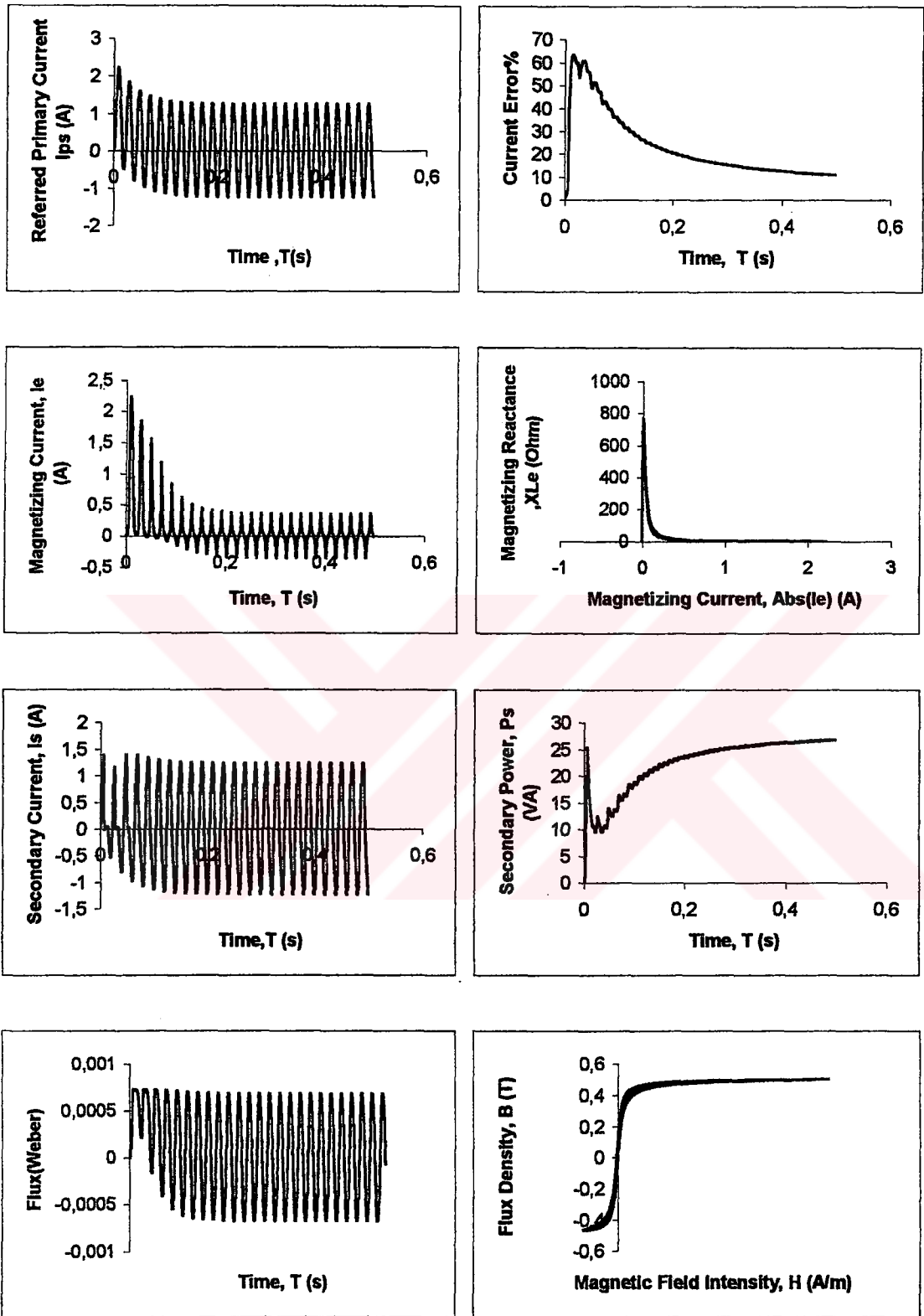


Figure 6.12 Variation of CT parameters with respect to load resistance

$I_{pm} = 500 \text{ A}$, $R_b = 40 \Omega$

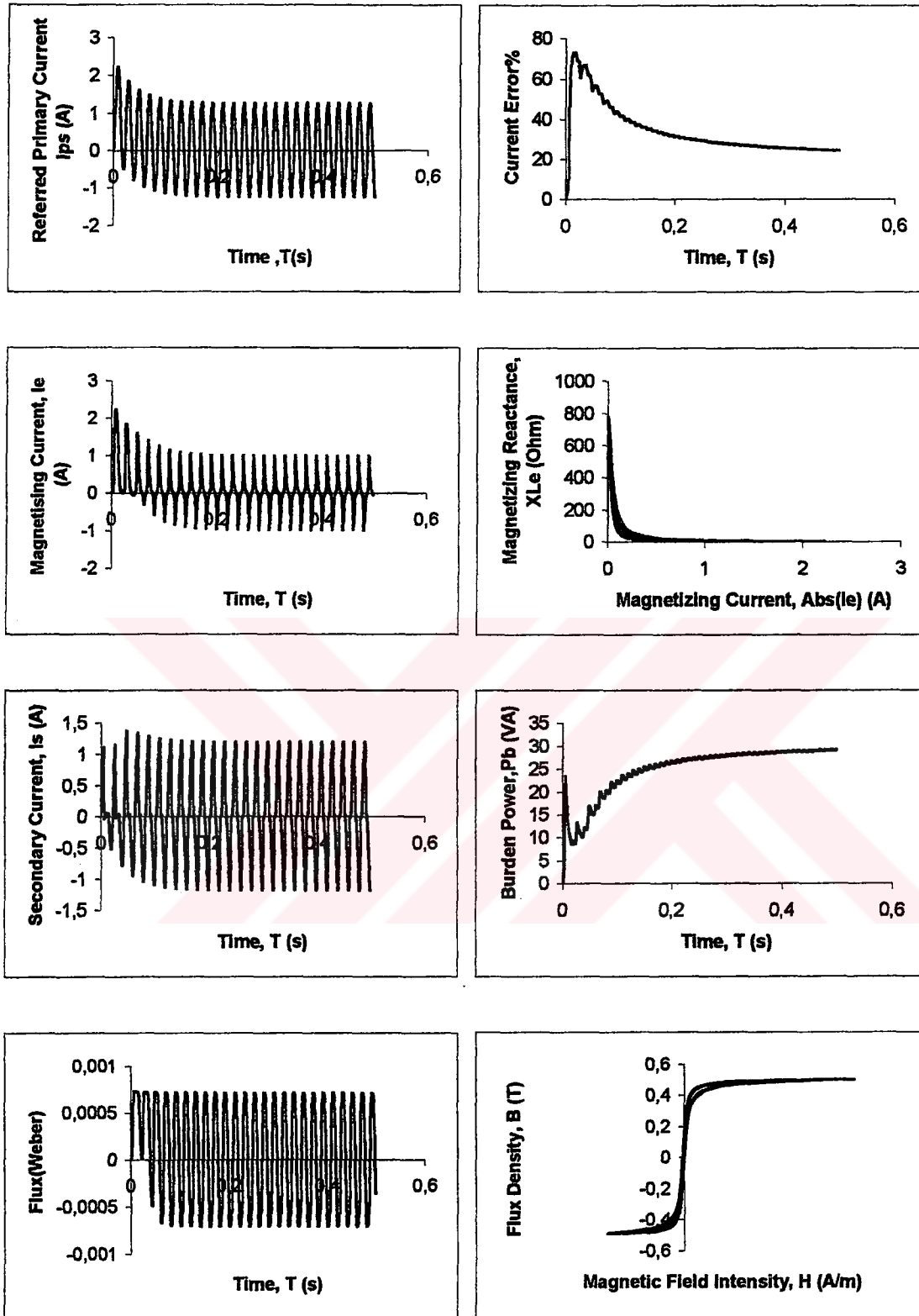


Figure 6.13 Variation of CT parameters with respect to load resistance

$$I_{pm} = 500 \text{ A}, R_b = 60 \Omega$$

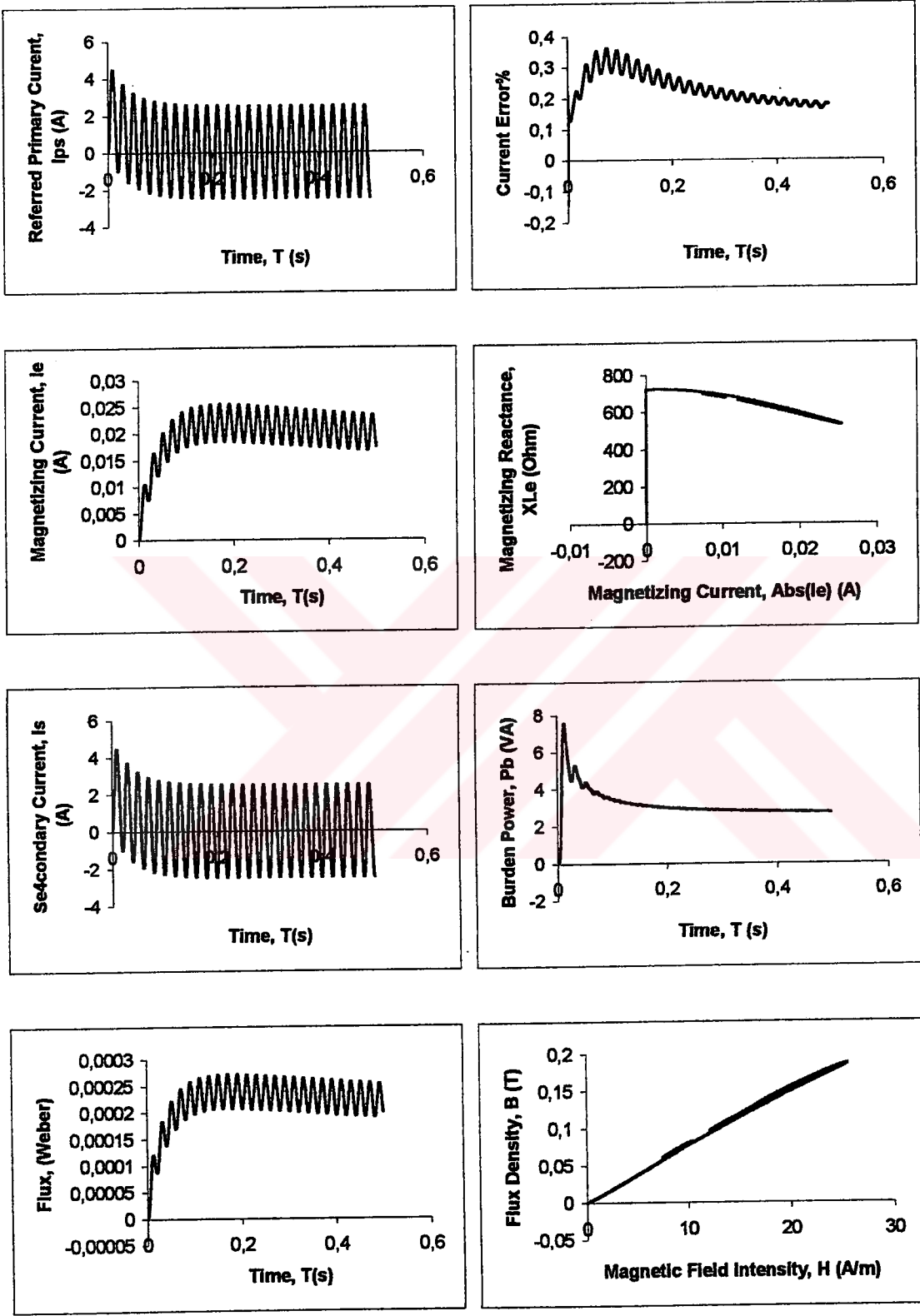


Figure 6.14 Variation of CT Characteristics with respect to load resistance.

$I_p = 1000 \text{ A}$, $R_b = 0.5 \Omega$

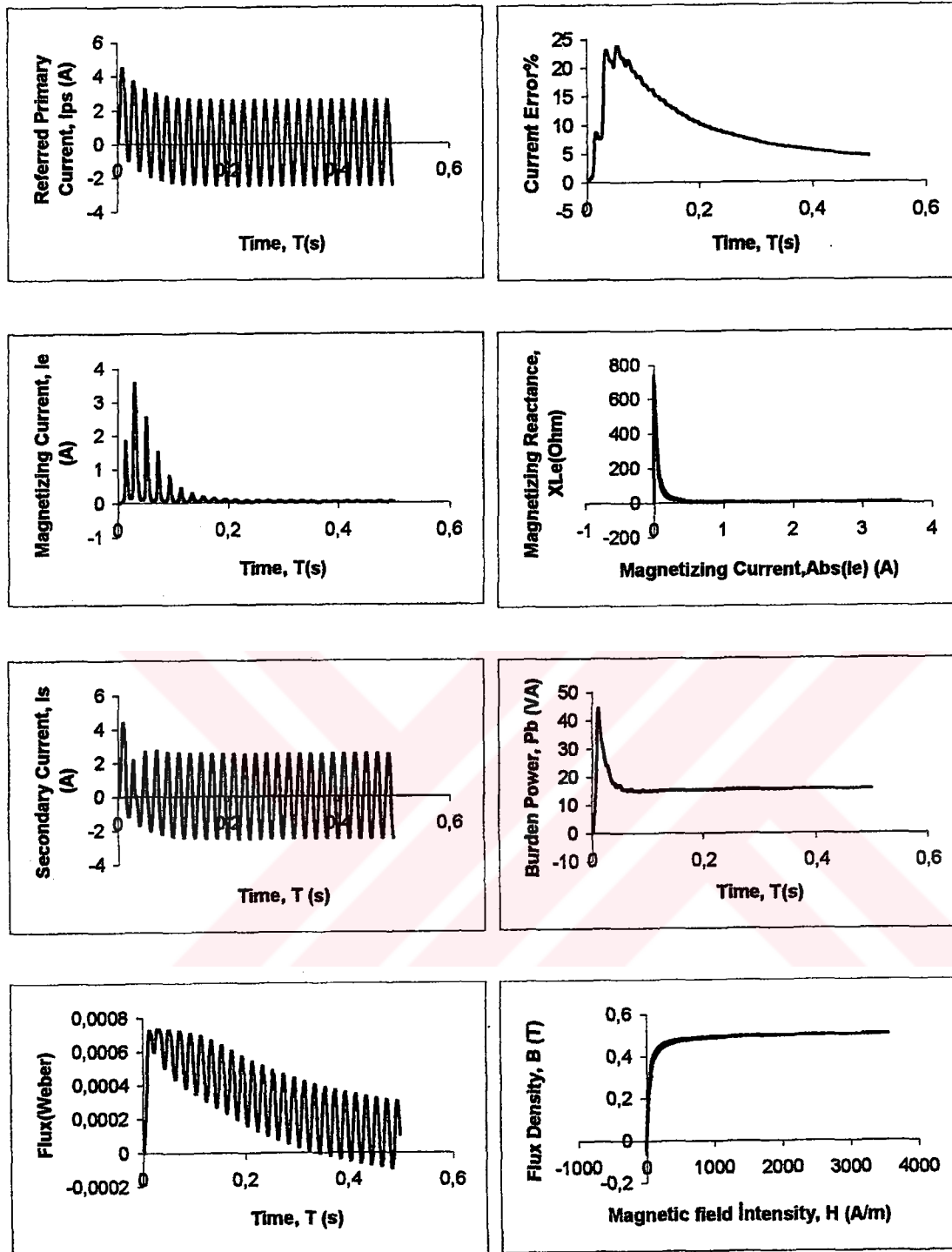


Figure 6.15 Variation of CT characteristics with respect to load resistance.

$$I_{pm}=1000\text{ A}, R_b=5\ \Omega$$

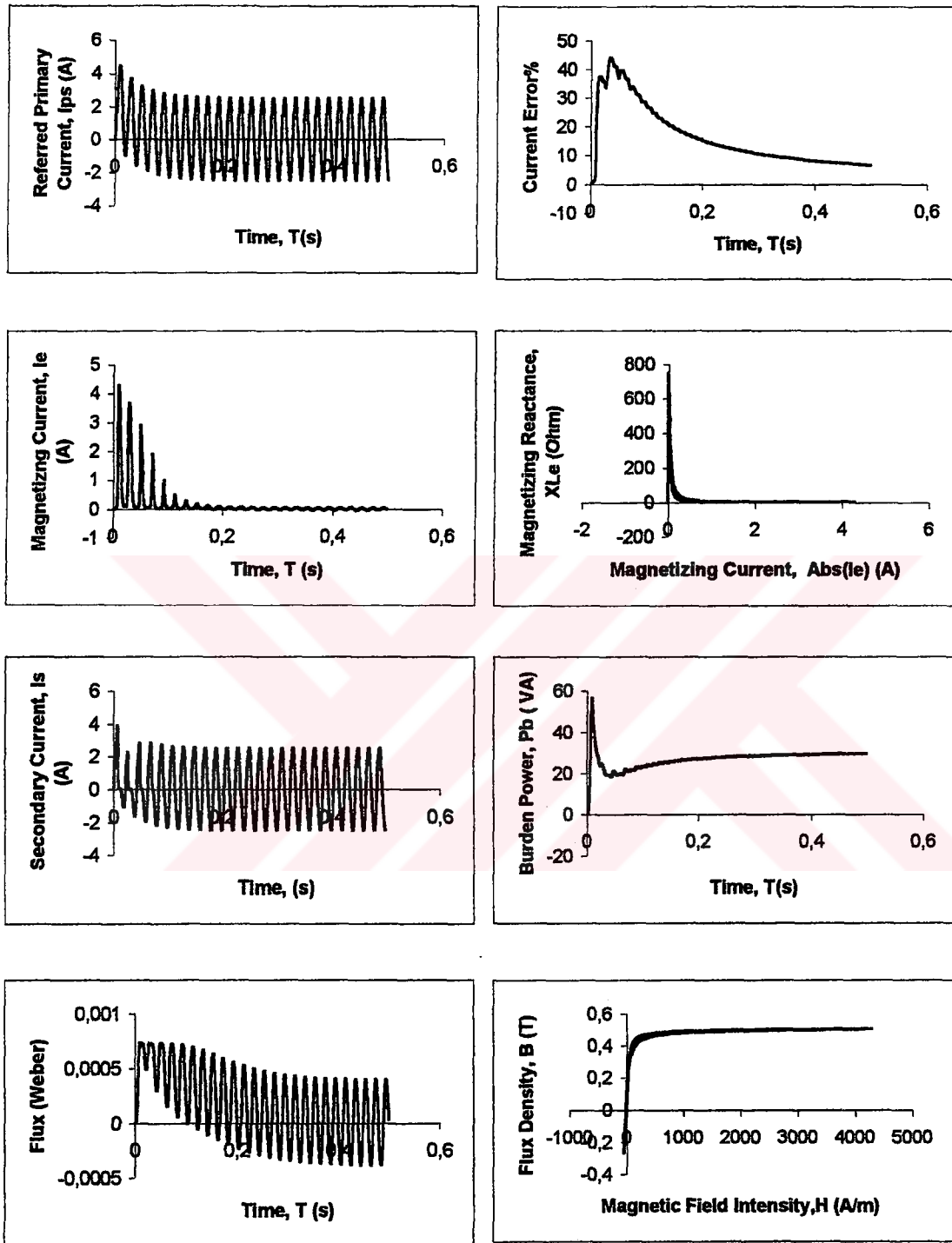


Figure 6.16 Variation of CT characteristics with respect to load resistance.

$$I_{pm}=1000 \text{ A, } R_b=10 \Omega$$

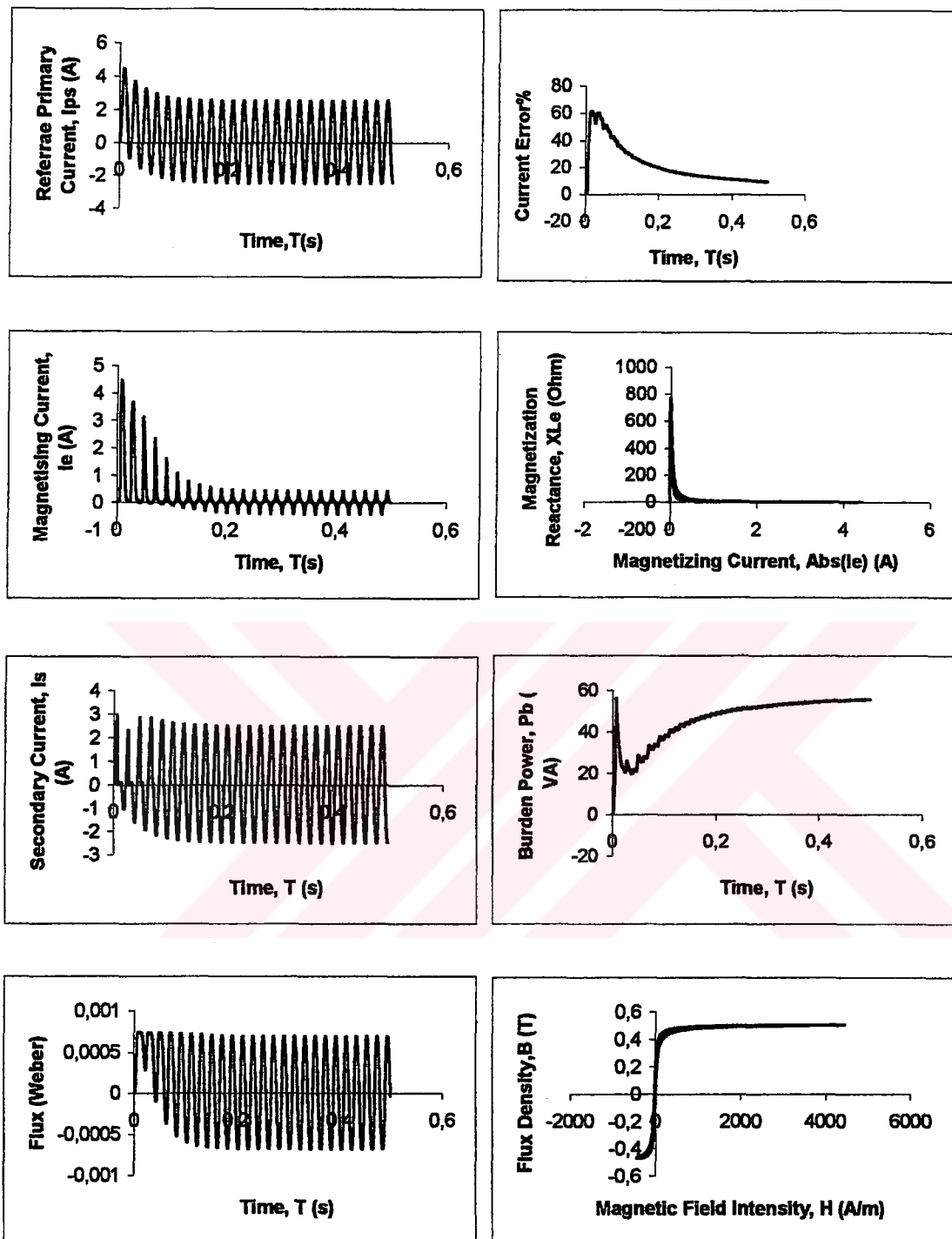


Figure 6 .17 Variation of CT characteristics with respect to load resistance.

$$I_{pm} = 1000\text{ A}, R_b = 20\ \Omega$$

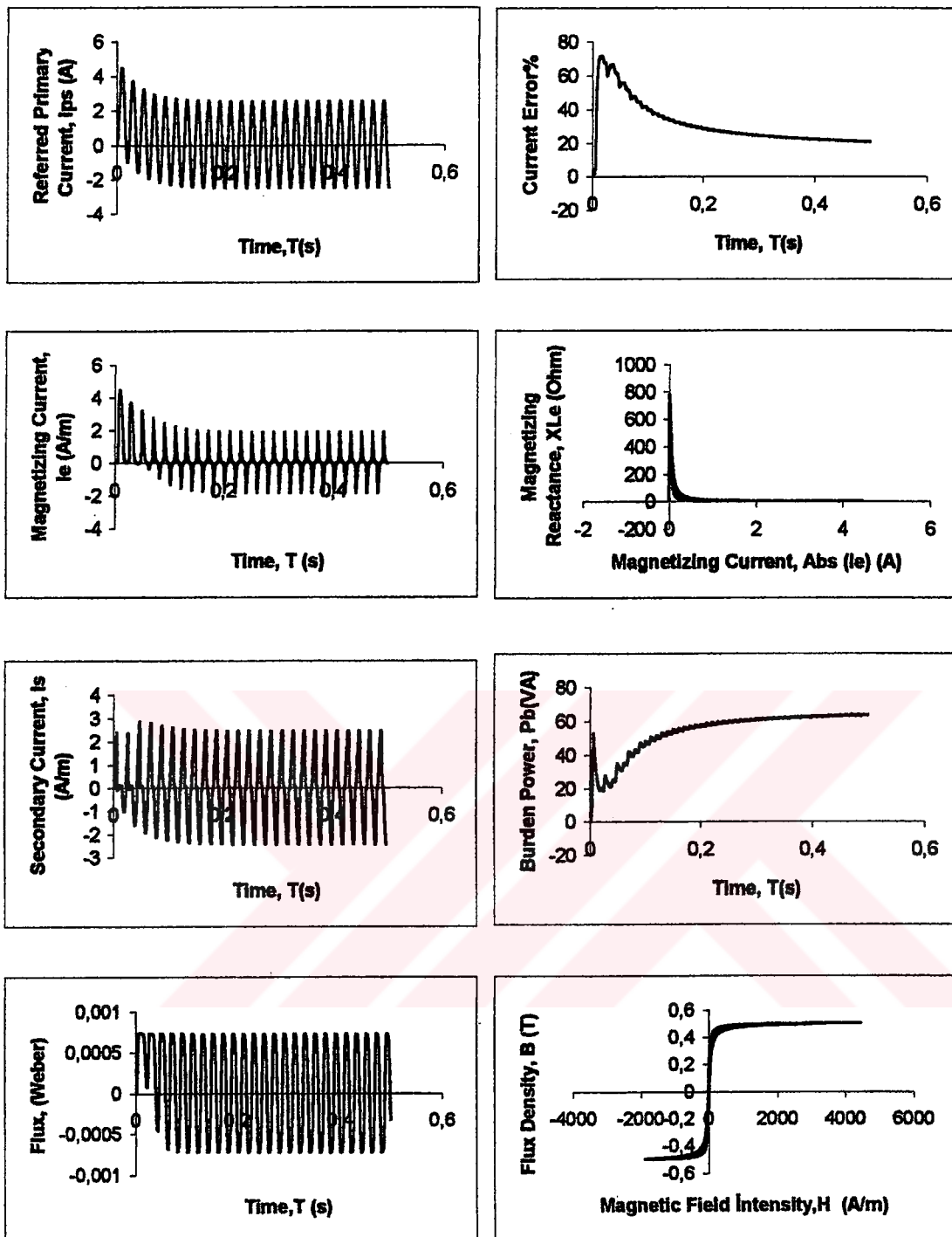


Figure 6.18 Variation of CT characteristics with respect to load resistance.

$$I_{pm} = 1000 \text{ A}, R_b = 30 \Omega$$

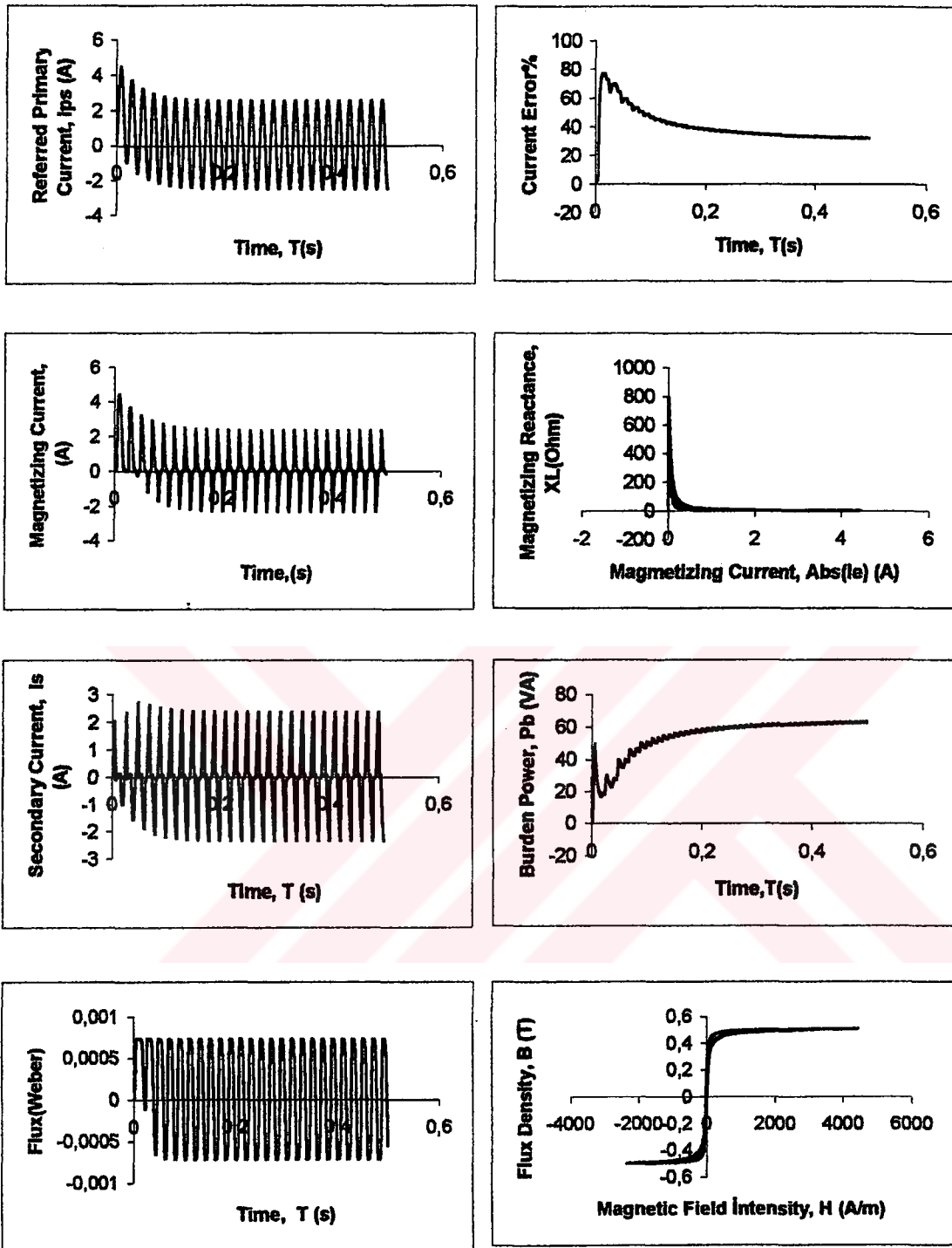


Figure 6.19 Variation of CT characteristics with respect to load resistance.

$$I_{pm} = 1000 \text{ A}, R_b = 40 \Omega$$

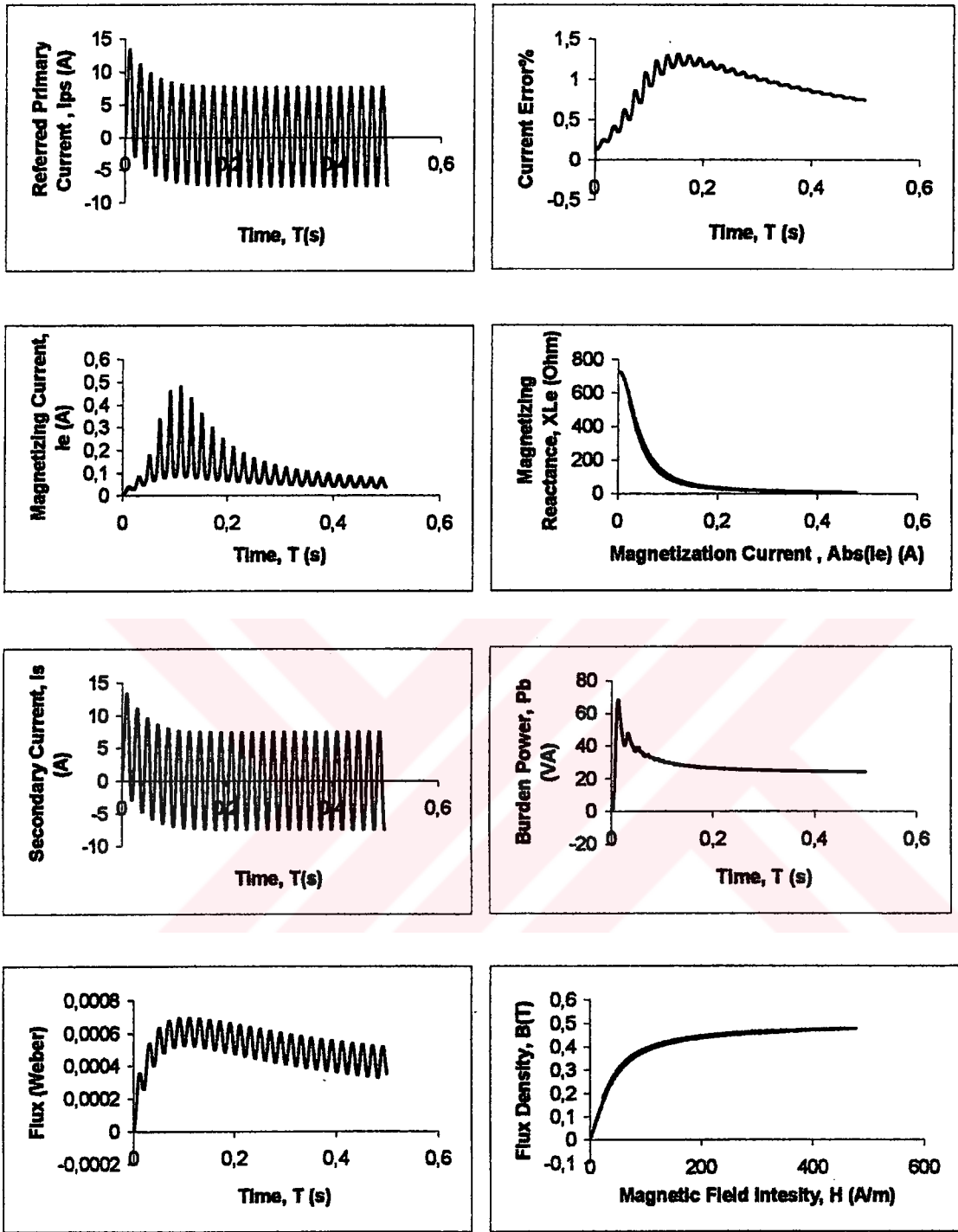


Figure 6.20 Variation of CT Characteristics with respect to load resistance.

$$I_{pm} = 3000 \text{ A}, R_b = 0.5 \Omega$$

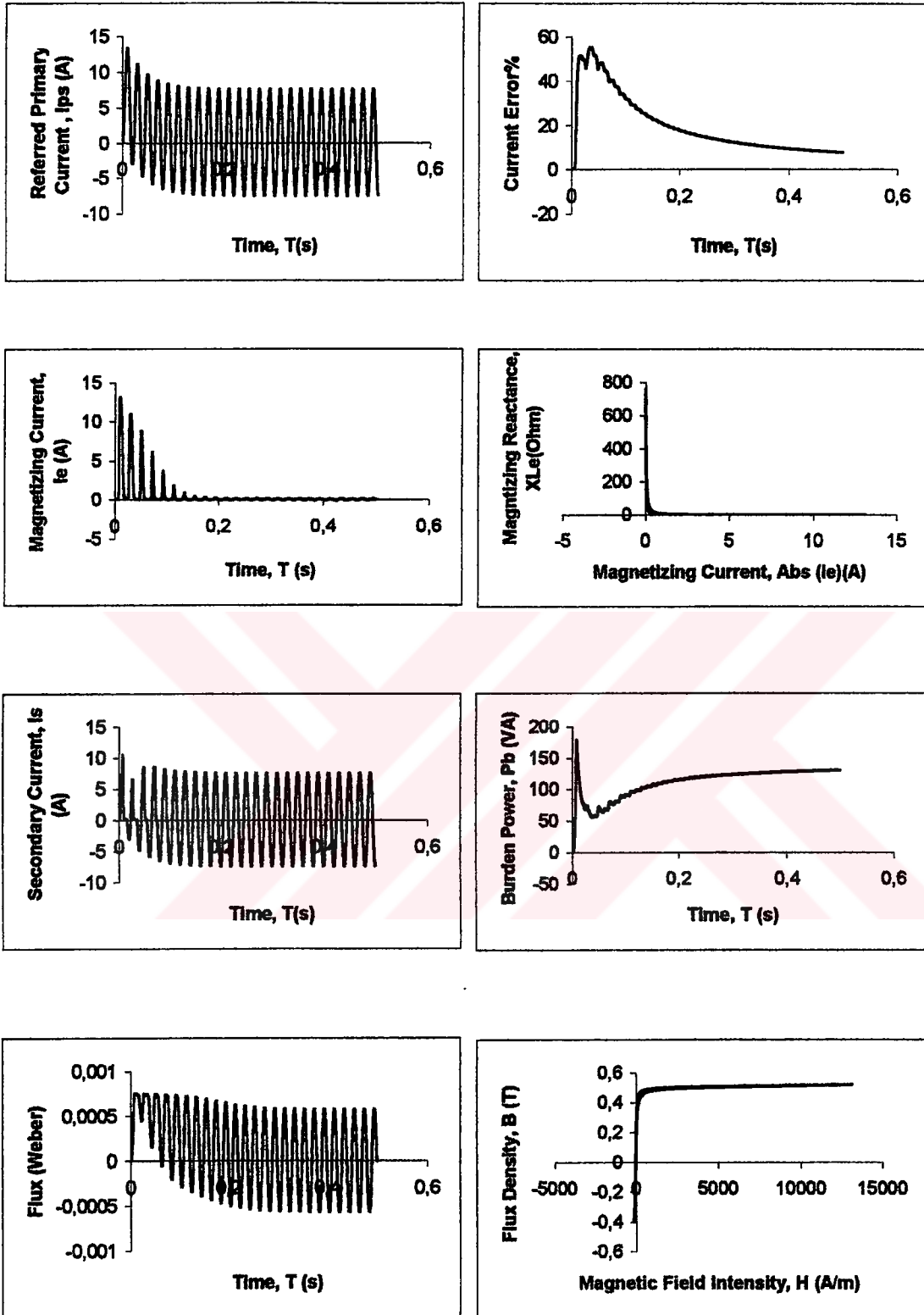


Figure 6.21 Variation of CT Characteristics with respect to load resistance.

$$I_{pm} = 3000 \text{ A}, R_b = 5 \Omega$$

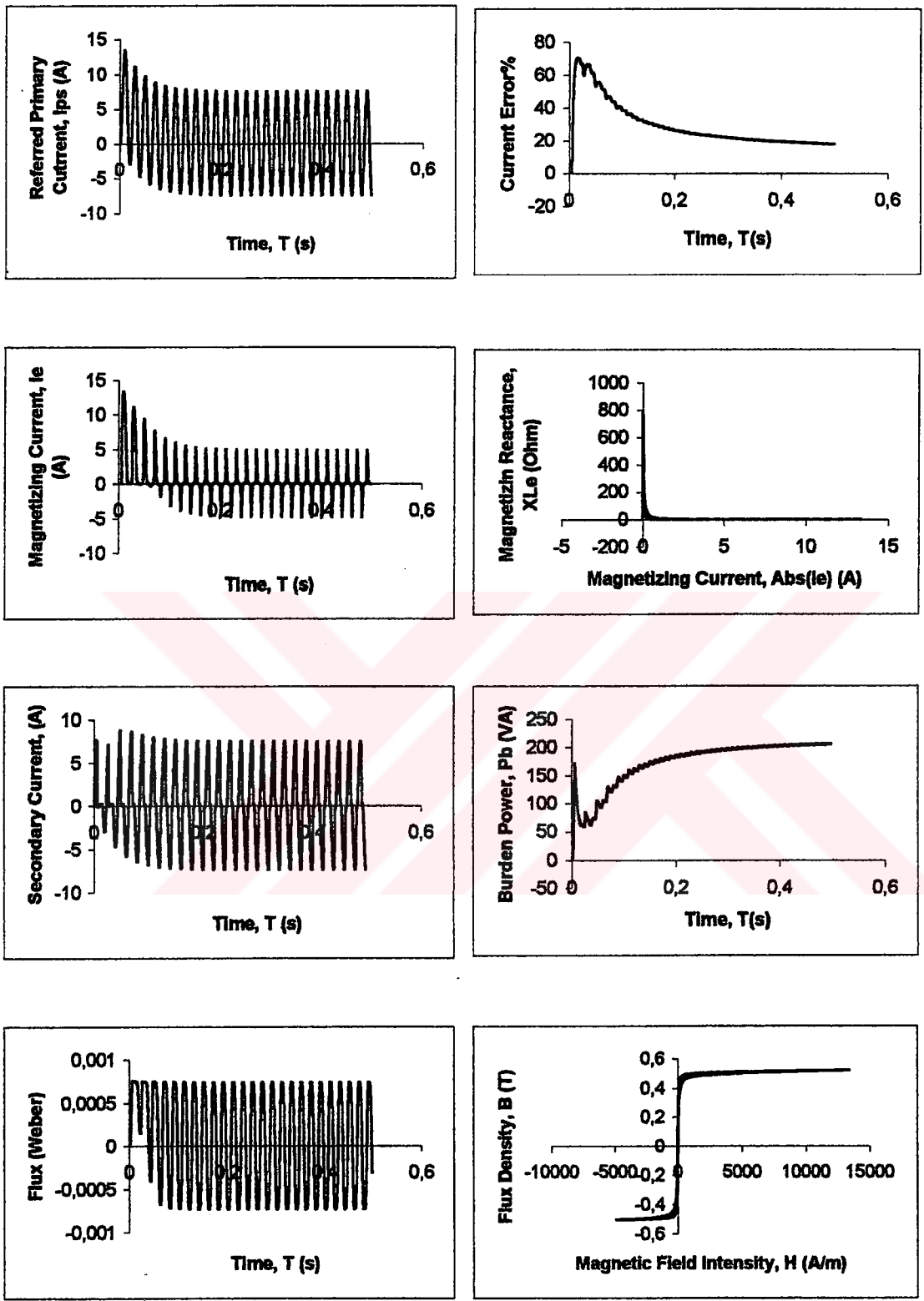


Figure 6.22 Variation of CT Characteristics with respect to load resistance.

$$I_{pm} = 3000 \text{ A}, R_b = 10 \Omega$$

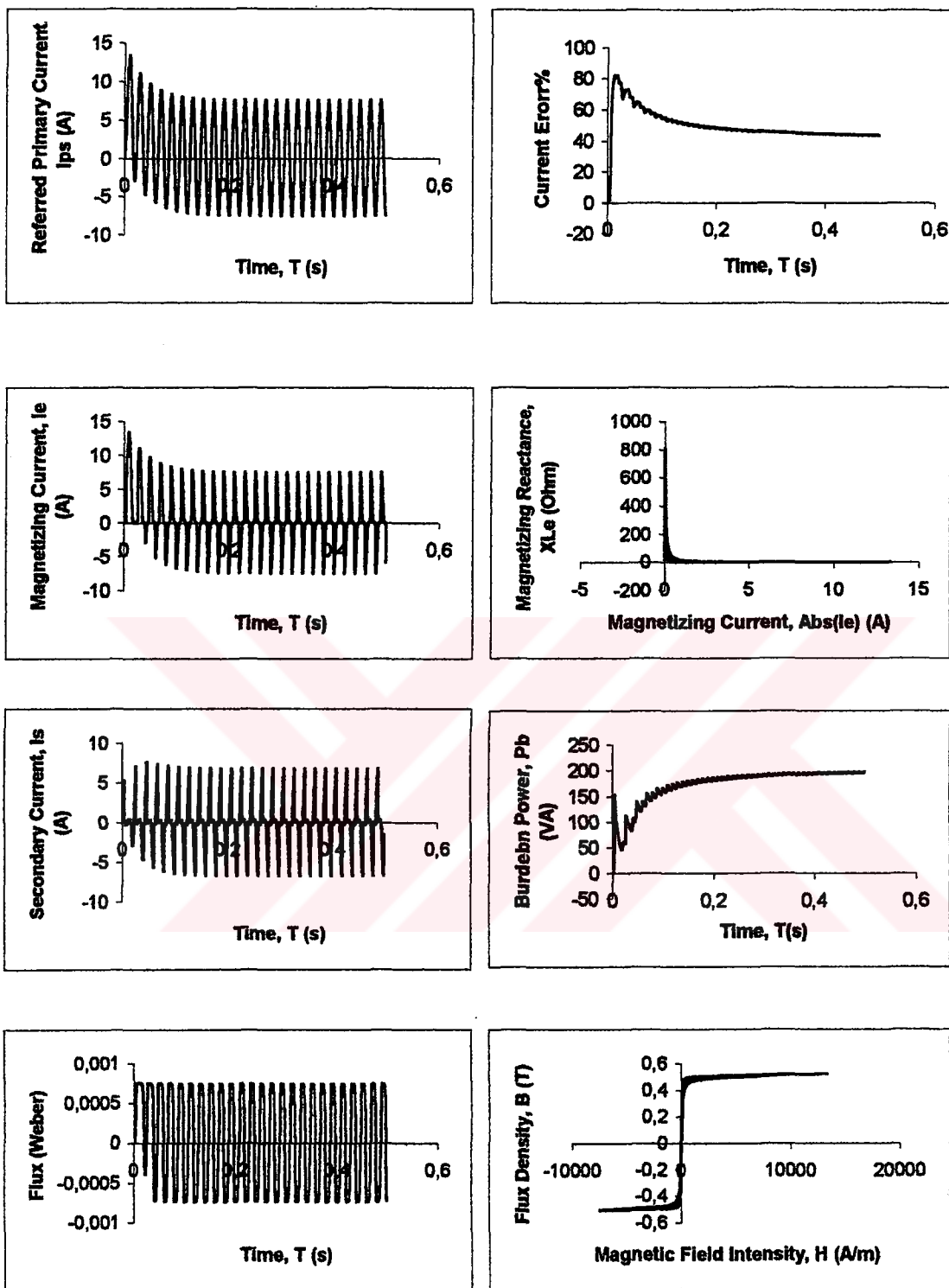


Figure 6.23 Variation of CT Characteristics with respect to load resistance.

$$I_{pm} = 3000 \text{ A}, R_b = 20 \Omega$$

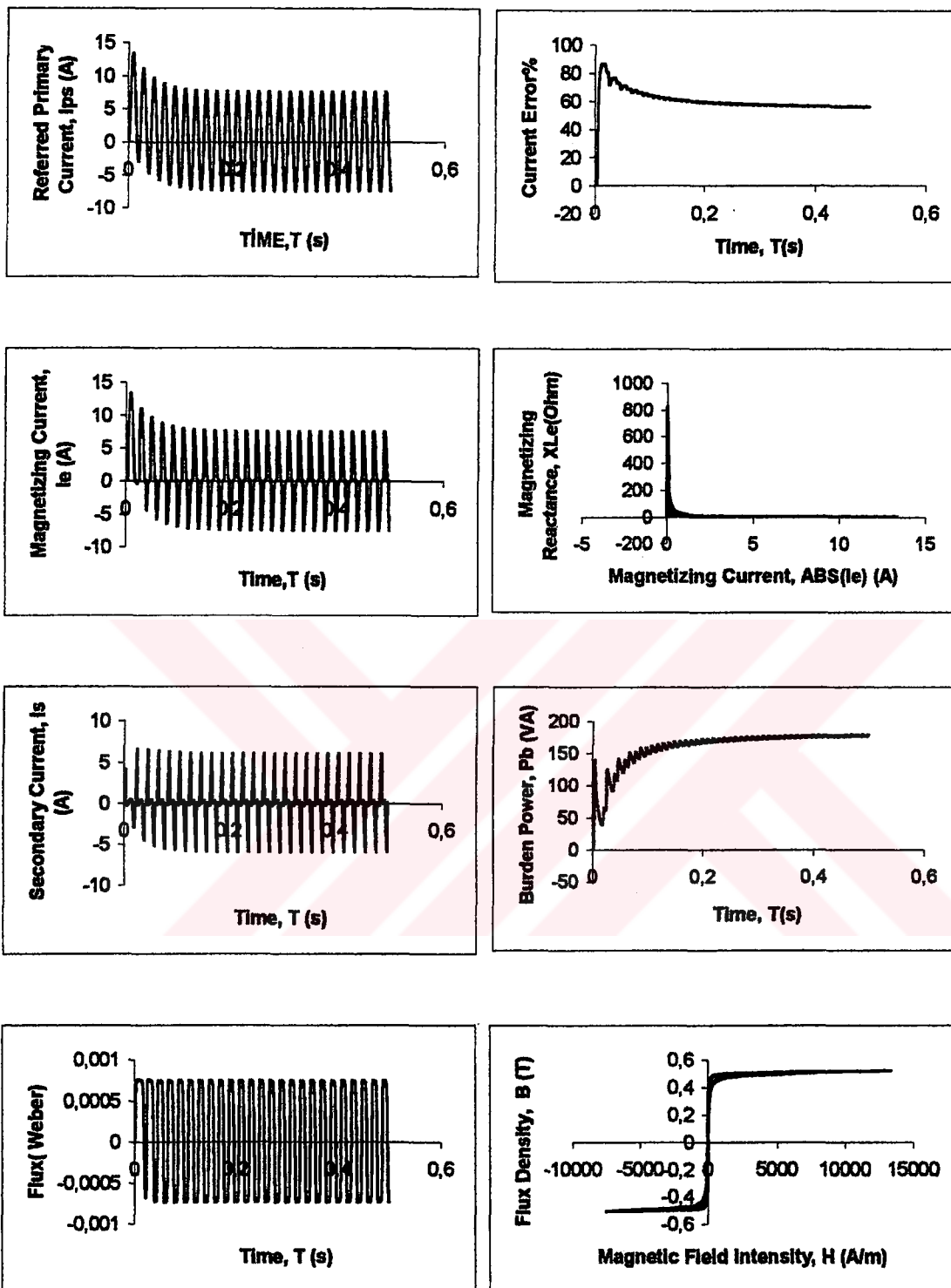


Figure 6.24 Variation of CT Characteristics with respect to load resistance.

$$I_{pm} = 3000 \text{ A}, R_b = 30 \Omega$$

CHAPTER 7

CONCLUSION AND SUGGESTIONS FOR FURTHER WORK

7.1 Conclusion

This thesis reports the development of an accurate core model for a current transformer suitable for use in current transformer transient analysis. A multi-valued hysteresis algorithm was developed for representing the B/H characteristic of the current transformer core. A protection CT was examined during the core-modeling process. After examining different core-modeling methods, Jiles–Atherton model was found to be sufficiently accurate for CT applications.

A computer program was developed for the transient analysis of the equivalent circuit of the current transformer using the core model previously described. Kirchhoff's current laws together with the explicit Fourth Order Runge Kutta Merson Routine are used to analyze the transient response of the current transformers. Simulation results were given in Chapter 6.

From the simulation results, it can be noted that CT errors depend on the magnitude of the fault current and burden impedance. Dominance of the resistance component in the burden impedance was the most significant in the distortion of the CT secondary current. Note that increasing the burden impedance would have a worst effect than an increase in the fault current level. On the other hand, inductance in the burden tends to reduce the distortion but this causes a phase angle error.

Since parameters of the J-A Model are obtained experimentally and there are limited numbers of experiments done on J-A model, we had a little difficulty in finding model parameters for different core types used in current transformers. As it is known that, every core does not give faithful results under fault conditions, different core types are

examined and it was found that 3C8 Mn-Zn ferrite core showed satisfactory results. For this reason, data of this core was used in our simulation. In order to test and compare the results of the simulation with the cores of the current transformers currently used in the market, more experiments should be done to get (J-A) model parameters.

7.2 Suggestions for Further Work

- Since it is a new model and model parameters depend on the experimental results, there are restricted numbers of core data in Jiles-Atherton model. So, experiments in a wide spectrum on different core types are suggested. This will provide us to compare the simulation results with the experimental results.
- The analysis carried out so far is on a single-phase circuit. Use of the AC model to study the transient response of current transformers in three-phase circuits is suggested.
- The use of the technique developed in this thesis to study inrush currents in three-phase power transformers is suggested. Following the same AC core-modeling procedure, a multi valued model of the transformer core characteristic can be developed, which can be used to study the effects of inrush currents in three-phase power transformers.
- Heating effects caused by transient asymmetric currents in transformer cores can also be studied.
- The use of the developed digital technique to study the effects of ferroresonance phenomena in circuits containing transformers is suggested. For such a study, modification of the fundamental circuit equations is required to adapt the technique to the examined network.

REFERENCES

1. IEEE Power System Relaying Committee Report, "Transient Response of Current Transformers" IEEE Power Engineering Society, IEEE number 76-CH1130-4 PWR, 1976
2. Wu. A.Y., "Analysis of Current Transformer Transient Response and its Effect on Relay Performance", IEEE Trans. on Industrial Applications, Vol. 1A-21, No. 4, May/June 1985, pp. 793-802.
3. Hall, J.E., Care, J.M., Light, M.R., "Development in CEGB System for Protection," IEEE Conference on Development in Power System Protection, March 1975, No. 125, pp. 318-324.
4. Schroot, C.H., "Digital Computation of the Transient Behavior of Current Transformers Under System Fault Conditions," IEEE Conference on Developments in Power System Protection, Publ. No.125, 1975, pp. 189-196.
5. Wright, A.,Carneiro, S., "Analysis of Circuits Containing Components With Cores of Ferromagnetic Materials", IEE Proc., Vol. 121, No.12, Dec.1974. pp. 1579-1581.
6. Hannala, A.Y.,Macdonald,D.C., "Representation of Soft Magnetic Materials", IEE Proc., Vol. 127, Pt. A, No. 6, July 1980, pp. 386-391.
7. Bradley, D.A., Gray, C.B. and O'Kelly, D., "Transient Compensation of Current Transformers", IEEE Trans. on PAS. Vol.97, No.4, July 1977, pp.1264-1268.
8. Mora, E.,"Performance of Current Transformers with Nonlinear Loads", MSc Dissertation, UMIST, Jan. 1980.
9. Yacamini, Abu-Nasser, A., "Numerical Calculation of Inrush Current in Single Phase Transformers", IEE Proc.,Vol.128, Pt.B, No. 6, Nov. 1981, pp.327-334.
10. Frame, J.G., Mohan, N., Biu, T.H., Hysteresis Modeling in an Electromagnetic Transient Program", IEEE Trans. on PAS. Vol.101. No. 9, Sept. 1982, pp. 3403-3410.

11. Idoniboyebu, D.C., "Transient Response of Protection Current Transformers with Linear and Nonlinear Loads", MSc Dissrtation Thesis, UMIST, Oct. 1983.
12. BS 3918, 1982.
13. Tumay, M., Smith, J.R., "Basic Principles & Testing Procedures for Current & Voltage Transformers", Strachlide Univ. England, 1991-1995.
14. Cullity, B.D., "Introduction to Magnetic Materials", Addison -Wesley Publishing Company Inc. Reading, Massachusetts, 1972.
15. Braisford, F., Fogg, R., "Anomalous Iron Losses in Cold-Reduced Grain Oriented Transformer Steel at Very Low Frequencies", Proc. IEE, Vol. 111, No. 8, Aug. 1964, pp. 1463-1467.
16. Pray, R.M., Bean, C.P., "Calculation of Energy Loss in Magnetic sheet Materials Using a Domain Model", J. Appl. Phys. Vol. 29, No. 3, March 1958, pp. 532-533.
17. Boon, C.R., Robey, J.A., "Effect of Domain Wall Motion on Power Loss in Grain Oriented Silicon-Iron Sheet", Proc. IEE, Vol. 115, No. 10, Now. 1968, pp. 1535-1540.
18. Macfadyen, W.K., Simpson, R.R., Wood, W.S., "Representation of Magnetization by Exponential Series" , Proc. IEE, Vol. 120, No. 8, August 1973, pp. 902-904.
19. Shimatani, N., Fujita, H., "Approximation of Magnetization Curves", IEEE of Japan, Section J, Vol. 101, Oct. 1981.
20. Krisnamoorthy, T.S., Venugopal, M., "Determination of Best Fit Parameters for Excitation Curve", Proc. IEEE, Dec. 1973, pp. 1762-1764.
21. Prusty, S., Rao, M.V.S., "New Method for Predetermination of True Saturation Characteristic of Transformers and Nonlinear Reactors", Proc. IEE, Vol. 127, Pt. C, No. 22, March 1980, pp.106-110.
22. O'Kely. D., "Simulation of Transient and Steady State Magnetization Characteristics with Hysteresis", Proc. IEE, Vol. 124, No. 6, June 1977, pp. 578-582.
23. Lin, C.E., Wei, J.B.,Huang, C.L., Huang, C.J., "A New Method for Representation of Hysteresis Loops", IEEE Trans. on Power Delivery, Vol. 4, No. 1, January 1989, pp. 413-420.

24. Hannala, A.Y., Macdonald, D.C., "Representation of Soft Magnetic Materials", Proc. IEE, Vol. 127, Pt. A, No. 6, July 1980, pp. 386-391.
25. Rivas, J., Zamaro, J.M., Martin, E., Pereira, C., "Simple Approximation for Magnetization Curves and Hysteresis Loops", IEEE Trans. on Magnetics, Vol. MAG17, No. 4, July 1981, pp. 1498-1502.
26. Macfadyen, W.K., Simpson, R.R., Wood, W.S., "Representation of Magnetic Characteristics Including Hysteresis by Exponential Series", Proc. IEE, Vol. 120, August 1973, pp. 1019-1020.
27. Jiles, D.J., Thoelke, J.B., Devine, M.K., Numerical Determination of Hysteresis Parameters for the Modeling of Magnetic Properties Using the Theory of Ferromagnetic Hysteresis", IEEE Transactions on Magnetics, Vol. 28, No. 1, January 1992, pp. 27-35
28. Carpenter, Kenneth H., "A Differential Equation Approach to Minor Loops in the Jiles- Atherton Hysteresis Model", IEEE Transactions on Magnetics, Vol. 27, No. 6, November 1991, pp. 4404-4406.
29. Bi, Y, Jiles, D.J., "Measurements and Modeling of Hysteresis in Materials Under the Action of an Orthogonal Bias", IEEE Transactions on Magnetics, Vol. 35, No. 5, September 1999, pp. 3787-3789.
30. Liorzou, F., Phelps, B. Atherton, D.L., "Macroscopic Models of Magnetization", IEEE Transactions on Magnetics, Vol. 36, No. 2, March 2000, pp. 418-428.
31. Calkins, F.T., Smith, R.C., Flatau, A.B., "Energy Based Hysteresis Model for Magnetostrictive Transducers", IEEE Transactions on Magnetics, Vol. 36, No. 2, March 2000, pp. 429-439.
32. Brachtendorf, H.G., Laur, R., "A Hysteresis Model for Hard Magnetic Materials", IEEE Transactions on Magnetics, Vol. 33, No. 1, Jan. 1997, pp. 723-727.
33. Jayasinghe, R.P., McLaren, P.G., "Transformer Core Models Based on Jiles-Atherton Algorithm", IEEE Cat. No. 97CH36117, 1997, pp121-125.

APPENDIX 1

Runge Kutta (Merson) 4th Order Integration Routine

$$\frac{dY}{dX} = f(X, Y)$$

Then,

$$C1 = Hf(X, Y)$$

$$C2 = Hf(X + H/3.0, Y + C1/3.0)$$

$$C3 = Hf(X + H/3.0, Y + C1/6.0 + C2/6.0)$$

$$C4 = Hf(X + H/2.0, Y + C1/8.0 + 3.0C3/8.0)$$

$$C5 = Hf(X + H, Y + C1/2.0 - 3.0C3/2.0 + 2.0C4)$$

$$Y = Y + (1.0/6.0) (C1 + 4.0C4 + C5)$$

$$X = X + H$$

Where,

H is the increment (of X)

For good accuracy, H should be small as much as possible.

APPENDIX 2

Langevin Function

$$\ell(a) = \left[\coth a - \frac{1}{a} \right] = \left[\frac{e^a + e^{-a}}{e^a - e^{-a}} - \frac{1}{a} \right]$$

$\ell(a) = \left[1 - \frac{1}{a} \right]$ for large a values. Where,

$\ell(a)$ is the Langevin function

The function rises from zero to unity as a increases and has a slope of,

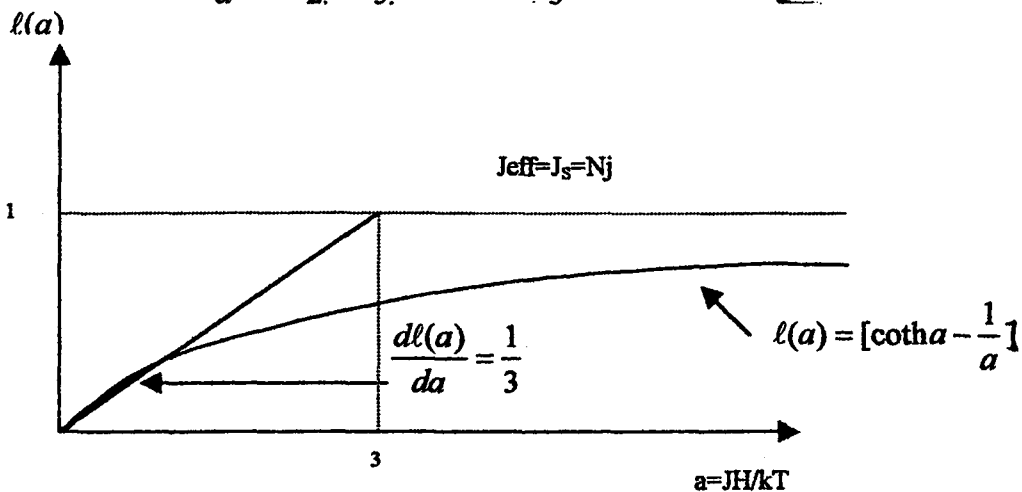
$$\frac{d\ell(a)}{da} = \frac{1}{3} \quad \text{near the origin.}$$

If e^a is written in the series form, then

$$\begin{aligned} \ell(a) &= \frac{1}{a} \left[\frac{1 + a^2/2! + a^4/4! + \dots}{1 + a^3/3! + a^5/5! + \dots} - \frac{1}{a} \right] \\ &= \ell(a) = \frac{1}{a} \left[\frac{1 + a^2/2! + a^4/4! + \dots}{1 + a^3/3! + a^5/5! + \dots} - 1 \right] \end{aligned}$$

for $a \ll 1$ dropping the fourth order terms and inverting the denominator, we have

$$\ell(a) = \frac{1}{a} \left[1 + \frac{a^2}{2!} - \frac{a^3}{3!} + \dots - 1 \right] = \frac{1}{3}$$



$a = JH/kT$, is the ratio of the magnetostatic energy to energy per particle. And the effective intrinsic flux density is proportional to $\ell(a)$, $J_{\text{eff}} = N_j \ell(a)$.